Development of an Autonomous Facade System with Individually-Controllable Photovoltaic Louvers

李, 晗

DOCTORAL THESIS

Development of an

Autonomous Facade System with

Individually-Controllable Photovoltaic Louvers

JULY 2019

Department of Architecture

Graduate School of Human-Environment Studies

Kyushu University

LI HAN

ACKNOWLEDGEMENTS

TABLE OF CONTENTS

NOMENCLATURE

a_v	luminous extinction coefficient of the atmosphere
A	azimuth angle of sun [deg]
A'	azimuth angle of window [deg]
A_s'	angle between the window and south [deg]
α	azimuth angle of the sky element respecting the sun azimuth [deg]
α_{sun}	sun profile angle [deg]
β	angle between the axes of PV louvers and vertical plane [deg]
E_{vd}	horizontal diffuse illuminance [lx]
E_{vo}	luminous solar comstant [lx], which equals to 133800 lx
E_{voh}	horizontal extraterrestrial illuminance [lx], $E_{voh} = E_{vo} \sin \gamma_s$
E_{vds}	south diffuse vertical illuminance [lx]
E_{vdw}	west diffuse vertical illuminance [lx]
$E_{\theta Ts}'$	sun-shading thresholds of global illuminance on PV-louver [lx]
E_{Ts}	sun-shading thresholds of south vertival global illuminance [lx]
γ	angle between the PV surface normal and the incident direction of the sunlight [deg]
γ_s	angle of elevation of the sun above the horizon [deg]
$G_{h,d}$	diffuse horizontal irradiance [W/m^2]
$G_{t,global}$	global irradiance on a tilt plane [W/m^2]
$G_{t,ground}$	ground-reflected irradiance on a tilt plane [W/m^2]
H	solar altitude [deg]
η_m	module efficiency
I_{DN}	normal direct irradiance [W/m^2]
I_{DH}	horizontal direct irradiance [W/m^2]
θ	louver tilt angle [deg]
$\theta_{\text{cut-off}}$	cut-off angle of louver [deg]
L_a	luminance at sky selement [cd/m^2]
L_{vz}	zenith luminance [cd/m^2]
m	relative optical air mass
P_{in}	input power [W]
P_{out}	output power [W]
R_d	diffuse transposition factor
S_b	direct-beam-illuminated PV area [m^2]
T_v	luminous turbidity factor
χ	shortest angular distance between a sky element and the sun [deg]
Z	zenith angle of the sky element [deg]
Z_s	zenith angle of the sky element and zenith angle of the sun [deg]

Chapter I

Introduction

1.1   Background

Global greenhouse gas emissions from fossil fuels have led to the increase in the global warming [1-2]. A report of the Intergovernmental Panel on Climate Change (IPCC) estimated that the energy consumed by buildings accounts for 32% of global final energy consumption and 19% of energy-related greenhouse gas emissions [3]. It also pointed out that the existing building stock, at the same time, could offer a great potential for CO_2 mitigation of up to 50–90% by using existing technologies [3]. Of these proposed technologies, building integrated photovoltaics (BIPV) have been recognized as a viable path to satisfy the energy needs of a building [4-5].

Over the last century, the proportion of the office buildings' envelope that is transparent has increased significantly [6]. Due to low thermal insulation of glass in comparison to opaque building materials, it is more important to control the solar energy inflow as the transparent fraction of building's envelope becomes larger. For this, transparent facades need an additional sun-shading control system that helps avoid solar radiation during the overheated period, allows enough solar radiation during the cold period and ensures comfortable visual conditions during operating hours.

Developments of efficiency and costs of thin-film PV technologies have brought new design possibilities. Their lightweight and flexible nature contributes to easier and more aesthetically pleasing integration into the building envelope. One example is the application of thin film PV on glazed surfaces to create a semi-transparent BIPV system [7]. Such systems not only generate electricity, but also influence the thermo-optic properties of a building, which in Los Angeles can reduce the HVAC (heating, ventilation and air conditioning) energy demand by 30%. However, when used in colder climates, the reduction of solar heat gains results in a net HVAC loss [8].

A dynamic sun-shading control system can mitigate this loss by actively controlling direct and indirect radiation into the building, while still responding to the occupant's desires. Using thin film solar panels as a shading element will also achieve the simultaneous production of photovoltaic electricity. As today photovoltaic integrated shading devices (PVSDs) attract more and more designers and researchers' attentions, there are still many areas need to be developed and improved.

PVSDs influence the performance of buildings in multiple aspects, including the air-conditioning energy consumption, electricity lighting energy consumption, electrical energy generating, indoor visual comfort, and architectural aesthetic, but some of them are contradictory. Thus, balancing the competing parameters is the key issue in the design and application of PVSDs. Based on the fixed-tilt-angle type of PVSDs, some researchers are working on sun tracking methods and corresponding rotation angles. These researches mostly focus on how to avoid shadows on the PV surface, and to enable daylighting without glare [9-10].

However, there has been barely sun tracking methods of PVSDs considering the angle control under no-direct-sunlight sky condition, when the skylight become to the critical factor to the multi-objective optimization. As mentioned before, during wintertime, the reduction of solar heat gains will result in increase of heating energy. Besides, it has reported that people in indoor spaces generally like to have access to a window for daylight provision and outside view [11-12]. Thus, to provide the flexibility of preventing direct solar radiation from entering the room and, at the same time, give access to diffuse daylight as well as a certain amount of view to the outside, a new angle control strategy (sun tracking method) of PVSDs needs to be proposed.

Automatically controlled blinds are usually equipped with sunshine sensors for direct sunlight presence judgements. For example, Inoue et al. proposed a blind control system with an automatic sun-tracking device installed on the roof to measure direct solar irradiance [13]. However, despite the costs and maintenance, monitoring sky conditions on the roof of buildings is insufficient to grasp exact daylight conditions for each window. The method to monitor the sky conditions should be simpler and more reliable.

1.2 Objectives

Towards this end, the objectives of this research are:

(1) To develop a new form of the autonomous facade system with photovoltaic integrated louvers (PV-louver system) that can be controlled individually as an integrated solution for daylight control and solar energy supply.

(2) To derive a new approach that using daylight illuminance on windows (PV-louvers) for sunshine presence judgements.

(3) To present the control strategy and configuration design of the PV-louver system to improve daylight operation and optimize the electrical power generation.

(4) A group of measurements is used to investigate the balance between the electric energy generated by the PV-louvers and energy needs for heating, cooling and lighting of an open-plan office with the autonomous PV facade system.

1.3   Methodology

To ensure the accuracy of this research work, it was decided to adopt the actual data from the "Station IDMP: Vaulx-en-Velin Cedex" in Lyon, France [14]. IDMP stands for International Daylight Measure Programme, which was conducted by International Commission on Illumination (CIE) in the 1990s. The measurement station is collecting data at one-minute intervals, 24 hours a day. The daylight and solar radiation data at the IDMP measuring station is provided by D. Dumortier, a professor of the National University of Public Works and Engineering (ENTPE) in Lyon.

The location of measurement station is in 46 degrees north and 5 degrees east. The measurement detail of IDMP is shown in Table 1-1. In this research, data from January 2012 to December 2016 were used to i) obtain a set of daylight illuminance thresholds for sunshine monitoring; ii) calculate and analyze the electrical power generation of the PV-louvers, air-conditioning and lighting energy consumption in a proposed standard office with the planned PV autonomous facade system. The electric generation is assessed by computer simulation, the thermal environment is assessed by software THERB for HAM and the luminous environment is assessed through both physical modelling and computer calculation.

Table 1-1. The measurement detail of IDMP in Lyon

Location	Vaulx-en-Velin, Lyon City, France, IDMP: FRA2, Latitude: 45.78° N, Long: 4.92° E
Measurements of ENTPE	-Horizontal global and diffuse irradiances [W/m^2] -Horizontal direct irradiance [W/m^2] -Horizontal global and diffuse illuminances [lx] -Vertical global illuminances [lx] (North, East, South, West) -Zenith luminance [cd/m^2] -Temperature [°C] -Humidity [%] -Wind speed [m/s] -UVA and UVB [W/m^2]
Others	-Date and Time -Altitude of the sun [deg] -Azimuth of the sun [deg]

1.4   Structure

The structure of this doctoral thesis altogether divides into 6 chapters:

Chapter 1 describes the background, objectives and methodology of this research and the structure of this thesis.

Chapter 2 describes the current state of the solar control devices applied to buildings. Firstly, it introduces the benefits and disadvantages of daylight and solar energy in buildings. Then, it overviews previous studies to analyze the current techniques and situation of photovoltaic integrated shading devices (PVSDs), and pointed out problems in both hardware and software.

Chapter 3 introduces the framework and design characteristics of the developed autonomous facade system with individually-controllable PV-louvers. The daylight-responsive control strategy is proposed for partly cloudy and overcast sky conditions. Besides, the improved PV-louvers configurations are also proposed to solve the PV efficiency loss under high sun profile angle conditions.

Chapter 4 explains how to use the daylight measurements at the IDMP station in France to obtain the thresholds of vertical global illuminance for judging direct sunlight presence. Then it shows a way to use ISO/CIE Standard General Skies to obtain the theoretical daylight illuminance thresholds for sunshine judgements. Finally, it explains application of the thresholds to the proposed PV louvers system.

Chapter 5 analyzes impacts of the proposed PV-louver system on electrical power generation, air-conditioning and lighting energy consumptions in a standard office. The electricity generated from the PV-louvers in different control cases was calculated and analyzed. Simulations were conducted to suggest the optimum control method and PV-louvers configuration for the autonomous PV facade system.

Chapter 6 summarizes the main results and presents the outlook of this paper.

REFERENCES

[1] United Nations (UN), Kyoto protocol to the United Nations framework convention on climate change, UN (1998)

[2] Intergovernmental Panel on Climate Change (IPCC), Climate change 2007: synthesis report, IPCC (2007)

[3] Fifth assessment report, mitigation of climate change. In: Intergovernmental Panel on Climate Change (2014), pp. 674–738

[4] P. Defaix, W. van Sark, E. Worrell, E. de Visser, Technical potential for photovoltaics on buildings in the EU-27, Solar Energy, 86 (9) (2012), pp. 2644-2653

[5] M. Raugei, P. Frankl, Life cycle impacts and costs of photovoltaic systems: current state of the art and future outlooks, Energy, 34 (3) (2009), pp. 392-399

[6] G. Bizzarri, M. Gillott, V. Belpoliti, The potential of semitransparent photovoltaic devices for architectural integration. The development of device performance and improvement of the indoor environmental quality and comfort through case-study application, Sustainable Cities and Society, 1 (2011), pp. 178-185.

[7] D.H. Li, T.N. Lam, W.W. Chan, A.H. Mak, Energy and cost analysis of semi-transparent photovoltaic in office buildings

[8] Y.T. Chae, J. Kim, H. Park, B. Shin, Building energy performance evaluation of building integrated photovoltaic (BIPV) window with semi-transparent solar cells, Applied Energy, 129 (2014), pp. 217-227

[9] P. Jayathissa, M. Luzzatto, J. Schmidli, J. Hofer, Z. Nagy, A. Schlueter, Optimising building net energy demand with dynamic BIPV shading, Applied Energy, 202 (2017), pp. 726–735,

[10] Y. Gao, J.F. Dong, O. Isabella, R. Santbergen, A photovoltaic window with sun-tracking shading elements towards maximum power generation and non-glare daylighting, Applied Energy, 228 (2018), pp. 1454-1472

[11] M. Bodart, A. Deneyer, Analyse of the survey on the office workers' interest in windows, IEA 31, Subtask A, working document, (2005)

[12] B.L. Collins, Review of the psychological reaction to windows, Light. Res. Technol., 8 (1976), pp. 80-88

[13] Origara Y., Inoue T., Ichinose M., "Investigation Based on Automatic Blind and Effect of Daylight Use", The Society of Heating, Air-Conditioning Sanitary Engineers of Japan, No.2, pp. 943-946, 2011

[14] CIE 108-1994 Guide to Recommended Practice of Daylight Measurement, CIE, 1994.

Chapter II

Current State of the Solar Control Devices Applied to Buildings

2.1   Daylighting and solar energy in buildings

The sun is the primer source of light on the earth. Because photoreceptors in the human eye absorb energy only in the wavelength region between 370 nm to 780 nm and thereby initiate the process of seeing, the wavelength range is distinguished as visible spectrum. The solar radiance reaching the earth, about half is visible light, and half is in the infrared part of the electromagnetic spectrum, and a small amount of ultraviolet radiation.

Light from the sun can reach the earth in two ways: directly as sunlight, and indirectly as skylight after being scattered, reflected and absorbed by the atmosphere. Daylight is the combination of all direct and indirect sunlight. It includes direct sunlight, diffuse sky radiation, and both of these reflected by the earth and terrestrial objects, like landforms and buildings. Solar energy is harnessed for a range of ever-evolving technologies such as solar heating, photovoltaics, solar thermal energy, solar architecture, molten salt power plants and artificial photosynthesis [1]. Solar energy is viewed as one of the most popular renewable energy sources [2]. It is the most abundant, inexhaustible, cleanest and environmentally friendly among all renewable energy resources.

2.1.1 Benefits and disadvantages of daylighting in buildings

With the wide usage of LED lighting, daylighting no longer has obvious energy saving advantages. However, the daylight still have very positive effects on people: (i) Physiologically, daylight is an effective stimulant to the human visual system and the human circadian system; (ii) Psychologically, daylighting and a view out are desired and, in consequence, have benefits for human well-being. Unfortunately, daylighting can cause both visual and thermal problems if it is not properly delivered. For example, sunlight directly incident on people near a window can cause thermal and visual discomfort.

The visual problems of daylighting are glare and veiling reflections. Glare is caused by a direct view of either the sun or the bright sky. It is usually experienced when facing a window in a facade receiving direct sunlight. Veiling reflections are most commonly experienced by people sitting back to a window, when the high brightness impinging on a computer screen reduces the contrast of display. Besides, daylight entering a building causes a heat load. This may be useful in winter, but it can be an additional cooling load in summer. Therefore, it is essential to consider the contribution of daylight energy for the energy balance of the whole building. When developing or selecting shading devices, consideration should be given to these effects.

2.1.2 Solar control and solar energy technologies for buildings

Well-designed solar control and sun-shading devices can dramatically reduce building peak-heat-gain and cooling requirements and improve the daylighting quality in building interiors. It can also improve user visual comfort by controlling glare and reducing excessed contrast.

The design of effective shading devices will depend on the solar orientation of a particular building facade. For example, simple fixed overhangs are very effective in shading south-facing windows in the summer when sun angles are high. However, the same horizontal device is ineffective at blocking low afternoon sun from entering west-facing windows during peak-heat-gain periods in the summer.

Solar control and shading can be provided by a wide range of building components including [3]:

- Landscape features such as mature trees or hedgerows;

- Exterior elements such as overhangs, horizontal multiple panels or vertical fins;

- Horizontal reflecting surfaces called light shelves;

- Low shading coefficient (SC) glass; and,

- Interior glare control devices such as Venetian blinds or adjustable louvers.

Exterior shading devices are the most efficient thermally because they intercept the solar energy before it enters a room. They are particularly effective in conjunction with clear glass facades. Its effectiveness finally depends on its type and placement relative to the glazing.

When sunlight strikes a building, the building materials can reflect, transmit, or absorb the solar radiation. Solar technologies are broadly characterized as either oassive or active depending on how they capture and distribute solar energy or convert it into solar power. Passive solar techniques refer to the use of the sun's energy for the heating and cooling of interiors by exposure to the sun. The solar radiation heats interiors. In addition, the heat produced by the sun causes air movement that contributes the ventilation and structural cooling. Unlike active solar heating systems, passive systems are simple and do not involve substantial use of mechanical and electrical devices. However, passive solar techniques are commonly included at a very early stage of the building design. Active solar techniques include use of photovoltaic systems, concentrated solar power and solar water heating to harness the energy.

Building Integrated Photovoltaics (BIPVs) refers the integration of photovoltaic modules into the building envelope, with the dual roles of replacing building components and of simultaneously serving as electricity generators. In general, most building surfaces are available for the integration of PV modules, which can be grouped into four macro-categories: PV-facades (including curtain wall products, spandrel panels, glazing, etc), PV-roofs (including tiles, shingles, standing seam products, skylights, etc.), PV-windows and overhead glazing (including laminated glass, laser-etched thin films, transparent thin films, etc.) and PV-sunshades (including panels, louvres, blinds, etc.) [4]. It should be noted that a general consensus on the BIPV classification has not yet been reached [5]. In some studies, the integrated PV surfaces of parapets and balconies have been classified into a category called PV-accessories.

2.2 A review of photovoltaic integrated shading devices (PVSDs)

Vertical space bears great potential of solar energy especially for urban areas, where photovoltaic windows in high-rise buildings can contribute to both power generation and daylight harvest. The potential of PV-sunshade (photovoltaic integrated shading device) products have been verified as more technically efficient than other types of BIPV products, such as the PV-facades and PV-roofs [6-7]. It calls for more attention and research on photovoltaic integrated shading device (PVSD).

2.2.1 PV techniques applicable to PVSDs

Solar cells are typically named after the semiconducting material they are made of. Three kinds of PV solar cells have hitherto been developed. The kind of wafer-based cells are made of crystalline silicon, the commercially predominant PV technology, that includes materials such as polysilicon and monocrystalline silicon. The kind of thin-film cells includes amorphous silicon, CdTe and CIGS cells. They are commercially significant in utility-scale photovoltaic power stations, building integrated photovoltaics or in small stand-alone power system. There is kind of solar cells made of organic materials, often organometallic compounds as well as inorganic substances. The dye-sensitized photovoltaic (DSSP), organic photovoltaic (OPV) were regarded as alternative thin-film PV technologies but are essentially dead now, and those modules are rarely available in the market currently [8]. Despite the fact that their efficiencies had been low and the stability of the absorber material was often too short for commercial applications, there is a lot of research invested into these technologies as they promise to achieve the goal of producing low-cost, high-efficiency solar cells.

The crystalline silicon solar cell according to the material can be divided into monocrystalline photovoltaic cells (also known as single-crystal silicon cells or c-Si) and polycrystalline photovoltaic cells (also known as multi-crystalline silicon cells or p-Si). The former is made of high-purity single-crystal Si rods, which are sliced into thin wafers to produce cells. The 17–18% efficiency of monocrystalline silicon cells can be achieved owing to its purity [9]. The later can be manufactured from metallurgical-grade silicon through a chemical purification called the Siemens process. Given consideration of mitigating the cost of developing PV modules, polycrystalline silicon cells are regarded as more cost-effective than the monocrystalline silicon cells. The efficiency of polycrystalline silicon is 13-16% [10].

The thin-film solar cell mainly includes amorphous silicon solar cells (a-Si), cadmium telluride (CdTe) photovoltaic solar cells and copper-indium-gallium-selenide (CIGS) cells. Table 2-1 shows the basic information of the first- and second-generation solar cell [11]-[14].

Table 2-1. Basic information of the crystalline silicon and thin-film solar cells

Classification	Crystalline silicon solar cell		Thin-film solar cell		
	Mono-Si	Poly-Si	a-Si	CIGS	CdTe
Module efficiency	15-18%	13-16%	6-9%	10-12%	9-11%
Shading effect	High	High	Low	Low	Low
Harmful effect	No	No	No	No	Yes
Weigh (kg/m^2)	11.7	11.6	2.5	2.4	16.7

With regard to the PV properties, two factors were generally considered for the PVSDs: (i) practicality applicable to PVSDs and (ii) constructability applicable to PVSDs.

In terms of practical ability in a vertical PV-sunshade system, the shading effect of a PV cell should be considered. Although the efficiency of electricity generation of crystalline silicon PV products is higher than that of the thin-film PV counterparts (Table 2-1), the crystalline silicon PV products are less tolerant of partial shading with their efficiency precipitously declining than the thin-film PV counterparts. It has been reported that by shading 50% of a mono-Si or poly-Si PV cell the power production was reducing by more than 30% [15]. On the contrary, the thin-film PV products have smaller shading effect and resist elevated temperatures than the crystalline silicon PV products [4]. This alongside potentially lower production costs offered by the thin-film PV technology, illustrates the advantages of the thin-film PV products [16]. In addition, the production of CdTe PV cells entails the use of toxic materials, such as cadmium and tellurium, leading to potentially deleterious hazards. Thus, CdTe PV cells are not suitable for the application on PVSDs.

In terms of constructability, because the structure of a PV-sunshade system is commonly not as much as capable of load-bearing than the roof-integrated and facade-integrated PV system, the relatively light weight of the a-Si and CIGS PV cell enhances their applicability in shading systems.

A recent survey says greater emphasis has been placed upon studies on crystalline silicon [4] with a fact that crystalline silicon overwhelmingly predominates the global

market of PV cells (90%) [17]. However, as aforementioned, a-Si and CIGS deserve more emphasis in future studies to explore their potential for integration into shading devices, owing to their noticeable suitability of application (practicality and constructability) on PVSDs.

2.2.2 Optimum orientation and tilt angle of PVSDs

It is known that if the PV panel is tilted towards the sun, more solar energy can be captured by the PV panels for maximum conversion into electricity [19]. It lead to the concept of the optimum tilt of PVSDs. For this, ideal PVSDs have movable PV panels tracking the movement of the sun and keeping perpendicular to the direction of sunlight. However, the required tracking system can be costly, and the costs may not have advantage over the increase in the electricity generated from PVSDs. Hence, in most current cases, the PV panels of PVSDs are equipped on buildings with a fixed tilt angle.

The orientation and the tilt angle are regarded as two main factors influencing the performance of electrical generation of PVSDs.

In general, in the northern hemisphere the most favorable orientation is to the south, while in the southern hemisphere that is to the north [18]. Taking the electricity production oriented to the equator as a benchmark, the average decline in the efficiency of the electric production of a PVSD orientated away from the equator is about 1.1% for every five degrees [19]. It is also noted that the optimal orientation is influenced by the local conditions, such as weather and topography in reality [20].

A suggested fixed tilt angle [21] setting round the year can be estimated by empirical formula Eq. (2-1). It is noteworthy that this angle is the optimum tilt for fixed solar panels for all-year-round power generation.

$$\beta\_annual \quad \approx l_{PV} \qquad\qquad \text{Eq.}(2-1)$$

Where β_annual is the optimum fixed tilt angle setting round the year [deg]
L_{PV} is the latitude of the location of the PVSD [deg]

Accordingly, the best compromise in power output is achieved throughout the entire year and this implies the constituent monthly power output may or may not be optimal [19]. Relative to passive systems such as fixed louvers, a dynamically controlled PVSD with auto-rotation louvers can increase both visual and thermal comfort and energy efficiency.

2.2.3 Sun tracking systems

In views of the sun tracking system properties, two factors were considered for the PVSDs: the tracking method and the tracker type. The tracking method can be categorized into two types: (i) direct tracking method; and (ii) indirect tracking method [22, 23].

(i)   Direct tracking method: a method for controlling the tracking system based on the results of direct measurement from the PV system. The measurement data can be divided into two types (i.e., solar radiation and electricity generation). The solar radiation-based direct tracking method determines the tracking

direction by using a photo-sensor and evaluating the maximum solar radiation data. The electricity generation-based direct tracking method determines the tracking direction based on evaluation of the current data produced from the PV system. However, the direct tracking method has a disadvantage in that malfunction in tracking can occur as a result of temporary errors [24, 25].

(ii)   Indirect tracking method: a method for controlling the tracking system by calculating the position of the sun according to both the date and time. However, this method has a disadvantage in that it is difficult to reflect the difference of the electricity generation depending on the location and direction where the PV system is installed.

This research adopted the direct tracking method for the study on PV-louvers control.

Tracker types include single axis and dual axis tracker. In this study, the horizontal single-axis tracker (HSAT) type was selected to use in the proposed autonomous PV-louver system. The HSAT can track the daily rising and falling motion of the sun through the rotation horizontal to the ground.

2.3   Status and issues of PVSDs

A recent survey indicated that there are four types of buildings on the application of PVSD systems, including offices, residential buildings, school facilities, and laboratories. Additionally, a majority of studies focused on office buildings [4]. The reason for this attention to PVSD application on office buildings may partially be attributed to its greater energy consumption [26]. Besides, the architects' preference towards vast glazed envelopes and facades in the design of office buildings [27] causes glare and excessive heat gain in the summer [28]. Moreover, the effective functioning hours of photovoltaics match well with the working hours of offices since they are usually operating during the daytime when solar radiation is abundant and PVSD electricity production is high [29]. Hence, office buildings are suitable for PVSD application due to large energy consumption, large surfaces of glazed facades, and a schedule that matches well the building functions and electricity generation.

There are research studying 15 types of PVSDs, with the emphasis on inclined single panel, louvres embracing the horizontal louvres between double layers, horizontal louvres outward and inward, and vertical louvres outward [4]. It is suggested that future studies should put more attention to other types of PVSDs so as to ensure the adaptability of PVSDs under different design conditions, such as location, orientation, and others.

Nowadays, sun-tracking PVSDs integrate PV materials with auto-tracking shading devices (e.g. blinds, louvers, shutters, etc.), are attracting more and more researchers attentions. Luo et al. conducted a comparative study of PV blinds by varying the spacing between adjacent blinds (2.5 cm, 3.5 cm, and 4.5 cm) and by varying the slat angle (30°,

45°, and 60°) [30]. However, the analysis focused on the thermal performance of the PV blinds, instead of the PV power generation. Abdallah et al. developed a sun tracking system and concluded that the use of two axes tracking system results in an increase in total daily generation of about 41.34% as compared with that of the 32° tilted fixed surface [31]. However, the analysis was based on traditional single-layer solar panels, instead of the multi layers solar panels. In fact, for a multi layers PVSD type, the shading effect of the solar cell module plays a critical role in its performance. The shadows on a PV panel surface cast by the panel above it result in PV partial shading problems, which affect the PV performance, especially the module efficiency. Therefore, when designing a sun tracking method for PVSDs, factors such as orientation tilt angle, and the width/length of shading devices need to be considered to avoid shadows being cast on the PV surface, and to enable daylighting without glare.

Above all, PVSDs influence the performance of buildings in multiple aspects, including the energy consumption related to air-conditioning, electricity lighting, electrical energy generation, indoor visual comfort, and architectural aesthetic. However, As seen in Fig. 2-1, some of them are contradictory: for example, ensuring the maximum electric energy production with an optimum tilt angle may narrow the space between slats or panels, limit field of outside views or increase consumption of electricity lighting energy. Thus, balancing competing parameters is a key issue in the design and application of PVSDs, to which multi-objective optimization (balance energetic performance with architectural expression) may be a viable solution. Against this background, some studies were conducted. Zhang et al. studied the optimization of tilt angles of the horizontally inclined PV-shading panel, with the building energy consumption (cooling and lighting)

and electrical power production [33].
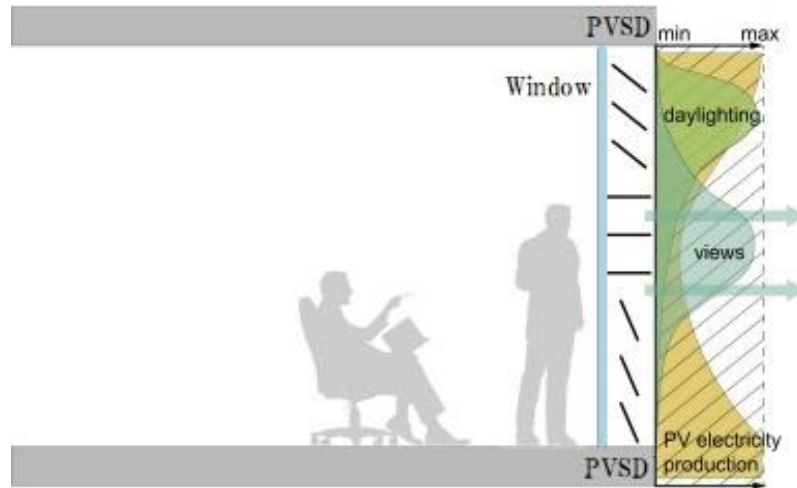
Fig.2-1 PVSD acting as a mediator between the interior and exterior environment, while fulfilling various functions. Modified from Jakica and Zanelli (2014) [32]

However, previous studies on the multi-objective optimization of PVSDs are still insufficient. There has been barely PVSDs research on the angle control of PV shading elements under no-direct-sunlight sky condition, when the skylight becomes to the critical factor to the multi-objective optimization. In some cases, the PV power generation is no longer the primary goal of the PV shading system. At higher latitude sites in winter, increase heating energy resulted by the reduction of solar heat gains might spoil the electrical power a PVSD can generate. Besides, as occupants desire daylight or outside views, open positions of shading elements are in need during automatic control strategies.

2.4   Conclusion

The chapter overviews the benefits of utilizing daylight and solar radiation in buildings as well as their negative impacts. It is useful to equip photovoltaic integrated shading devices (PVSDs) on large-scale windows of today's high-rise buildings. PVSDs can avoid excessive heating and glare, but also utilize solar energy for power supply. It highlights the technology of sun-tracking PVSDs, which integrates PV materials with auto-rotation shading devices (e.g. blinds, louvers, shutters, etc.). It concludes the previous study approaches including tilt angle, orientation, and control method of PVSDs. Finally, it summarizes the status and issues of PVSDs, and found the inadequacy of the current studies to define the direction of this research.

REFERENCES

[1] Solar Energy Perspectives: Executive Summary, International Energy Agency. (2011).

[2] S.K. Das, D. Verma, S. Nema, R.K. Nema, Shading mitigation techniques: State-of-the-art in photovoltaic applications Renew. Sustain. Energy Rev., 78 (2017), pp. 369-390.

[3] D. prowler, Sun control and shading devices, Whole building design guide, (2016).

< https://www.wbdg.org/resources/sun-control-and-shading-devices >

[4] X. Zhang, S. Lau, S.S.Y. Lau, Y. Zhao, Photovoltaic integrated shading devices (PVSDs): A review. Sol. Energy, 170 (2018), pp. 947-968.

[5] Frontini, F., Bonomo, P., Chatzipanagi, A., BIPV product overview for solar facades and roofs (2015).

[6] M. Mandalaki, T. Tsoutsos, N. Papamanolis, Integrated PV in shading systems for Mediterranean countries: balance between energy production and visual comfort, Energy Build., 77 (2014), pp. 445-456.

[7] E. Taveres-Cachat, K. Bøe, G. Lobaccaro, F. Goia, S. Grynning, Balancing competing parameters in search of optimal configurations for a fix louvre blade system with integrated PV, Energy Procedia, 122 (2017), pp. 607-612.

[8] M. Tripathy, P.K. Sadhu, S.K. Panda, A critical review on building integrated photovoltaic products and their applications, Renew. Sustain. Energy Rev., 61 (2016), pp. 451-465.

[9] M. Debbarma, K. Sudhakar, P. Baredar, Thermal modeling, exergy analysis, performance of BIPV and BIPVT: a review, Renew. Sustain. Energy Rev., 73 (2017), pp. 1276-1288.

[10] G.N. Tiwari, R.K. Mishra, S.C. Solanki, Photovoltaic modules and their applications: a review on thermal modelling, Appl. Energy, 88 (2011), pp. 2287-2304.

[11] K. Jeong, T. Hong, C. Koo, J. Oh, M. Lee, J. Kim, A prototype design and development of the smart photovoltaic system blind considering the photovoltaic panel, tracking system, and monitoring system, Appl. Sci., 7 (2017), p. 1077.

[12] S. Roberts, N. Guariento, Building Integrated Photovoltaics: A Handbook, Walter de Gruyter (2009).

[13] D.G. für Sonnenenergie, Planning and Installing Photovoltaic Systems: A Guide for Installers, Architects and Engineers, Planning and Installing Series, Earthscan (2008).

[14] G. Stapleton, S. Neill, Grid-connected Solar Electric Systems: The Earthscan Expert Handbook for Planning, Design and Installation, Routledge, New York, NY, 10001 (2012).

[15] A. Dolara, G.C. Lazaroiu, S. Leva, G. Manzolini, Experimental investigation of partial shading scenarios on PV (photovoltaic) modules, Energy, 55 (2013), pp. 466-475.

[16] A. Falk, C. Durschner, K.H. Remmers, Photovoltaics for Professionals: Solar Electric Systems Marketing, Design and Installation, Taylor & Francis (2013).

[17] S. El Gindi, A.R. Abdin, A. Hassan Building integrated Photovoltaic Retrofitting in office buildings Energy Procedia, 115 (2017), pp. 239-252.

[18] Prasad, D.K., Snow Dr, M., Designing with solar power: a source book for building integrated photovoltaics (2005).

[19] Boxwell, Michael, Solar Electricity Handbook 2017 Edition, eleventh E. ed. Greenstream Publishing Limited, Birmingham (2017).

<http://solarelectricityhandbook.com/solar-irradiance.html>.

[20] Gaiddon, B., Kaan, H., Munro, D., Photovoltaics in the urban environment: lessons learnt from large scale projects (2009).

[21] Prasad, D.K., Snow Dr, M., Designing with solar power: a source book for building integrated photovoltaics (2005).

[22] Mousazadeh, J., Keyhani, A., Javadi, A., Mobli, H., Abrinia, K., Sharifi, A., A review of principle and sun-tracking methods for maximizing solar systems output, Renew. Sustain, Energy Rev, 13(2009), pp. 1800–1818.

[23] Kwangbok, J., Taehoon, H., Choongwan, K., A Prototype Design and Development of the Smart Photovoltaic System Blind Considering the Photovoltaic Panel, Tracking System, and Monitoring System, Applied Sciences, 7(10), (2017), pp. 1077.

[24] Salas, V., Olías, E.A., Barrado, A., Lázaro, A., Review of the maximum power point tracking algorithms for stand-alone photovoltaic systems, Sol. Energy Mater, Sol. Cells, 90(2006), pp. 1555–1578.

[25] Ma, J., Man, K.L., Ting, T.O., Zhang, N., Lei, C.U., Wong, N., A hybrid MPPT method for photovoltaic system via estimation and revision method. In Proceedings of the 2013 IEEE International Symposium on Circuits and Systems, Beijing, China, (2013).

[26] EIA, Annual energy review 2011, (2011).

    <https://www.eia.gov/totalenergy/data/annual/pdf/aer.pdf>.

[27] S. El Gindi, A.R. Abdin, A. Hassan, Building integrated Photovoltaic Retrofitting in office buildings, Energy Procedia, 115 (2017), pp. 239-252.

[28] N. Lukač, S. Seme, K. Dežan, B. Žalik, G. Štumberger, Economic and environmental assessment of rooftops regarding suitability for photovoltaic systems installation based on remote sensing data, Energy, 107 (2016), pp. 854-865.

[29] S. El Gindi, A.R. Abdin, A. Hassan, Building integrated Photovoltaic Retrofitting in office buildings, Energy Procedia, 115 (2017), pp. 239-252.

[30] Abdallah, S., Nijmeh, S., Two axes sun tracking system with PLC control, Energy Conversion and Management, 45(2004), pp. 1931–1939.

[31] Luo Y., Zhang L., Wang X., Xie L., Liu Z., Wu J., A comparative study on thermal performance evaluation of a new double skin facade system integrated with photovoltaic blinds, Applied Energy, pp. 281–93.

[32] Jakica, N., Zanelli, A., Dynamic visualization of optical and energy yield co-simulation of new generation BIPV envelope in early design phase using custom ray tracing algorithm in python. In: Proceedings of the Advanced Building Skins (2014).

[33] W. Zhang, L. Lu, J. Peng, Evaluation of potential benefits of solar photovoltaic shadings in Hong Kong, Energy, 137 (2017), pp. 1152-1158.

Chapter III

A Developed Autonomous Facade System with Individually-Controllable PV Louvers

3.1 Design characteristics of the autonomous PV facade system

The buildings benefit from daylight owning to a good window system. Energy saving is the most serious challenge for buildings with large glass facades. One of the solutions is using a sun-shading system. In the today's world, PVSDs have been attracting more and more attention from designers and researchers. Some of them focus on dynamic PVSD systems, which offer better controls for the direct into the building as well as responses to occupant's visual needs compared to the fixed and manual ones.

To judge if there is direct sunlight or not, an automatically controlled PVSD system needs to be equipped with some sensors for monitoring sunshine. However, it still leaves researchers with the work on making a simpler and more reliable method of sun-tracking. Besides, previous studies on dynamic PVSDs are normally about the performance of venetian blinds or horizontal louvers. However, this simple and common arrangement that with all slats arranged vertically in line, fails to consider shading-effect in spring and summer, when the sun profile angle is high, most PV panels will be in the shadow because of the shade casted by the panel above it. This shading-effect on solar cells reduces considerably the efficiency of their electrical power generation.

This research develops an autonomous facade system with photovoltaic integrated louvers (PV-louver system) that can be controlled individually as an integrated solution for daylight control and solar power supply (Fig. 3-1). This new system proposes a new element from hereafter called PV-louver, which has functions of not only sun shading and power supply, commonly seen in conventional autonomous facade systems, but also integrating the additional function of daylight monitoring essential for efficiency.
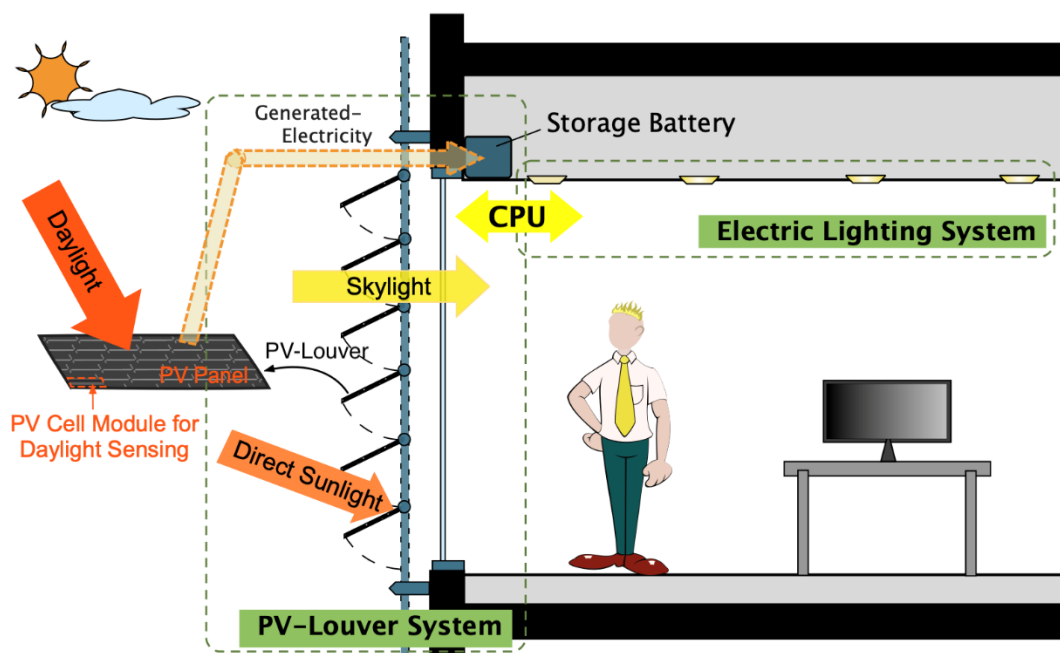

Fig. 3-1. Major parts of the proposed autonomous PV facade system

Fig. 3-1 shows the major parts of the proposed autonomous PV facade system, including a PV-louver system and an electric lighting system. The electricity generated from PV-louvers could supply for the automatic operation of this facade system and additionally support for an electric lighting system. PV sensors, PV modules located at the corner of the outer edge of PV-louvers, can monitor daylight illuminance by using the output of electricity. The real-time output would be sent to the central processing unit (CPU) so that the CPU can judge whether there is direct sunlight or not according to the pre-set thresholds. If it judges there is direct sunlight, it commands the PV-louvers to rotate to a specific angle to protect the interiors from direct sunlight. Meanwhile an electric lighting system is compensating insufficient daylight in the room.

To propose a suitable type of PV cell as the sensor to distinguish sky conditions by analyzing its output, two-stage experiments were conducted to evaluate properties of PV cell modules and devise a way to utilize them for the proposed PV-louver system.
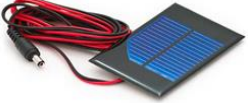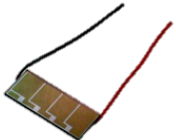
3.2   Correlation between the electricity from PV cells and daylight illuminance

3.2.1 Overview of the experiments

The experiments were conducted between March 2014 and April 2017 in the following two stages: (1) The first stage was devoted to testing which kinds of PV cell modules are appropriate for measuring solar radiation, and (2) the second stage was carried out to investigate the relationship between the electricity from the PV cell modules and daylight illuminance. Consequently, how to utilize the PV cell modules was determined.

Six types of PV cell modules were selected for the experiments. Table 1 shows their images and dimensions. There were monocrystalline silicon type (No. 1, 2, 3) made of single crystal silicon (c-Si), and amorphous silicon type (No. 4, 5, 6) made of amorphous crystal silicon (a-Si).

Table 3-1. PV cell modules used in the experiments

Type	Image	Dimensions (mm)
Monocrystalline silicon (c-Si)		
No. 1 Single crystal silicon solar cell		L: 180 W: 96 T: 3
No. 2 Single crystal silicon solar cell		L: 90 W: 50 T: 3
No. 3 Single crystal silicon cell		L: 94 W: 61 T: 2
Amorphous silicon (a-Si)		
No. 4 Spherical silicon solar cell		L: 159 W: 59 T: 1.2
No. 5 Flexible solar cell		L: 114 W: 25 T: 0.2
No. 6 Amorphous silicon solar cell		L: 25 W: 10 T: 1.3

L: length, W: Width, T: Thickness

The experiments were conducted on the roof of a building in Fukuoka, Japan ($130°$ E, $33°$ N). The voltage generated from each PV cell module on a horizontal plane was measured and recorded by a data logger, Midi LOGGER TYPE GL820. Irradiance on a horizontal plane was measured by ML-01 EKO pyranometer (Accuracy: ±10 W/m^2). Illuminance was measured by CL-200A chroma meter (Accuracy: $\pm2\%$ ±1 digit of displayed value). Measurements were taken at one-minute intervals. The PV cell modules was measured under various sky conditions with solar radiation measurements.

Fig. 3-2 shows the output of each PV cell module and global irradiance over time on 8 April 2014. The PV cell as a light sensor should have a fast response to the changing solar radiation. The experiment results showed that the No. 1 and No. 3 of the c-Si type and No. 5 and No. 6 of the a-Si type presented a relatively good response to the changing solar radiation.

Fig. 3-3 (a)-(b) shows the relationship between the global irradiance and output of PV cell No. 3 and No. 5. The output of the PV cell module is available for calculating the solar irradiance, determines whether it can be deployed as a daylight sensor to detect the presence of direct sunlight. However, the result shows the output rapidly increased with global irradiance in the range from 0 W/m^2 to 1100 W/m^2. It almost saturated at around 300 W/m^2. As the output showed no clear linear correlation with irradiance, it indicated that the PV cell modules could not be used for daylight sensing as they were. Therefore, this research work devised a way to utilize the PV cell module for distinguishing sky conditions.
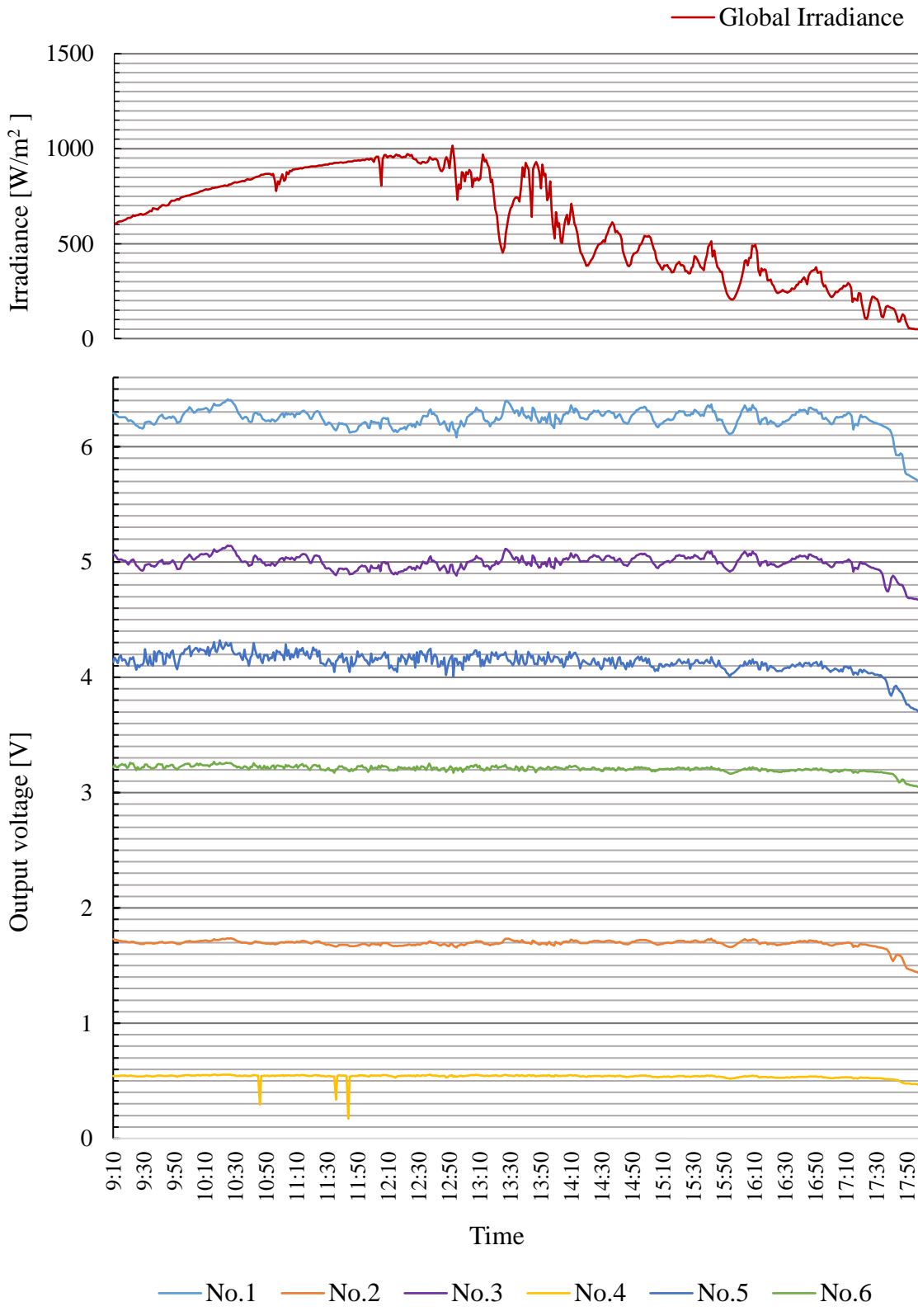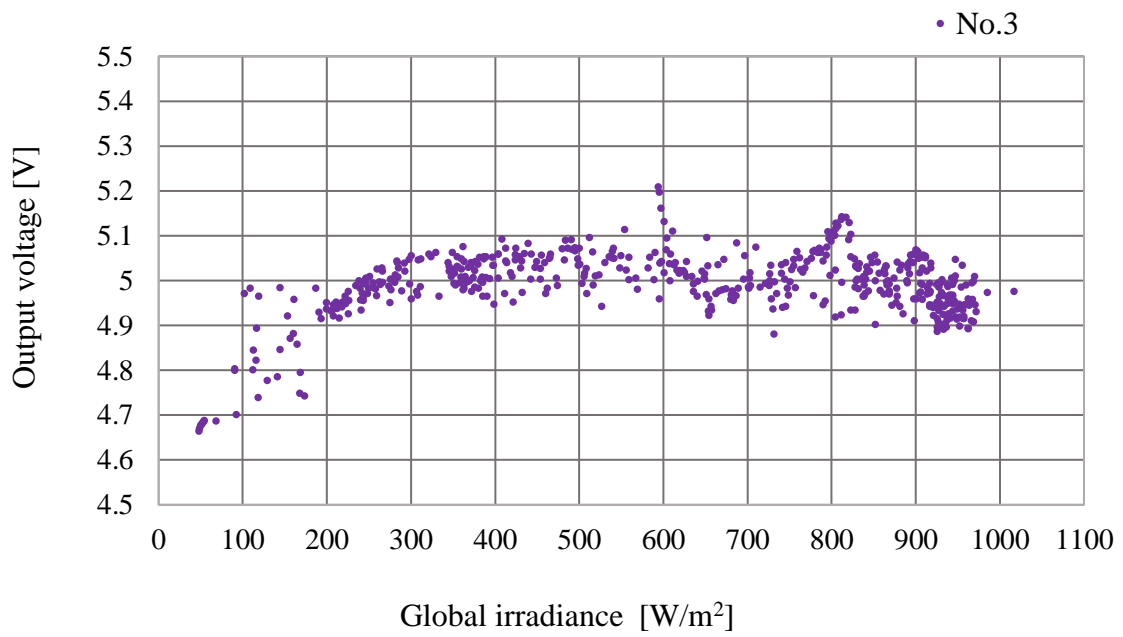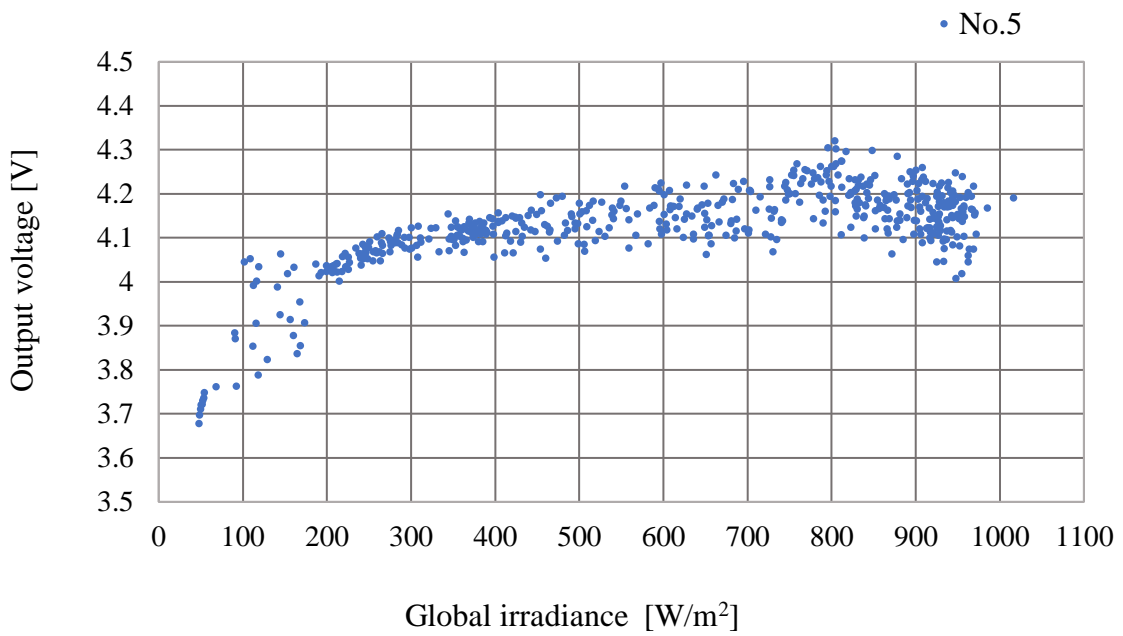
Fig. 3-2. Diurnal fluctuation of the PV cell outputs and global irradiance (8 April 2014)

(a) The PV cell of monocrystalline silicon type

(b) The PV cell of amorphous silicon type

Fig. 3-3 (a)-(b). Outputs of two type PV cells and global irradiance (8 April, 2014)

3.2.2 Utilization of the PV cell for daylight sensing

Due to their material properties, PV cell modules have different spectral responses. For example, the c-Si type has the spectral response extending up to the wavelength of 1100 nm with its peak at about 1000 nm. The a-Si type has that ranging from about 400 nm to 800 nm and similar to the photopic spectral luminous efficiency. In this research, the proposed thresholds of daylight illuminance for determining the presence of direct sunlight ranged between 0 lx and 30000 lx [1] (The specific content about thresholds for sunlight judgement is in chapter 4). Therefore, A UV and IR cutting filter was applied to cover the c-Si type PV cell module to obtain the spectral response to the wavelengths of the visible range. The natural density filters were applied to cover the a-Si and c-Si PV cell modules to reduce the incident radiation.

The output of the a-Si flexible solar cell (No. 5) with 0.001% ND and UV and IR cutting filters showed a fairly good relation to the daylight illuminance. The output of the filtered a-Si PV cell presented an approximate logarithmic increase along with the illuminance. The Fig. 3-4 shows the diurnal fluctuation of the PV cell output and daylight illuminance over time on 1 April 2017. Fig. 3-5 shows the relationship between the daylight illuminance and output of the filtered PV cell modules No. 5.

Above all, the thin-film PV cells were selected to form the PV-louver that can monitor sunshine, owing to its lightweight, higher cost-effective and lower shading effect which were introduced in Chapter 2.
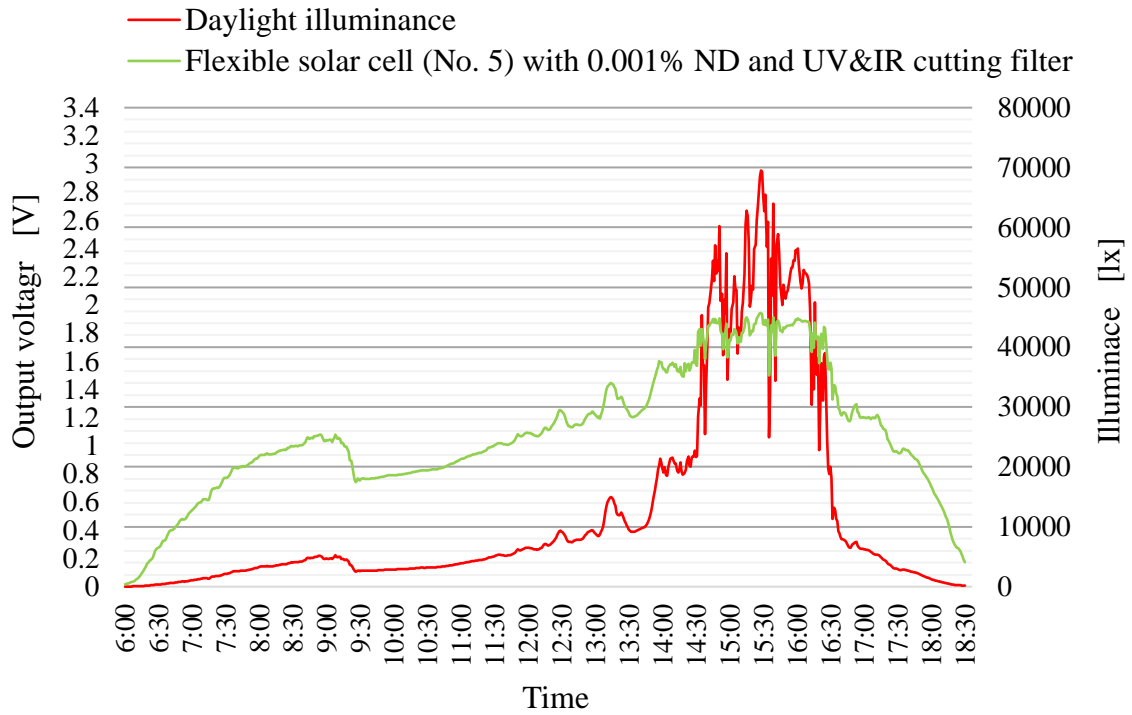
Fig. 3-4. Diurnal fluctuation of daylight illuminance and PV cell output (1 April 2017)
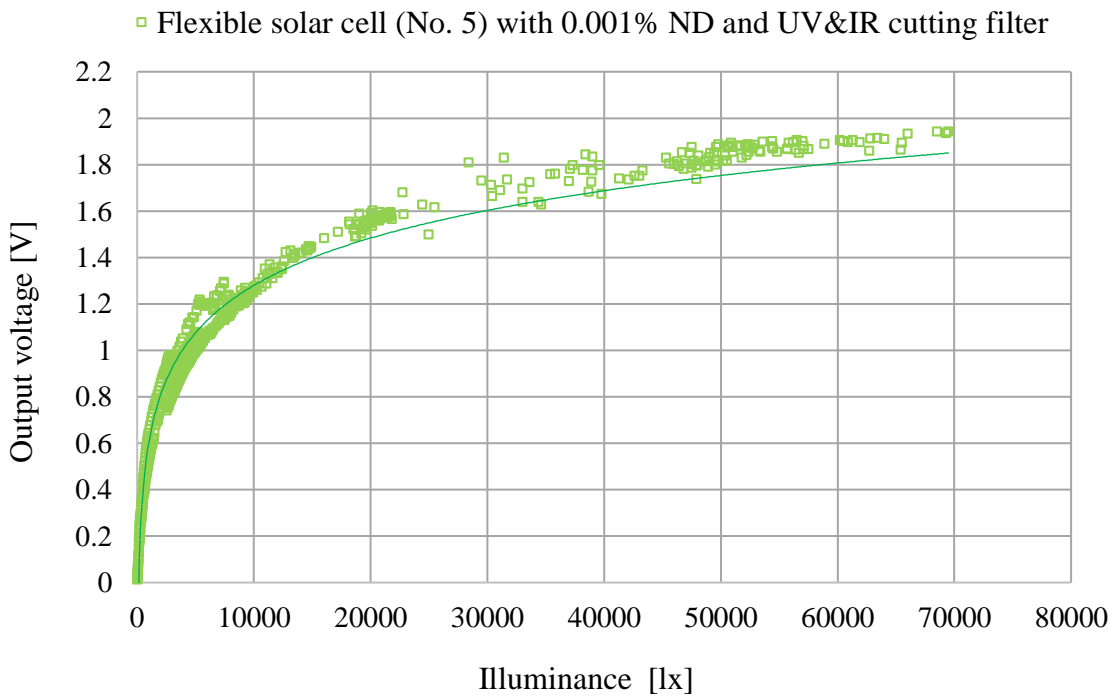
Fig. 3-5. Output of filtered PV cell and daylight illuminance (1 April 2017)

3.3 Improved PV-louver control strategy and PV-louvers configuration

3.3.1 Electric energy generated by PV modules on a tilt plane

There is a common misconception, that sun-tracking method of BIPV is to orientate the PV surface perpendicular to the sunlight. This misconception might come from the sun-tracking method commonly used in conventional PV power stations, where sun trackers (or solar trackers) are used to orienting flat PV panels towards the sun in order to increase the energy collection [2]. Theoretical explanation of the perpendicular sun-tracking method bases on a basic model of global irradiance on a tilt plane [3], that is,

$$G_{t,global} = I_{DN} \cos\gamma \ + G_{h,d} \ R_d + G_{t,ground} \qquad \text{Eq. (3-1)}$$

Where $G_{t,global}$ is the global irradiance on a tilt plane [W/m^2]

I_{DN} is the normal direct irradiance [W/m^2]

γ is the angle between the PV surface normal and the incident direction of the sunlight [deg]

$G_{h,d}$ is the diffuse horizontal irradiance [W/m^2]

R_d is the diffuse transposition factor

$G_{t,ground}$ is the ground-reflected irradiance on a tilt plane [W/m^2]

On a cloudless day, the product $I_{DN} \cos\gamma$ represents the direct irradiance on the tilt plane ($G_{t,bean}$), which is a dominant component contributing more than 90% of the global irradiance [4]. The other two components, diffuse irradiance ($G_{t,diffuse} = G_{h,d} \ R_d$) and ground-reflected irradiance ($G_{t,ground}$), contribute a small proportion to the clear sky condition, and vary with the orientation of the PV elements plane.

If the variations of those two components caused by the orientation are ignored and such components are taken as orientation-independent constants because of their small contribution, it can be concluded that the maximum $G_{t,global}$ is achieved when γ equals to zero, that is to say the PV surface is perpendicular to the incident sunlight.

According to the Eq. (3-2), because the direct-beam-illuminated PV area (S_b) remains as a constant, the maximum $G_{t,global}$ leads to the maximum incident energy per unit time, namely the maximum input power (P_{in}).

$$P_{in} = G_{t,global}S_b \qquad\qquad \text{Eq.} (3-2)$$

Where $\quad P_{in} \quad$ is the input power [W]

$\qquad\qquad S_b \quad$ is the direct-beam-illuminated PV area [m^2]

However, the perpendicular sun-tracking method is not necessarily applicable to PVSDs due to complicated building environment and multiple purposes of slat controls. Compared with conventional single layer PV products, PVSDs make a profound difference because S_b shrinks when shadows appear on the PV surface caused by adjacent elements. In this case, a maximum $G_{t,global}$ with a reduced S_b cannot guarantee a maximum P_{in} any more. Furthermore, the shadows on the PV surface not only lead to a decreased S_b, but also result in PV partial shading problems, which affect the PV performance, especially the module efficiency (η_m). The η_m drops dramatically when uneven shadows are found on series-connected solar cells. PV module performs the best when no shadow casts upon it.

According to the Eq. (3-3), in order to get the maximum P_{out} at a given time, a straightforward way is to keep the PV surface towards the optimal orientation, where it receives the maximum P_{in}; and no shadow appears on it, resulting in the maximum η_m.

$$P_{out} = P_{in}\eta_m \qquad \text{Eq.} (3-3)$$

Where P_{out} is the output power [W]
η_m is the module efficiency

Therefore, one of the purposes of sun tracking is to preserve the maximum P_{out} at every tracking moment, so that the PV module generates the maximum energy E, which is the integral of P_{out} over a certain period of time t, as show in Eq. (3-4).

$$E = \int P_{out}(t)\, dt \qquad \text{Eq.} (3-4)$$

As to PVSDs, sun-tracking strategy is not only aiming at the maximum electric energy, but also the capability to fulfill building functions.

3.3.2 Daylight-responsive control strategy

The objectives of the PV-louver control method for the proposed facade system are to receive the maximum possible P_{in} to avoid shadows on the PV surface, as well as enable daylighting utilization without glare from direct sunlight, which causes visual disability or discomfort for indoor occupants.

The amount of direct sunlight incident on the window varies with the sun profile angle, which formed by the incident direction of direct sunlight and the normal direction of the window surface, as shown in Fig. 3-6. The sun profile angle can be calculated from Eq. (3-5).
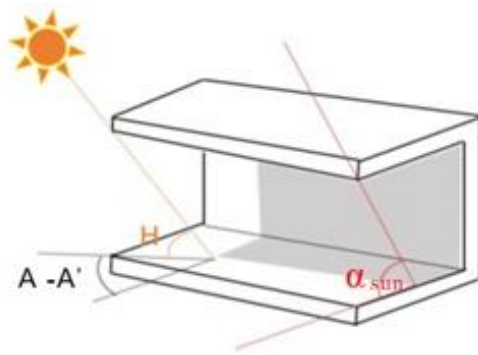
Fig. 3-6. Illustration of the sun profile angle.

$$\alpha_{sun} = \tan^{-1} \times \frac{\tan H}{\cos(A - A')} \qquad \text{Eq.}(3-5)$$

Where α_{sun} is the sun profile angle [deg]

         H is the solar altitude [deg]

         A is the azimuth angle of sun [deg]

         A' is the azimuth angle of window [deg]

This research used the longitude and latitude of the IDMP station in Lyon to calculate sun profile angles by each minute over the day and then estimated the louver control angle of the PV-louver system. For a south-facing window, the altitude of the sun (Alts), the azimuth of the sun (Azis) and corresponding sun profile angle, which is calculated for each season (spring, summer, fall and winter) are presented in Table 3-2.

Table 3-2. Sun profile angle for a south-facing window using the geographical factors of the IDMP station in Lyon (spring, summer, fall and winter).

Date	Time [h]	Alts [deg]	Azis [deg]	Sun Profile Angle [deg]
2015/3/4	9	17	118	32.1
	10	25	132	35.4
	11	32	147	36.9
	12	37	164	37.6
	13	38	183	37.8
	14	36	201	37.6
	15	31	218	36.7
	16	23	232	35.0
	17	14	245	30.9
	18	5	256	18.6
2015/6/18	9	41	97	81.5
	10	51	111	73.8
	11	60	129	69.8
	12	66	156	68.0
	13	67	191	67.7
	14	63	222	68.9
	15	54	243	72.0
	16	44	258	78.0
	17	34	270	89.6
	18	(The sun is in the west side of the building)		
2016/9/21	9	25	118	45.0
	10	34	132	44.9
	11	40	149	44.8
	12	44	168	44.7
	13	44	189	44.7
	14	41	209	44.7
	15	34	226	44.8
	16	26	241	44.8
	17	16	253	45.2
	18	6	264	47.6
2016/12/11	9	6	132	8.9
	10	13	144	15.8
	11	18	157	19.4
	12	21	172	21.0
	13	21	187	21.1
	14	19	201	19.7
	15	14	214	16.3
	16	7	227	10.0
	17	(sunset)		
	18	(sunset)		

When the sun comes out, the required tilt angle (θ) in our study should reach the cut-off angle (θ$_{cut-off}$) which is defined as the blind/louver tilt angle beyond where just no direct radiation is being transmitted through the slats. It is a typical automatic blind control used in several previous studies [5]. Fig. 3-7 shows the slats in cut-off position.

Factors that affect the cut-off angle include the sun profile angle, slat width (W) and spacing distance (S) between slats. The cut-off angle can be calculated easily using the sun profile angle if the slat width and slat spacing distance are equal, is calculated from Eq. (3-6). If the slat width and slat spacing distance are unequal, the cut-off angle is calculated from Eq. (3-7).
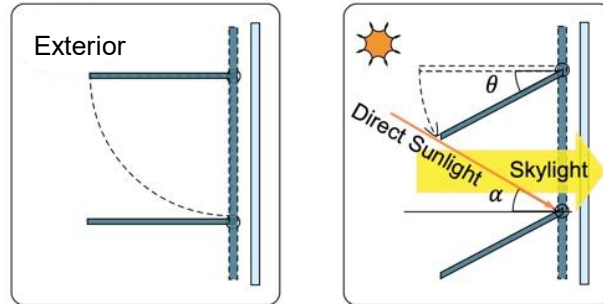

Fig. 3-7. Slats in the cut-off position when there is direct sunlight

$$\theta_{cut-off} = 90° - 2\alpha_{sun} \qquad \text{Eq.} (3-6)$$

$$\theta_{cut-off} = \tan^{-1}\left\{\frac{S}{W}\frac{\cos\alpha_{sun}}{\sqrt{1 - \left(\frac{S\cos\alpha_{sun}}{W}\right)^2}}\right\} - \alpha_{sun} \qquad \text{Eq.} (3-7)$$

As illustrated in Fig. 3-7, the slats are rotated to an angle θ as the direct sunlight enter the room at a sun profile angle α. The range of θ is from −90° to 90°, where a negative θ means slats being rotated toward the ground, a positive value toward the sky and zero for horizontal slats. Note that a slat control method with negative angles, the (directly) reflected rays might be directed towards occupants, causing significant glare from daylight [6]. Considering that PV panels often have a specular top panel surface, this research limits tilt angle of PV-louvers in the range of 0° to 90°. That is, for example, when the louver width and spacing distance are 100 mm, the louvers are supposed to be kept horizontally ($\theta = 0°$) when sun profile angles are above 45˚. When the ratio of louver width and spacing are 1.2, the louvers are supposed to be kept horizontally when sun profile angles are above 39.8˚.

Daylight-responsive strategy is proposed for better daylight use on the base of cut-off angle control method and sunshine monitoring for partly cloudy and overcast sky conditions. To be exact, if direct sunlight would fall into the room, the PV-louvers are automatically rotated to the cut-off position to block sunshine. Unless direct sunlight is available, it then attempts to save lighting energy with incoming daylight by automatically opening the louvers (Fig. 3-8). In addition, keeping horizontal angle contributes to the PV-louvers in receiving the maximum possible diffuse irradiance for energy generation.
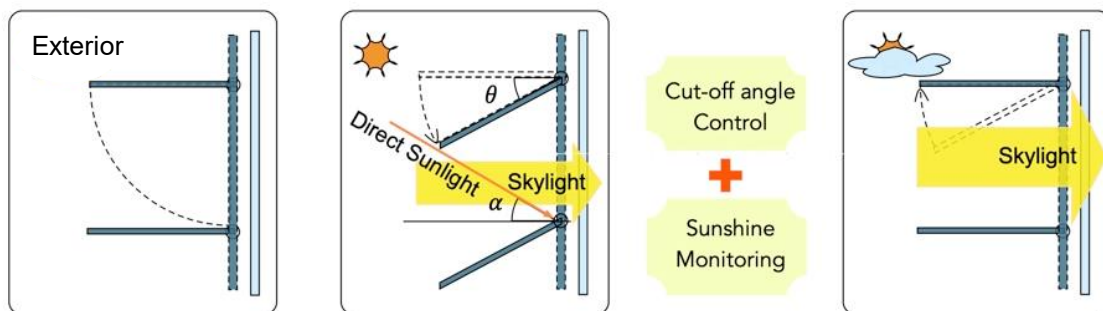
Fig. 3-8. Daylight-responsive controls for partly cloudy and overcas sky conditions.

In other to compare the difference between the cut-off angle and daylight-responsive angle controls, two louver types (W/S=1 and W/S=1.2) are examined. The measured normal direct solar irradiances (I_{DN}) of four partly cloudy days in each season were taken to judge sunlight presences. It is defined that there is sunshine when the normal direct solar irradiance is 120 W/m^2 or more. Table 3-3 presents examples of the louver angles by both control methods for each season in Lyon. It is noticeable, when the sun profile angle was high, PV-louvers were just remained horizontal weather there was direct sunlught or not. It means a loss of the PV-louver efficiency of electrical power generation caused by the shade casted by the panel above it.

Table 3-3. Example of the louver angle according to the cut-off angle and daylight-responsive control method for each season (for a south-facing window)

Date	Time [h]	Sun Profile Angle [deg]	I_{DN} [W/m²]	Is There Direct Sunlight	Louver Control Angle [deg] W/S=1		W/S=1.2	
					Cut-off	Responsive	Cut-off	Responsive
2015 3/4	9	32.1	0	No	25.8	0.0	12.8	0.0
	10	35.4	2	No	19.2	0.0	7.4	0.0
	11	36.9	0	No	16.2	0.0	4.9	0.0
	12	37.6	293	Yes	14.8	14.8	3.7	3.7
	13	37.8	0	No	14.3	0.0	3.3	0.0
	14	37.6	874	Yes	14.9	14.9	3.8	3.8
	15	36.7	0	No	16.7	0.0	5.3	0.0
	16	35.0	0	No	20.1	0.0	8.1	0.0
	17	30.9	603	Yes	28.2	28.2	14.7	14.7
	18	18.6	0	No	52.7	0.0	33.5	0.0
2015 6/18	9	81.5	802	Yes	0.0	0.0	0.0	0.0
	10	73.8	863	Yes	0.0	0.0	0.0	0.0
	11	69.8	0	No	0.0	0.0	0.0	0.0
	12	68.0	1	No	0.0	0.0	0.0	0.0
	13	67.7	1	No	0.0	0.0	0.0	0.0
	14	68.9	1	No	0.0	0.0	0.0	0.0
	15	72.0	2	No	0.0	0.0	0.0	0.0
	16	78.0	0	No	0.0	0.0	0.0	0.0
	17	89.6	0	No	0.0	0.0	0.0	0.0
2016 9/21	9	45.0	5	No	0.0	0.0	0.0	0.0
	10	44.9	2	No	0.3	0.0	0.0	0.0
	11	44.8	70	No	0.5	0.0	0.0	0.0
	12	44.7	3	No	0.6	0.0	0.0	0.0
	13	44.7	682	Yes	0.6	0.6	0.0	0.0
	14	44.7	153	Yes	0.6	0.6	0.0	0.0
	15	44.8	646	Yes	0.4	0.4	0.0	0.0
	16	44.8	620	Yes	0.4	0.4	0.0	0.0
	17	45.2	545	Yes	0.0	0.0	0.0	0.0
	18	47.6	194	Yes	0.0	0.0	0.0	0.0
2016 12/11	9	8.9	19	No	72.1	0.0	46.5	0.0
	10	15.8	273	Yes	58.4	58.4	37.5	37.5
	11	19.4	612	Yes	51.2	51.2	32.4	32.4
	12	21.0	0	No	48.0	0.0	30.1	0.0
	13	21.1	0	No	47.8	0.0	29.9	0.0
	14	19.7	599	Yes	50.6	50.6	32.0	32.0
	15	16.3	523	Yes	57.4	57.4	36.8	36.8
	16	10.0	0	No	70.1	0.0	45.2	0.0

3.3.3 Improved PV-louvers configurations for high sun profile angle condition

The issues emphasized in the upper section, loss of energy generation caused by the partial shading effects of PV cells in summer and spring when sun profile angles are high, needs to be solved. According to Eq. (3-1) and Eq. (3-2), the global irradiance on a tilt plane can be increased by i) narrowing the angle (γ) between the PV surface normal and the incident direction of the sunlight; and ii) increasing the direct-beam-illuminated PV area (S_b). As the occupied area for a facade system is fixed, here considered two way to improve the electric energy generation by only changing configuration of the PV-louvers. Fig.3-9 shows the PV-louvers configurations investigated:

- Type-A, horizontal PV-louvers are arranged vertically in a line and the louver width and louver spacing distance are equal;

- Type-B, horizontal PV-louvers are also arranged vertically in a line but the ratio W/S is 1.2;

- Type-C, horizontal PV-louvers are arranged in a slant layout and the angle between the axes of PV louvers and vertical plane is 10°. The PV-louvers do not overlap each other when they are in closed position.
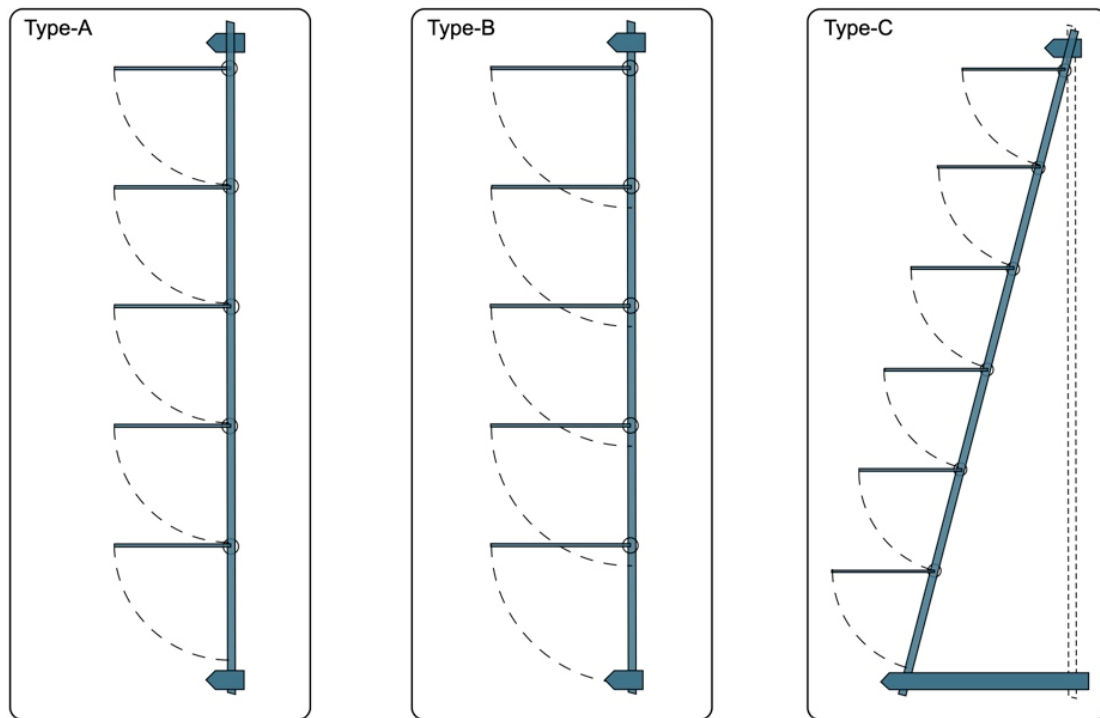
Fig. 3-9. Proposed PV-louvers configurations

Obviously, the PV cells area of Type B configuration is wider than that of Type A. The cut-off angle of Type-C is calculated from Eq. (3-8), where β represents the angle between the axes of PV-louvers and vertical plane. According to Eq. (3-6), the $\theta_{cut-off}$ of Type C is bigger than Type A, resulting in a smaller γ.

$$\theta_{cut-off} = 90° - 2\alpha_{sun} + \beta \qquad\qquad \text{Eq. } (3-8)$$

Where β is the angle between the axis of PV-louvers and vertical plane [deg]

3.4 Conclusion

The chapter introduces the design characteristics of the developed autonomous PV facade system with individually-controllable PV-louvers that can be used for daylight sensing, power supply and sun shading. The electric lighting system is designed to compensate insufficient daylight in the room. Considering exterior shading devices can intercept solar energy before it enter the room and avoid efficiency reduction of PV panels caused by window glazing, this research takes the type of exterior multi-horizontal louvers as a basic configuration for the autonomous PV facade system.

Experiments were conducted to investigate the relationship between the daylight illuminance and the output of different types of PV cells. According to the results, the type of thin-film PV cells were selected for the proposed PV-louvers and an approach to utilize them for daylight sensing was derived.

Besides, a daylight-responsive control strategy was proposed for partly cloudy and overcast sky conditions, which can make better use of daylight. Improved PV-louvers configurations were also proposed to solve the PV efficiency loss at high sun profile angle condition. The impacts and evaluations of the above proposals were further expounded in later chapters.

REFERENCES

[1] T. Koga, H. Li, Y. Koga, "A Method of Judging Sky Conditions by Vertical Global Illuminance", Summaries of Technical Papers of Architecture Institute of Japan Annual Meeting, D-1, 2016, pp. 499-500.

[2] H. Mousazadeh, A. Keyhani, A. Javadi, H. Mobli, K. Abrinia, A. Sharifi, A review of principle and sun-tracking methods for maximizing solar systems output, Renew Sustain Energy Rev, 13 (8) (2009), pp. 1800-1818.

[3] Gueymard CA. Direct and indirect uncertainties in the prediction of tilted irradiance for solar engineering applications. Solar Energy (3), pp. 432–44.

[4] A. Smets, K. Jäger, O. Isabella, R. van Swaaij, M. Zeman, Solar energy: the physics and engineering of photovoltaic conversion, technologies and systems, UIT Cambridge (2016).

[5] A. Tzempelikos, The impact of venetian blind geometry and tilt angle on view, direct light transmission and interior illuminance, Solar Energy, 82 (2008), pp. 1172-1191.

[6] Y.-C. Chan, A. Tzempelikos, Efficient venetian blind control strategies considering daylight utilization and glare protection, Sol. Energy, 98 (Part C) (2013), pp. 241-254.

[7] S. Hong, A.S Choi, M. Sung, Development and verification of a slat control method for a bi-directional PV blind, Appl. Energy, 206 (2017), pp. 1321-1333.

Chapter IV

Detection of Sunshine on Windows by Daylight Illuminance on the PV-Louvers

4.1   Vertical global illuminance thresholds for sunlight presence judgments drawn from measurements

4.1.1 Methodology of obtaining monthly thresholds of vertical global illuminance

As the problems mentioned before, compared with the direct solar illuminance/irradiance, using vertical global illuminance for judging sunshine can simplify the sensing approach. Moreover, determining illumination through each window by the sensors on it can achieve an individual control of sun shading.

In order to obtain thresholds of vertical global illuminance for the sun-shading control, this research analyzed two-year measurements collected from 1 January 2012 to 30 December 2013 at Ecole Nationale des Travaux de Publics de l'Etat (ENTPE) in France (4.9° E, 45.8° N). In this research work, the global illuminance on the south and west vertical planes were examined. Firstly, the normal direct irradiance is derived from the horizontal direct irradiance and the solar altitude recorded at ENTPE by Eq. (4-1).

$$I_{DN} = I_{DH} \times \frac{1}{\sin H} \qquad\qquad \text{Eq.} \, (4-1)$$

Where I_{DN} is the normal direct irradiance [W/m^2]

              I_{DH} is the horizontal direct irradiance [W/m^2]

              H is the solar altitude [deg]

World Meteorological Organization defines that there is direct sunlight when the normal direct irradiance is 120 W/m^2 or more. According to the measurements of normal direct solar irradiance, the monthly data of vertical global illuminance were classified into "direct sunlight" group and "no direct sunlight" group by month. Fig. 4-1 shows an example of the measured south vertical global illuminance in March (2012~2013). The orange points stand for the data with direct sunlight, and the blue points stand for the data without direct sunlight. Although there is an overlapping part, the boundary of the two groups can be seen as a linear relationship to the solar altitude.
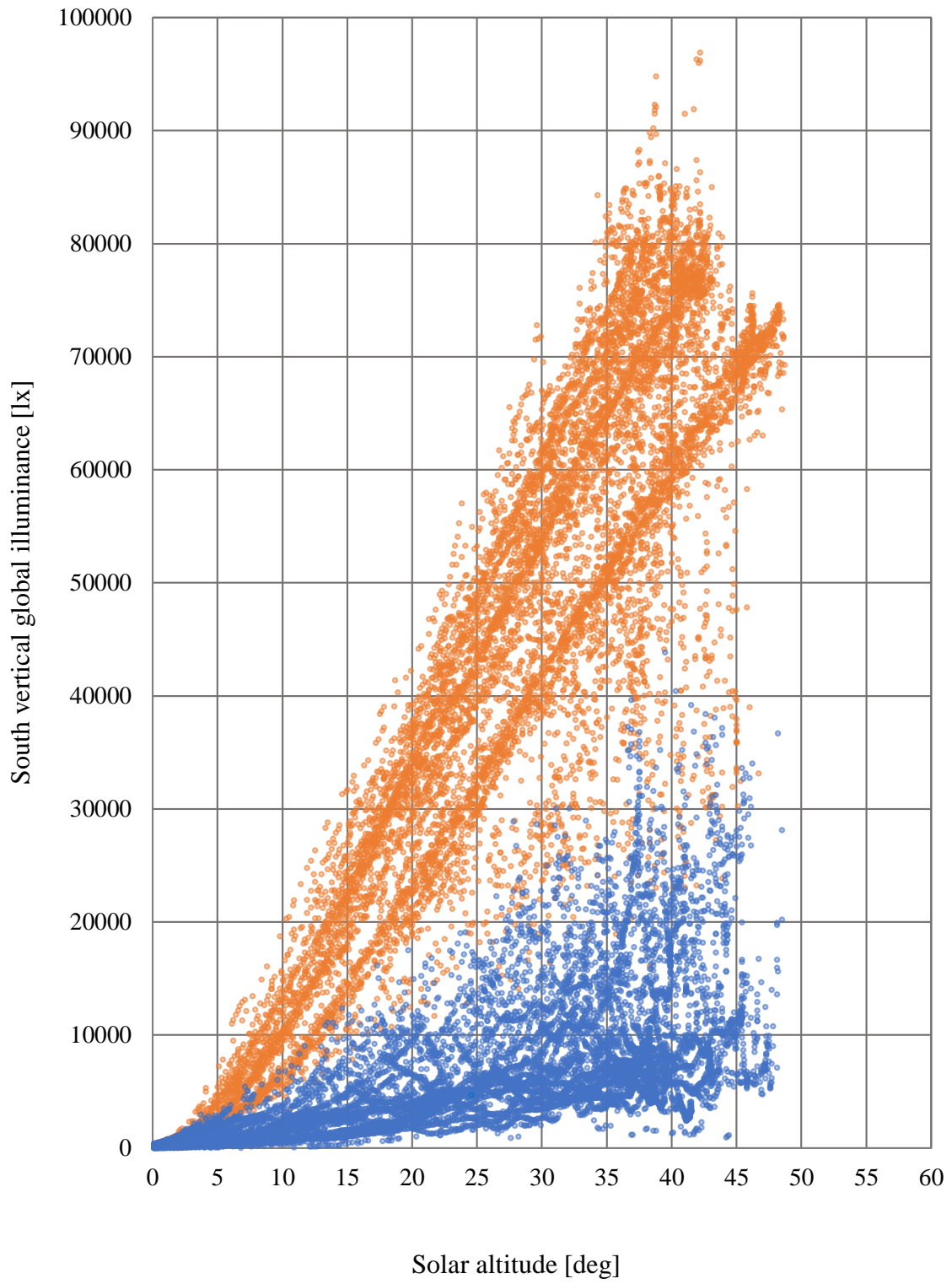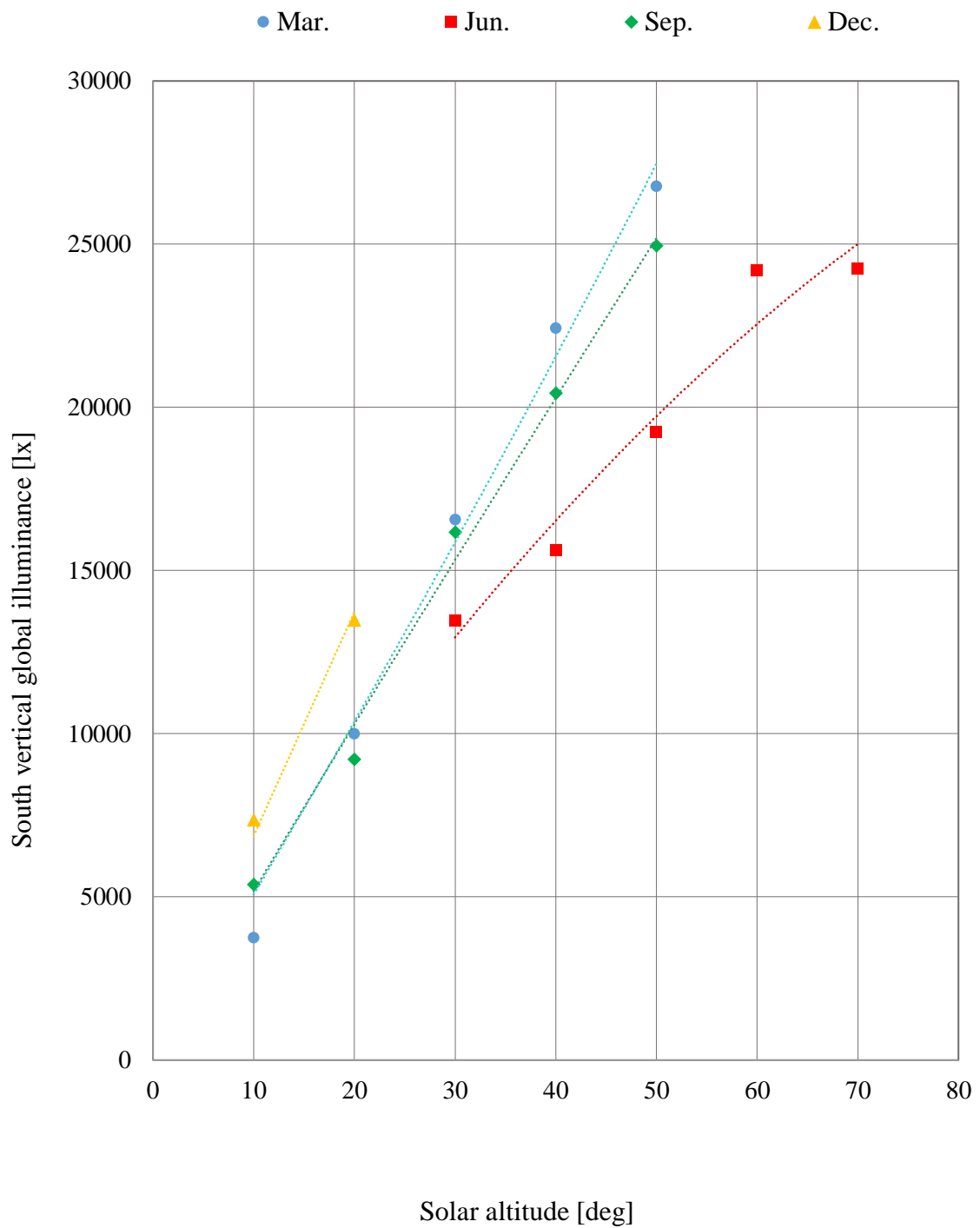
Fig. 4-1. The south vertical global illuminance and solar altitude (March 2012~2013)

Secondly, in each group, the monthly data were sorted by solar altitude in 10-degree intervals. Data above 5 degrees in solar altitude were selected for this study. For the "direct sunlight" group, global illuminance at a cumulative frequency of 90% from the highest value was found and taken as the lower limit value. For "no direct sunlight" group, global illuminance at a cumulative frequency of 90% from the lowest value was found and taken as the upper limit value. The thresholds of "direct sunlight" group and "no direct sunlight" group were derived from the lower and limit upper values.

Considering safety conditions of sun shading, this study uses the thresholds for no direct sunlight as the vertical global illuminance thresholds for the louver control because the illuminance values are lower than direct sunlight case. Table 4-1 shows the selected values of south and west vertical global illuminances in "no direct sunlight" groups. Fig. 5-2 shows the monthly thresholds of the south and west vertical global illuminance by solar altitude in 10-degree intervals of March, June, September and December.

Table 4-1. South and west thresholds for "no direct sunlight" condition

South thresholds for "no direct sunlight" condition						
	Solar altitude [deg]					
Month	5～15	15～25	25～35	35～45	45～55	55～65	65～75
	South vertical global illuminance [lx]						
1	5354	11890	16200	—	—	—	—
2	5452	13180	17210	20240	—	—	—
3	3742	9990	16560	22420	26770	—	—
4	4545	8550	13730	19400	27060	18330	—
5	—	8500	10970	16040	20810	25900	17500
6	—	—	13460	15620	19220	24190	24260
7	—	—	11150	15570	18190	20890	20420
8	5930	8390	11980	13520	17050	23450	—
9	5382	9210	16170	20430	24950	—	—
10	6254	12240	18860	24440	—	—	—
11	5441	13870	18710	—	—	—	—
12	7360	13490	—	—	—	—	—
West thresholds for "no direct sunlight" condition						
	Solar altitude [deg]						
Month	5～15	15～25	25～35	35～45	45～55	55～65	65～75
	West vertical global illuminance [lx]						
1	5252	9470	11810	—	—	—	—
2	6961	13800	13270	11840	—	—	—
3	7420	15410	17820	18290	21080	—	—
4	6884	14990	20310	23790	21960	15260	—
5	7670	14780	17680	24090	24890	23950	17260
6	9770	16040	22260	24080	23980	22950	20830
7	8300	15960	18720	26290	24000	21420	14530
8	9990	17940	19120	19770	17620	21920	—
9	9690	14150	19390	19200	19080	—	—
10	10380	15020	16860	17600	—	—	—
11	6695	12370	11690	—	—	—	—
12	7680	9320	—	—	—	—	—

(a) The south vertical global illuminance thresholds

Fig. 4-2 (a). The south vertical global illuminance thresholds of the measurements in Lyon
with solar altitude (Mar., Jun., Sep. and Dec.)
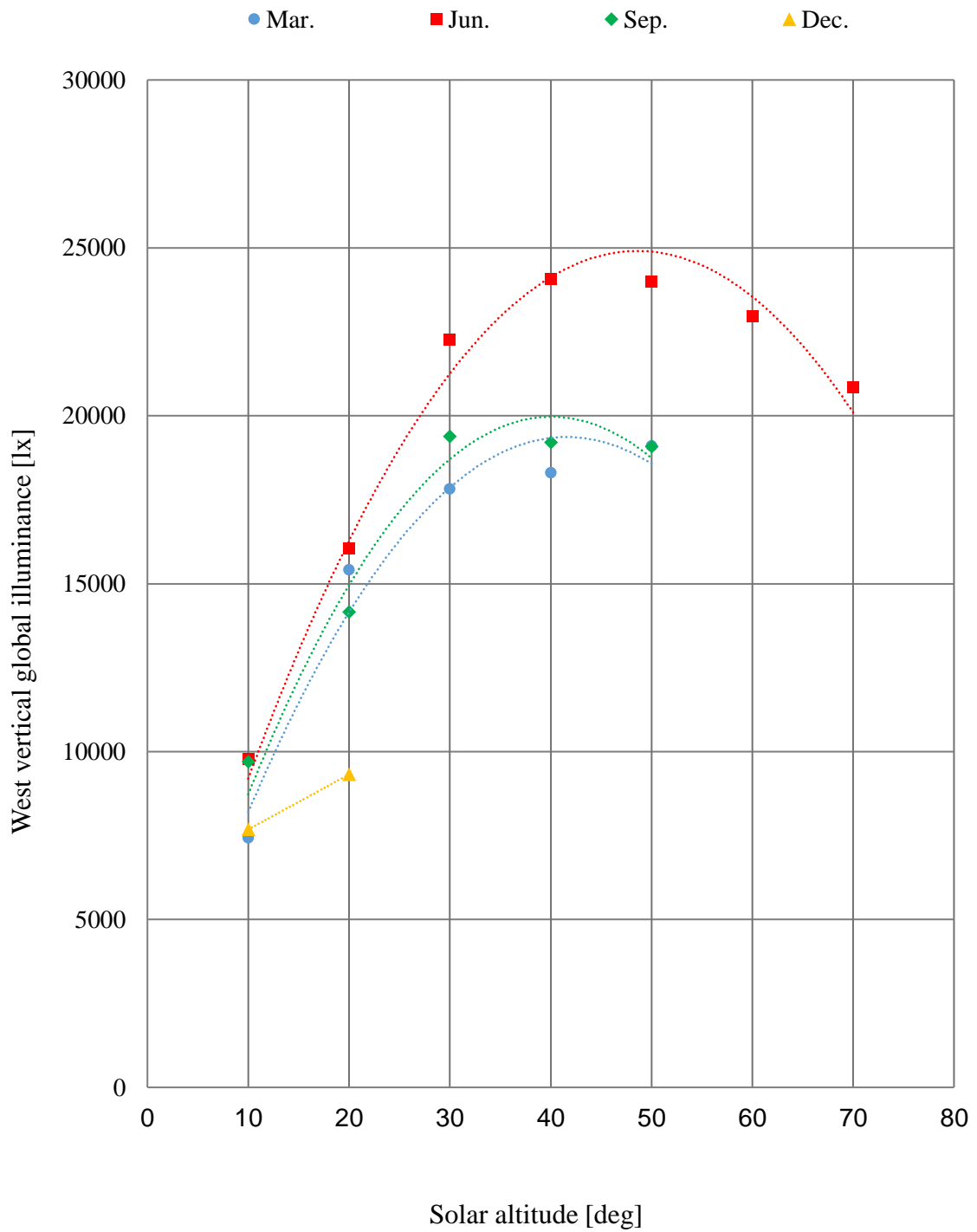
(b) The west vertical global illuminance thresholds

Fig. 4-2 (b). The west vertical global illuminance thresholds of the measurements in Lyon with solar altitude (Mar., Jun., Sep. and Dec.)

4.1.2 Diurnal variations of sun profile angle considering window directions

Apparent solar altitude to the window depends on window directions. The angle formed by the incident direction of direct sunlight and the normal direction of the window surface is called the sun profile angle. The amount of direct sunlight incident on the window varies with the sun profile angle. The schematic diagram and function are shown in Fig. 3-6 and Eq. (3-5) in Chapter 3.

In order to examine diurnal variations of sun profile angle, it checked the data of ten target days in 2012, at ENTPE in Lyon. They are days of the vernal equinox, summer solstice, autumnal equinox, winter solstice and other eight days in every mouth else. It shows that for the south facing window, the diurnal change of the profile angle was relatively small during 9 o'clock to 18 o'clock (Fig. 4-3 (a)). For the south-southwest facing window, the diurnal change became larger and was in the intermediate state between the south direction and the southwest direction cases (Fig. 4-3 (b)). For a southwest, west-southwest and west facing windows, the sun profile angle varied greatly with time (Fig. 4-3 (c) (d) (e)).
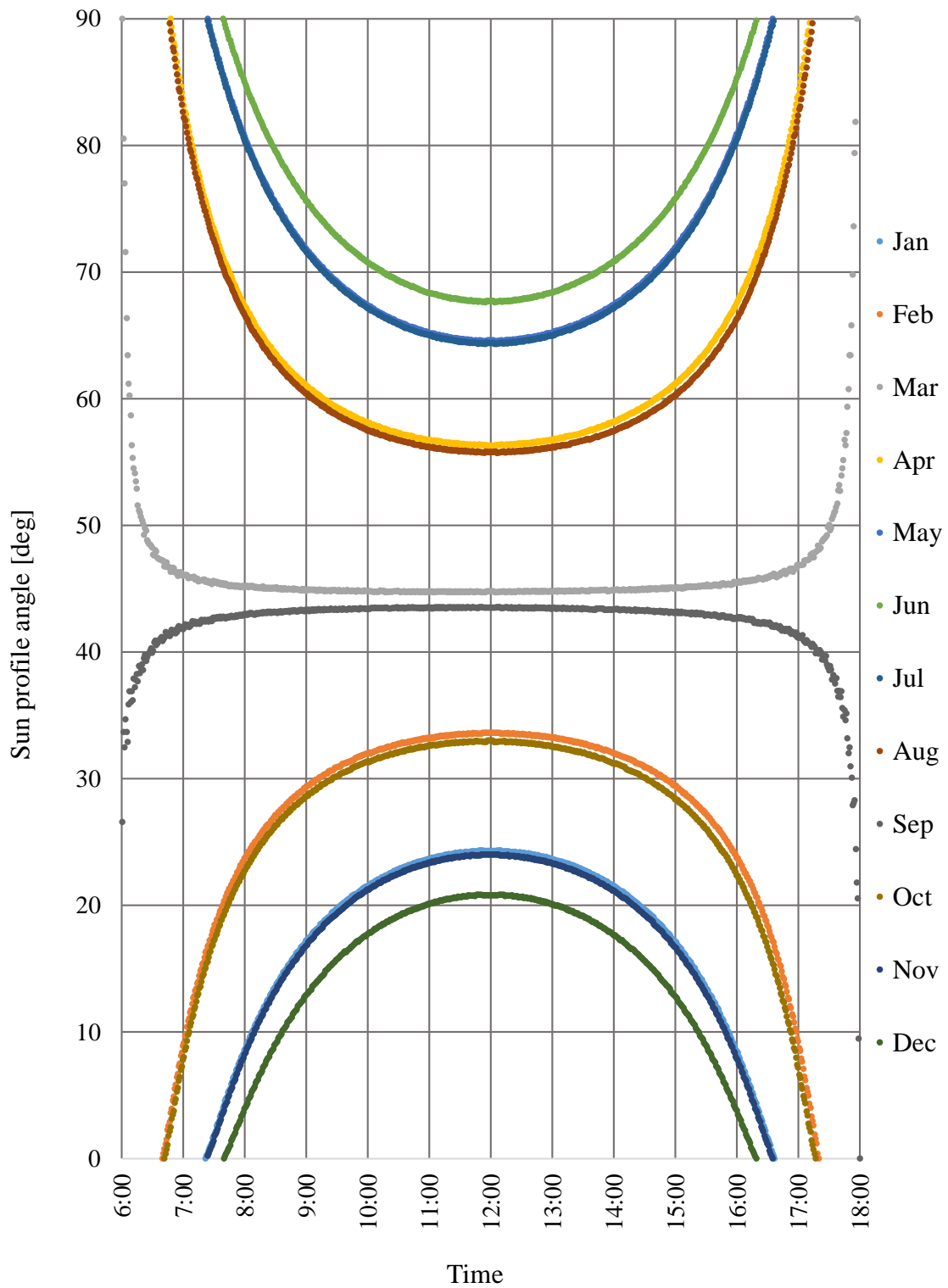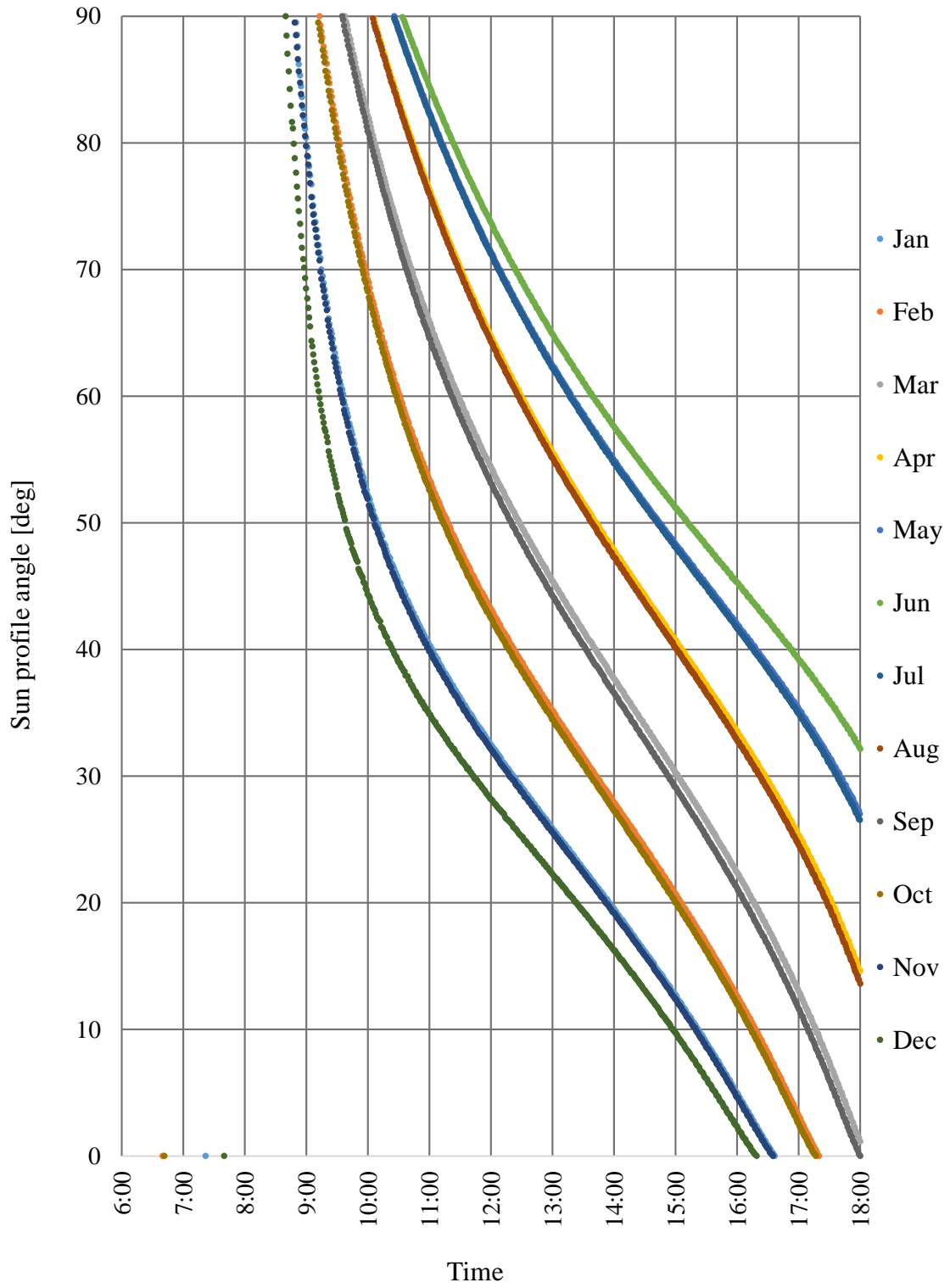
(a)   South direction

Fig. 4-3 (a). The diurnal variations of sun profile angle in Lyon throughout the year
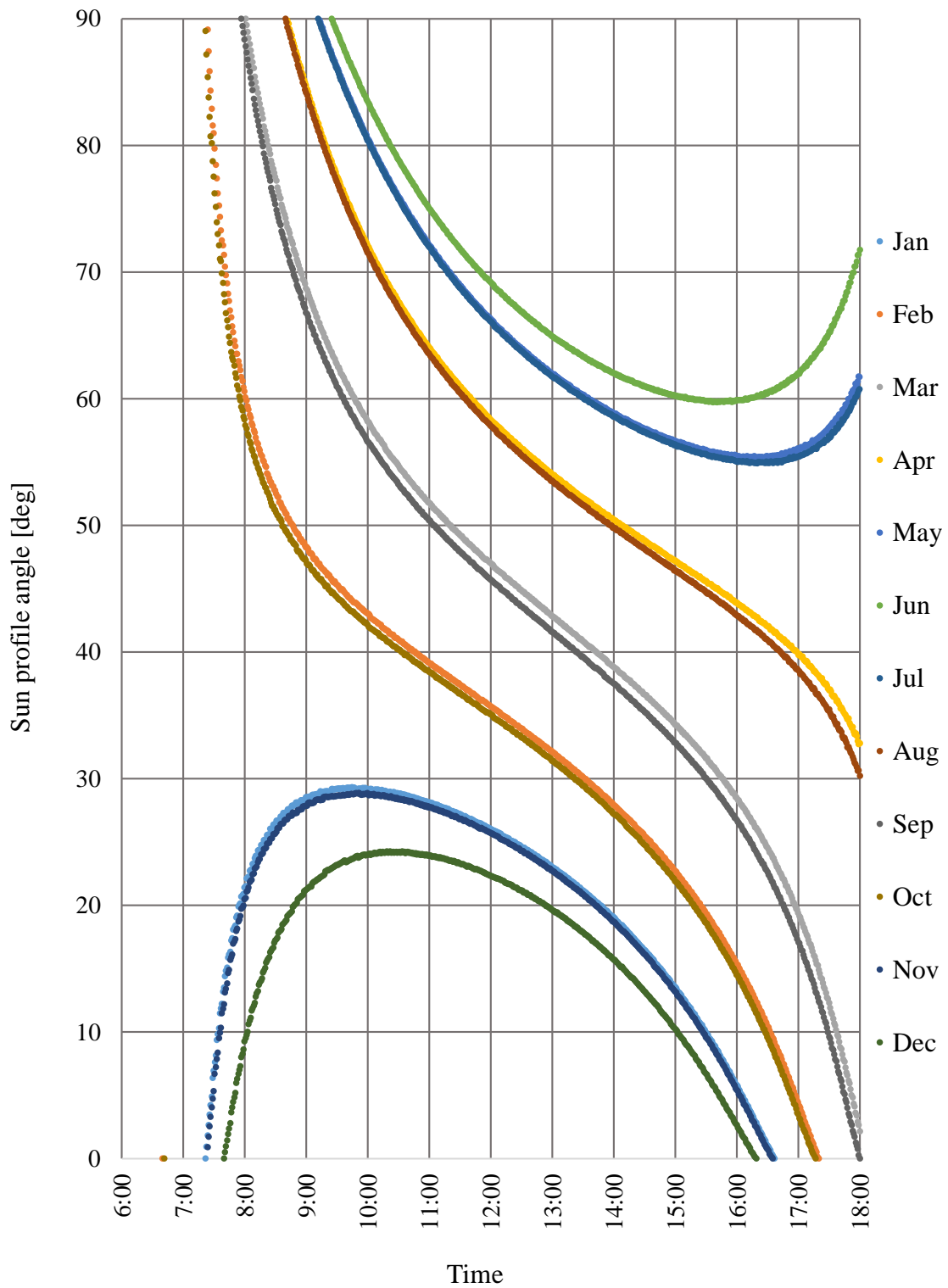
(b)   South-Southwest direction

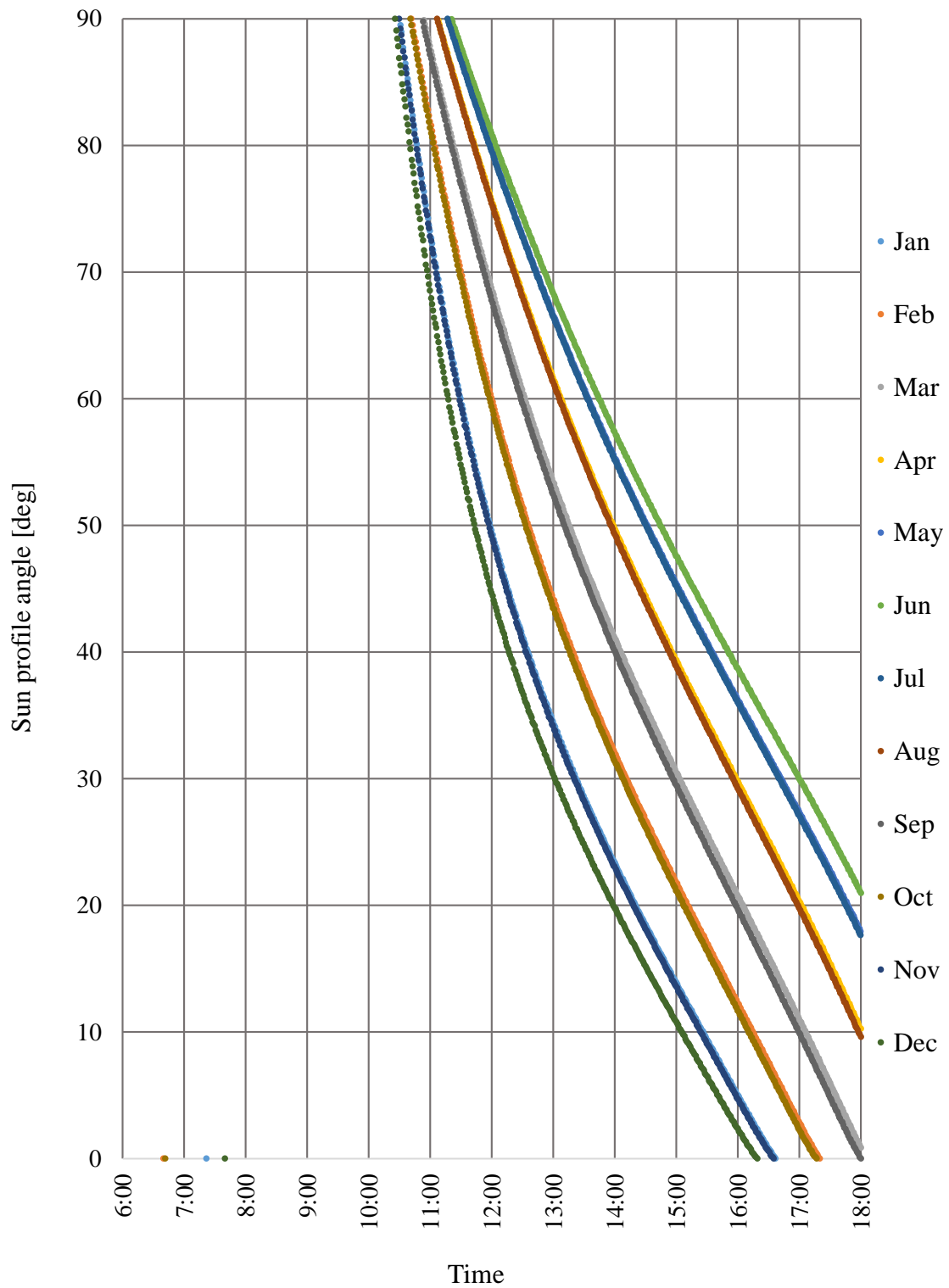Fig. 4-3 (b). The diurnal variations of sun profile angle in Lyon throughout the year
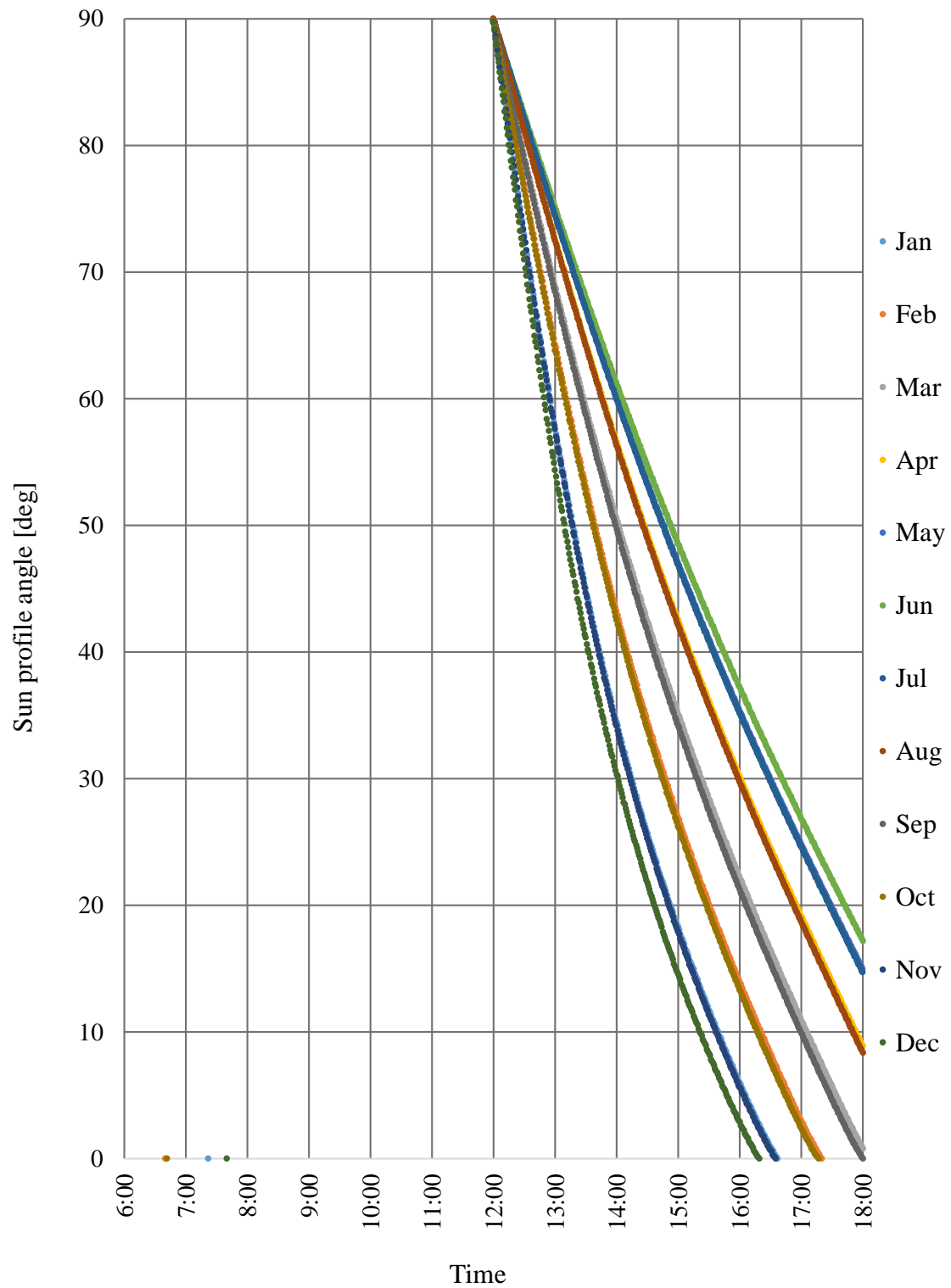
(c)   South-west direction

Fig. 4-3 (c). The diurnal variations of sun profile angle in Lyon throughout the year

(d) West-Southwest direction

Fig. 4-3 (d). The diurnal variations of sun profile angle in Lyon throughout the year

(e)   West direction

Fig. 4-3 (e). The diurnal variations of sun profile angle in Lyon throughout the year

Therefore, the sun profile angle is more suitable as a value than the solar altitude for the window facing the angle between the southwest and the west (or east to southeast). However, for the window facing between the southeast and southwest, it is considered that solar altitude is appropriate. Thus, with the same methodology, it obtained the west vertical global illuminance thresholds for direct sunlight presence judgments. Fig. 4-4 shows the monthly thresholds of the west vertical global illuminance, as a function of the sun profile angle, in March, June, September and December.
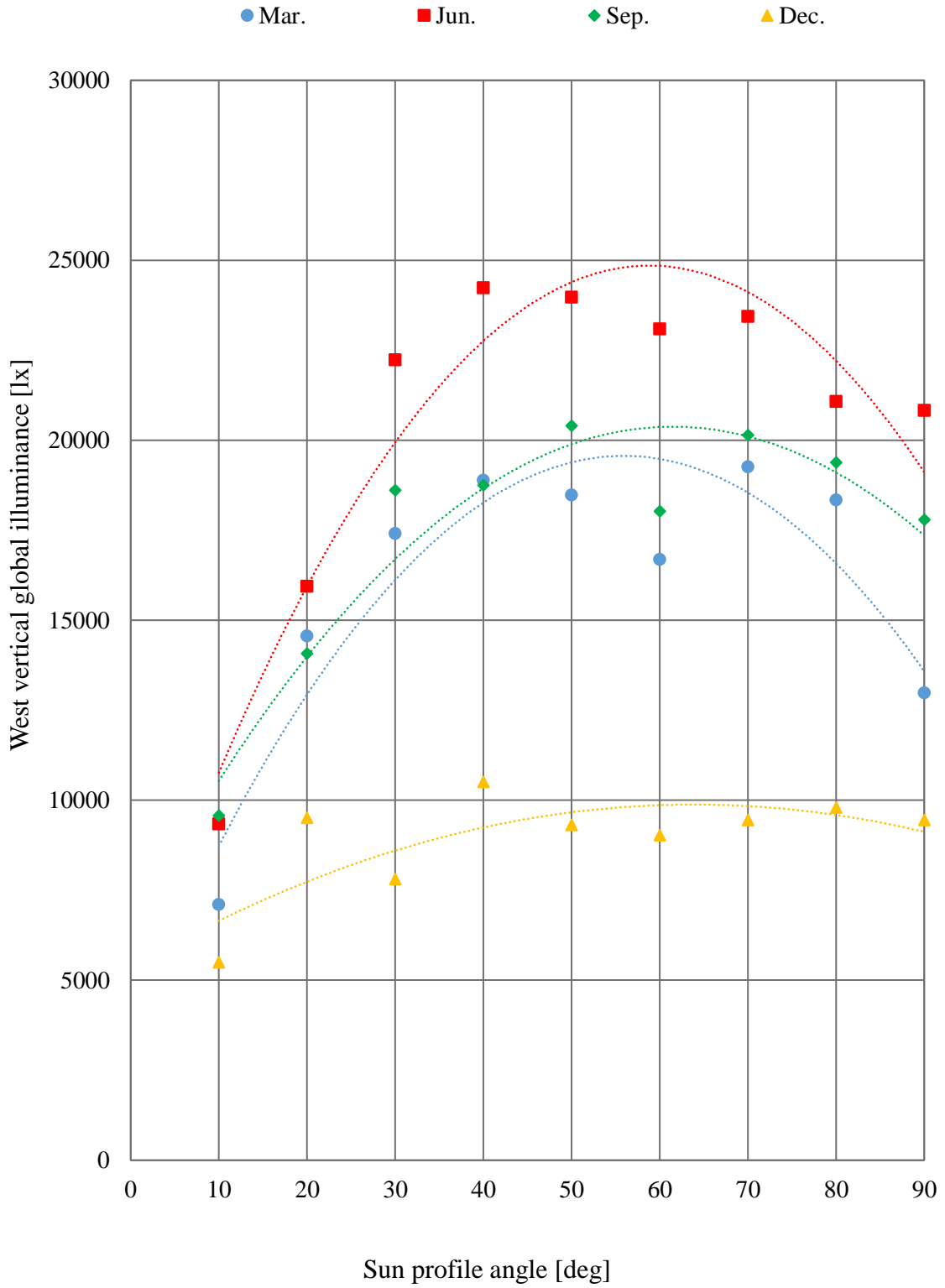
Fig. 4-4. The west vertical global illuminance thresholds of the measurements in Lyon
with sun profile angle (Mar., Jun., Sep. and Dec.)

4.1.3 Occurrence frequency of the measured thresholds of Lyon's sky conditions

The daylight measurement station in Lyon records sky conditions as five sky types, which are cloudless, intermediately cloudless, medium clouds, intermediately overcast and overcast sky types. Table 4-3 shows the thresholds of south vertical global illuminance and the sky types corresponding to the thresholds. The frequency of occurrences was 5.55% for cloudless sky, 5.55% for intermediately cloudless sky, 57.4% for medium-clouds, 31.5% for intermediately overcast and 0% for overcast. The partly cloudy sky conditions, which include intermediately cloudless, medium clouds and intermediately overcast, were up to 94.4%. Thus, it is the sky condition that with the highest occurrence frequency of the south global illuminance picked as thresholds.

Table 4-3. Thresholds of the south vertical global illuminance and the recorded sky types

Month	Solar altitude [deg] South vertical global illuminance [lx]						
	5〜15	15〜25	25〜35	35〜45	45〜55	55〜65	65〜75
1	5354 III	11890 III	16200 IV	- -	- -	- -	- -
2	5452 III	13180 III	17210 IV	20240 III	- -	- -	- -
3	3742 II	9990 III	16560 III	22420 III	26770 III	- -	- -
4	4545 III	8550 III	13730 III	19400 IV	27060 III	18330 IV	- -
5	- -	8500 IV	10970 III	16040 III	20810 IV	25900 III	17500 IV
6	- -	- -	13460 III	15620 IV	19220 III	24190 IV	24260 III
7	- -	- -	11150 III	15570 III	18190 IV	20890 III	20420 I
8	5930 III	8390 IV	11980 III	13520 III	17050 I	23450 II	- -
9	5382 IV	9210 III	16170 I	20430 IV	24950 II	- -	- -
10	6254 III	12240 IV	18860 IV	24440 IV	- -	- -	- -
11	5441 IV	13870 III	18710 III	- -	- -	- -	- -
12	7360 III	13490 III	- -	- -	- -	- -	- -
I: Cloudless sky II: Intermediately cloudless sky III: Medium-clouds IV: Intermediately overcast V: Overcast							

71

4.2   Theoretical daylight illuminance thresholds for sunlight presence judgments estimated by ISO/CIE standard general skies

To make the blind/louvers control system available in any specific location, it is necessary to generalize theoretical thresholds of vertical daylight illuminance for judging sunshine on a window. In order to generalize the thresholds of vertical global illuminance, this research work i) examined feasibility of utilizing ISO/CIE Standard General Skies to obtain theoretical illuminance thresholds; ii) propose monthly theoretical thresholds of daylight illuminance on windows, as functions of solar altitude or sun profile angle, to judge whether the windows receive direct sunlight or not.

4.2.1 CIE Standard General Sky

ISO/CIE joint standard on spatial distribution of daylight - CIE Standard General Sky defines relative sky luminances of fifteen sky types [1]. The CIE Standard adoped the standard skies proposed in a final report - *A set of standard skies characterizing daylight conditions for computer and energy conscious design* by Kittler R. et al. [2]. The modelled exterior daylight conditions can be used for various design purposes or expert comparisons and evaluations. CIE Standard General Sky Guide shows methods to use the relative sky luminance distributions to calculate diffuse illuminance for daylighting design procedures [3].

It utilized the ratio of zenith luminance to horizontal diffuse illuminance (L_{vz}/E_{vd}) to characterize properties of homogeneous skies in 15 basic types which cover the whole spectrum of usual skies found in reality. Three groups of overcast, intermediate and clear

skies were recommended while each group containing 5 sky types. The 15 sky types are

formed by chosen combinations of the relative luminance distribution for luminance (L_a)

at sky element as:

$$L_a = L_{vz} \frac{f(\chi)\varphi(Z)}{f(Z_s)\varphi(0)}$$

Eq. $(4-2)$

Where L_a is the luminance at sky selement [cd/m^2]

          L_{vz} is the zenith luminance [cd/m2]

          Z   is the zenith angle of the sky element [deg]

          Z_s is the zenith angle of the sky element and zenith angle of the sun [deg]

          χ is the shortest angular distance between a sky element and the sun [deg]

The twin set of gradation functions $\varphi(Z)$ and indicatrix functions $f(\chi)$ each

modells by exponential approximations by the help of a, b, c, d and e parameters. Fig. 4-

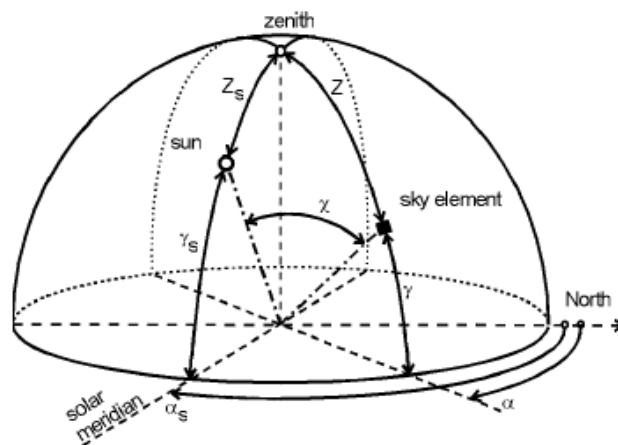4 shows the spatial position of the sun and a sky element.

Fig. 4-4. Angles defining the position of the sun and a sky element

Otherwise, the L_{vz}/E_{vd} ratio can be calculated using the integration as:

$$\frac{L_{vz}}{E_{vd}} = \frac{\varphi(0°)f(Z_s)}{\int_{Z=0}^{\pi/2}\int_{\alpha=0}^{2\pi}[\varphi(Z)f(\chi)\sin Z \cos Z]d\alpha \, dZ} \qquad \text{Eq.}(4-3)$$

Where α is the azimuth angle of the sky element respecting the sun azimuth [deg]

$\varphi(Z)$ is the gradation functions

$f(\chi)$ is the indicatrix functions

The Guide provides two alternative formula for calculating absolute zenith luminance (L_{vz}) of 15 sky types:

- If no other information is available but the assumption of a certain standard sky, the absolute zenith luminance L_{vz} of any sky type without direct sunlight is:

$$L_{vz} = \frac{E_{vd}}{E_{voh}}\left[B\frac{(\sin \gamma_s)^C}{(\cos \gamma_s)^D} + E \sin \gamma_s\right] \qquad \text{Eq.}(4-4)$$

Where E_{vd} is the horizontal diffuse illuminance [lx]

E_{voh} is the horizontal extraterrestrial illuminance [lx], $E_{voh} = E_{vo} \sin \gamma_s$

γ_s is the angle of elevation of the sun above the horizon [deg]

E_{vo} is the luminous solar comstant [lx], which equals to 133800 lx

- If the sunlight is influenced by atmospheric turbidity, the follownig formula can be used under clear and intermediate skies conditions:

$$L_{vz} = (A_1 T_v + A_2) \sin \gamma_s + 0.7 kcd \cdot m^{-2}(T_v + 1)\frac{(\sin \gamma_s)^C}{(\cos \gamma_s)^D}$$
$$+ 0.04 kcd \cdot m^{-2} T_v \qquad \qquad \text{Eq.} (4-5)$$

Where T_v is the luminous turbidity factor

Here T_v is the luminous turbidity factor, the ration of vertical optical thickness of a real turbid atmosphere to the vertical optical thickness of the pure and dry atmosphere. The recommended ratios E_{vd}/E_{voh} and parameters B, C, D, E, A₁, A₂ depend on a selected sky type.

Supposing the global horizontal illuminance (E_{vg}) and diffuse horizontal illuminance (E_{vd}) are measured, then the direct solar illuminance on horizontal surface (E_{vs}) is known, the T_v can be calculated as:

$$T_v = \frac{-\ln(E_{vs}/E_{vo})}{a_v m} \qquad \qquad \text{Eq.} (4-6)$$

Where a_v is the luminous extinction coefficient of the atmosphere

m is the relative optical air mass

The sun shading conditions affected either by atmospheric turbidity or by cloudiness of various thickness and light transparency. This attenuation and filtering of direct sun

beams can be expressed via the momentary value of the luminous turbidity factor [4]. Normal direct solar irradiance 120 W/m^2 is assumed to measure sunshine duration. The CIE sky types were considered that all overcast skies 1 to 6 without sunshine, and cloudy with clear sky types 7 to 15 with sunshine. The final report on standard skies [2] showed the usual T_v range of overcast skies is greater than 12, while T_v of partly cloudy sky are between 6~12.

Using the Eq. (4-3), Eq. (4-4), Eq. (4-5) and Eq. (4-6) can get diffuse illuminance of any sky type. Considering diffuse illuminance gets equal to global illuminance when there is no direct sunlight, it is feasible to find appropriate sky types to obtain the illuminance thresholds for determine direct sunlight on a window.

4.2.2 Calculation for diffuse vertical illuminance of the CIE partly cloudy skies

The previous study compared the calculated horizontal diffuse illuminance of CIE skies with the measured thresholds drawn from ENTPE data, it indicated the partly cloudy sky types 7 to 10, whose calculated diffuse illuminance have potential for sunshine judgement. Table 4-4 shows the SSLD (Standard Sky Luminance Distributions) descriptions of sky types 7 to 10.

Table 4-4. The SSLD descriptions of sky types 7 to 10

Type (SSLD code)	Description of SSLD
7 (III, 3)	Partly cloudy sky, no gradation towards zenith, brighter circumsolar region.
8 (III, 4)	Partly cloudy sky, no gradation towards zenith, distinct solar corona.
9 (IV, 2)	Partly cloudy, with the obscured sun.
10 (IV, 3)	Partly cloudy, with brighter circumsolar region.

The south diffuse vertical illuminance (E_{vds}) and the west diffuse illuminance (E_{vdw}) can be calculated by the integration of specific luminance in elements of the sky solid angle projected onto the vertical illuminate plane as Eq. (4-7) and Eq. (4-8).

$$E_{vds} = \int_{Z=0°}^{Z=90°} \int_{\alpha=90°}^{\alpha=270°} L_a \cos^2 Z \cos \alpha \, d\alpha \, dZ \qquad \text{Eq.} (4-7)$$

$$E_{vdw} = \int_{Z=0°}^{Z=90°} \int_{\alpha=360°}^{\alpha=180°} L_a \cos^2 Z \sin \alpha \, d\alpha \, dZ \qquad \text{Eq.} (4-8)$$

To grasp the differences between the sky types, the south vertical daylight illuminance of sky types 7 to 10 were calculated and compared with the measured south illuminance thresholds of Lyon in March, June, September and December (Fig. 4-5). The calculated values and measurements showed the same trend and the illuminance gap between sky types is increasing over the solar altitude.
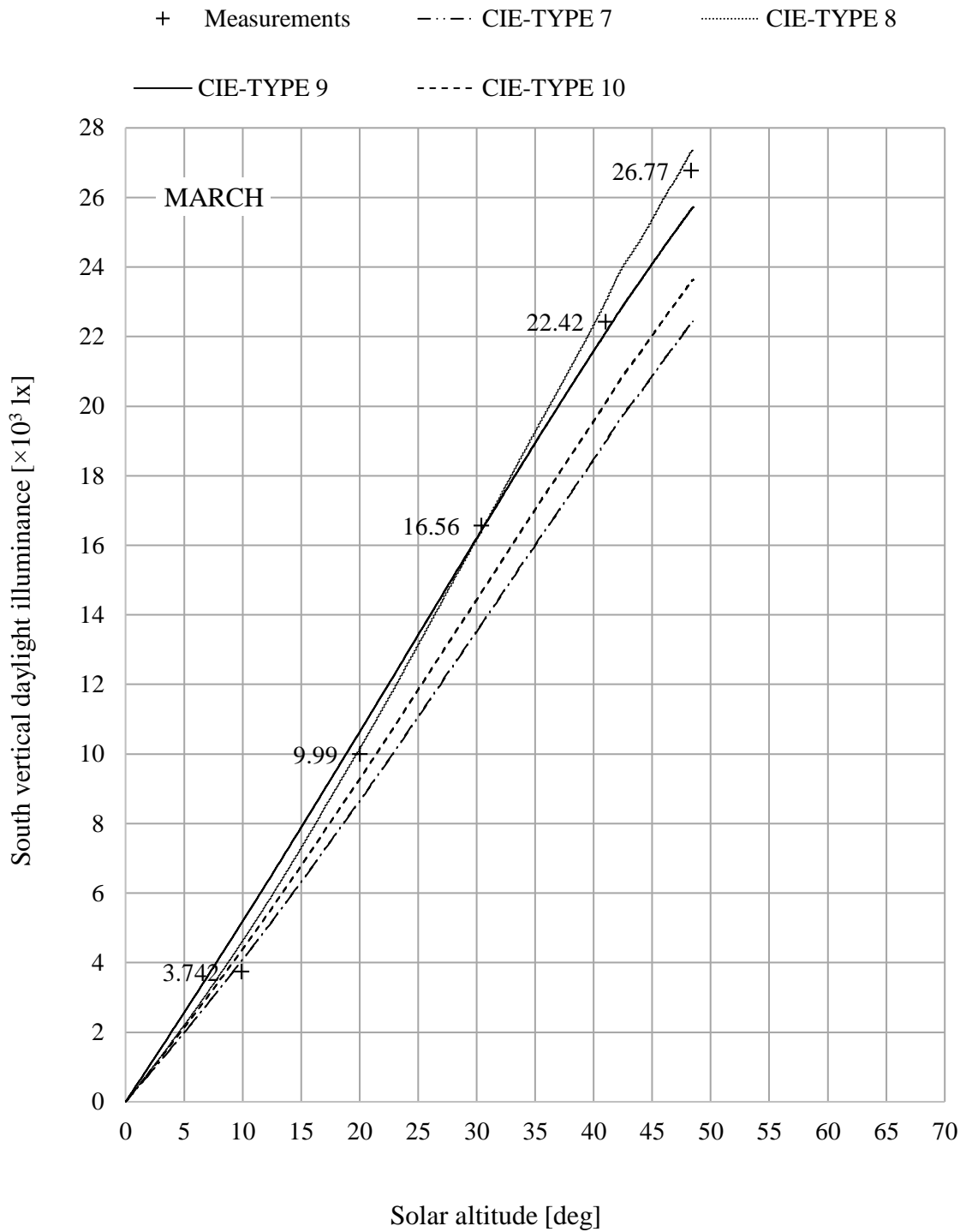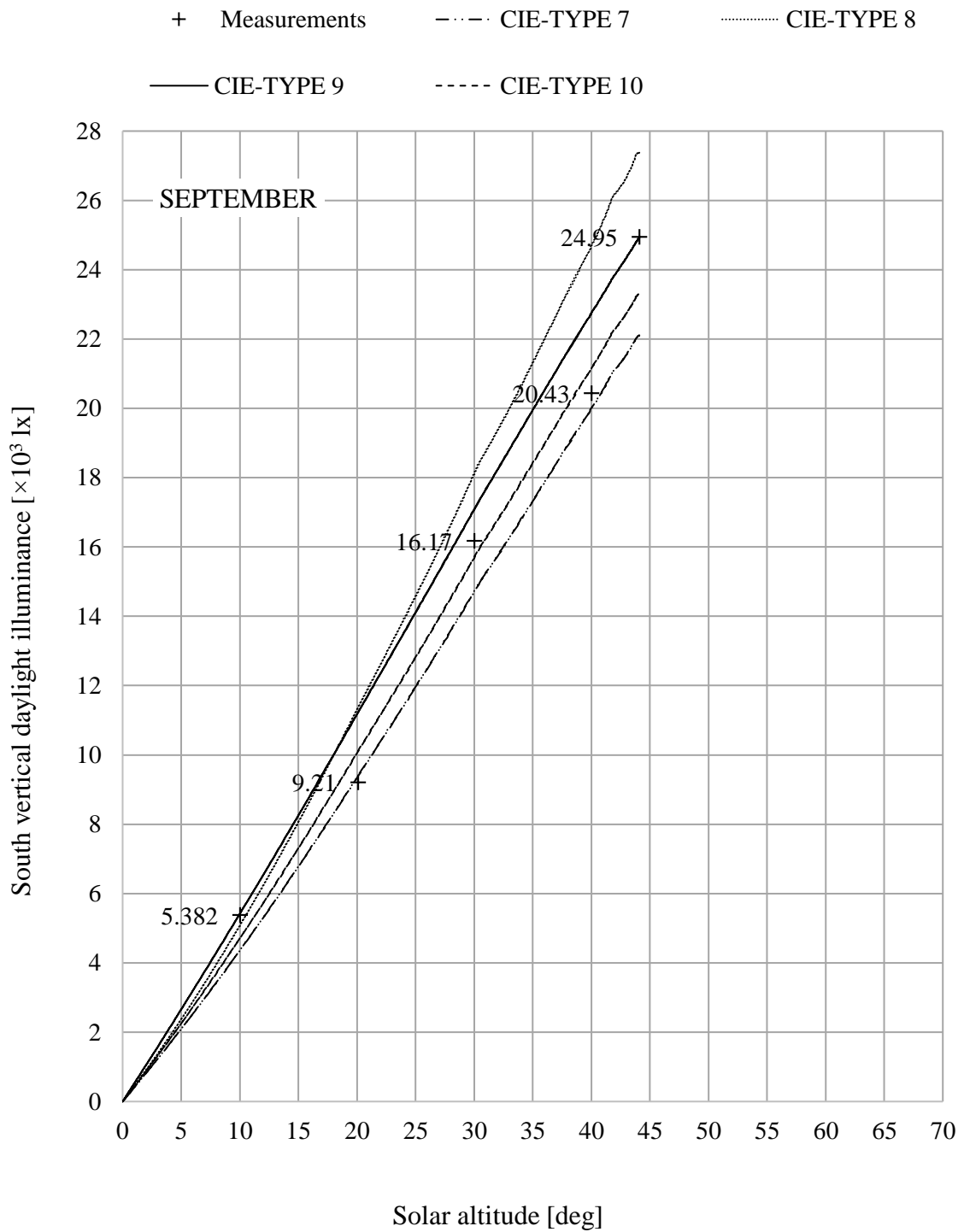
(a) March

Fig. 4-5 (a). The south vertical daylight illuminance of CIE sky types 7 to 10 and the south vertical daylight illuminance thresholds measured in Lyon
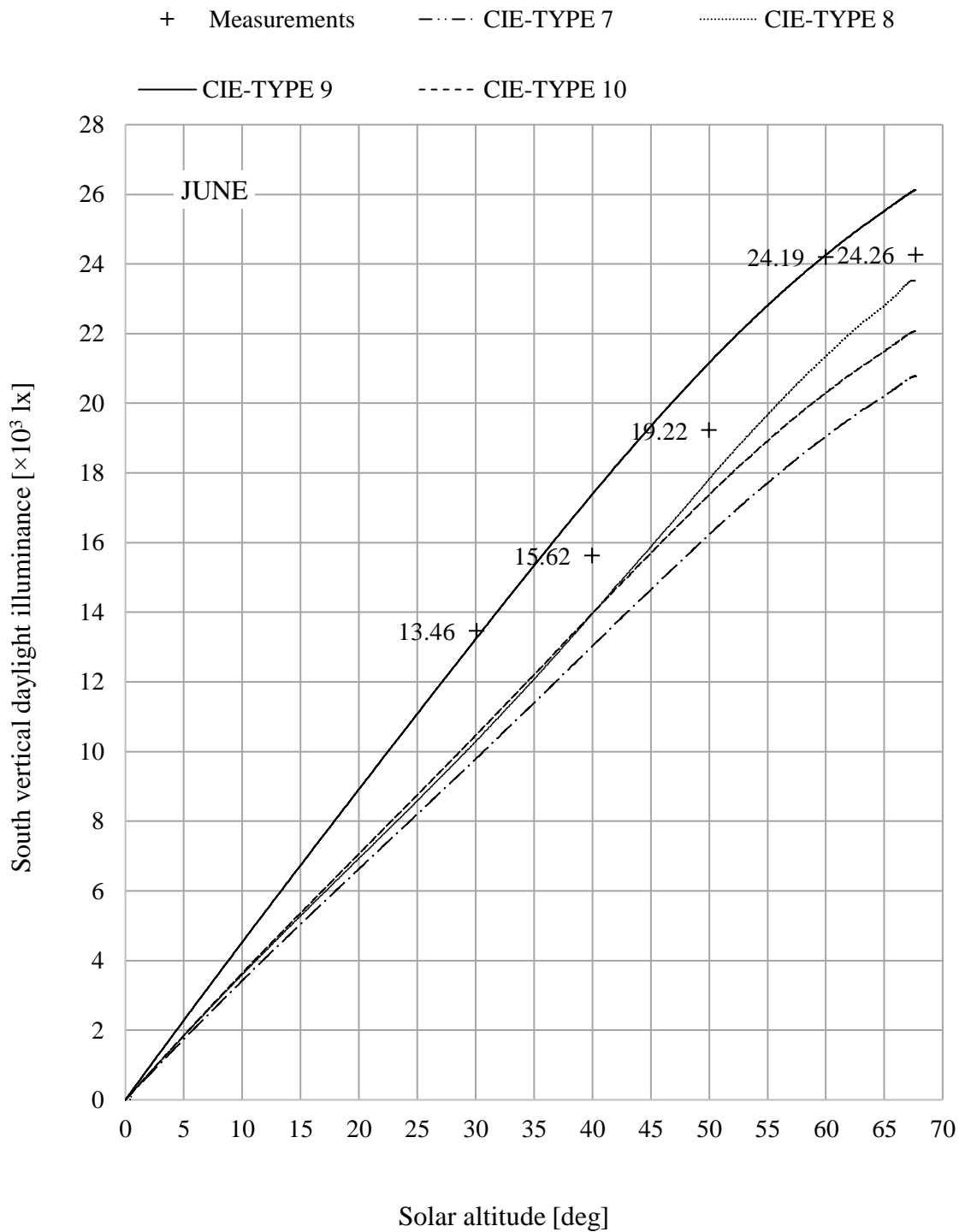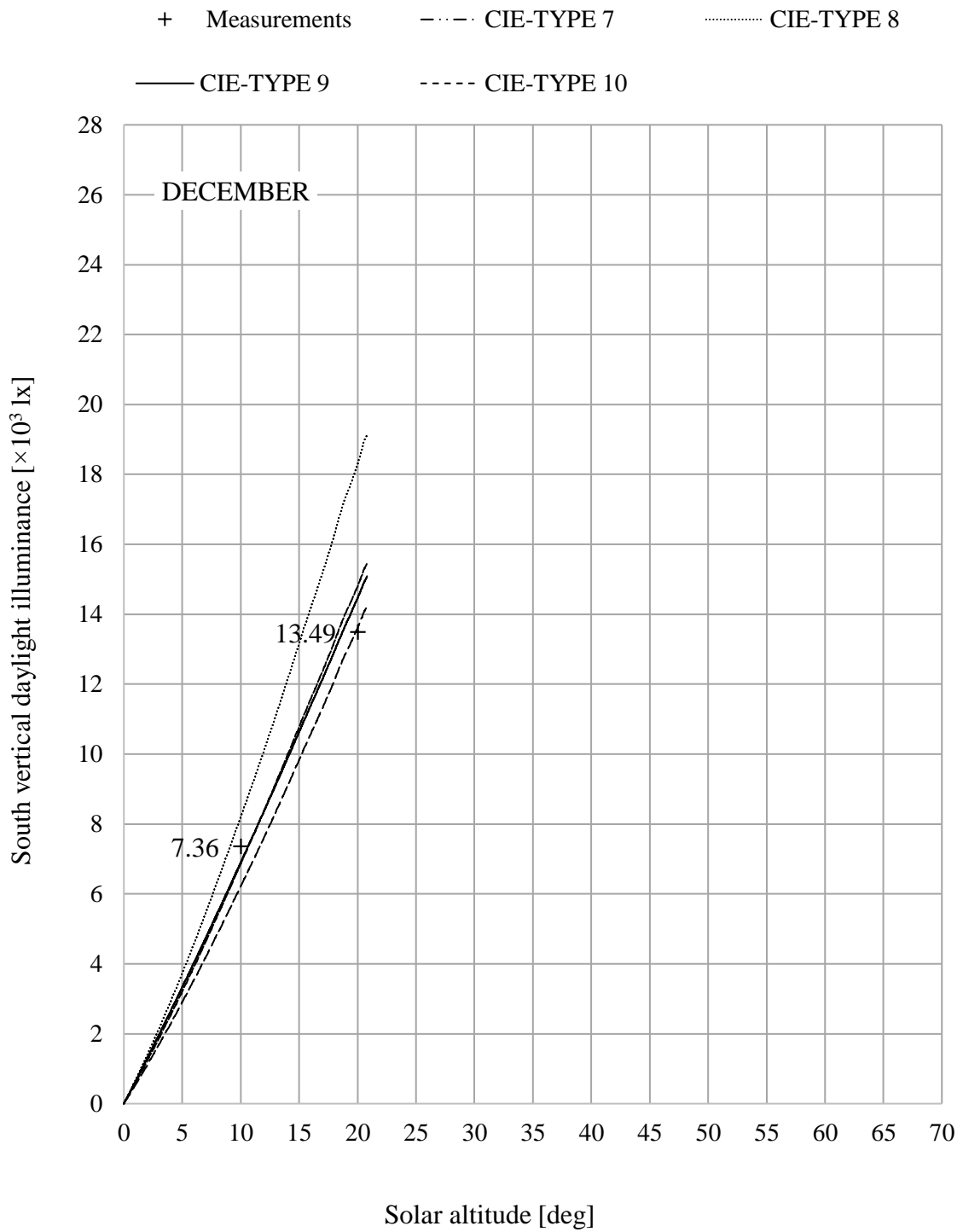
(b) June

Fig. 4-5 (b). The south vertical daylight illuminance of CIE sky types 7 to 10 and the south vertical daylight illuminance thresholds measured in Lyon

(c) September

Fig. 4-5 (c). The south vertical daylight illuminance of CIE sky types 7 to 10 and the south vertical daylight illuminance thresholds measured in Lyon

(d) December

Fig. 4-5 (d). The south vertical daylight illuminance of CIE sky types 7 to 10 and the south vertical daylight illuminance thresholds measured in Lyon

4.3 Proposed daylight illuminance thresholds and their applicability

4.3.1 Selection of the theoretical vertical daylight illuminance thresholds for Lyon

The final report on standard skies [2] gives the usual T_v range of every sky type. Table 4-5 shows the The T_v and sunlight comments of sky types 7 to 10. To find the suitable sky types to obtain vertical daylight illuminance thresholds, this study examined sunlight conditions when the measured south/west illuminance thresholds were acquired, by checking their calculated luminous turbidity factors that calculated from Eq. (4-6).

Table 4-5. The T_v and sunlight comments of sky types 7 to 10

Type	Usual T_v range	Comment of sunlight
7	Usually around 12	Filtered direct sunlight, exceptionally darker skies.
8	Usually 5-12	Filtered or no direct sunlight.
9	Over 10	Filtered or no direct sunlight.
10	Usually 6-12	Filtered direct sunlight.

The calculated results showed the T_v within the control range of solar altitudes mostly floated between 10 to 20. As for the sky type 9, whose T_v range is supposed to be usually over 10 (Table 4-5). Besides, as shown in Fig. 4-5, because the calculated south vertical daylight illuminances of sky type 9 were almost slightly above the measured thresholds, there is a guarantee of safety conditions for sun shading. It indicated that sky type 9 can be served to get the vertical daylight illuminance thresholds. Fig. 4-6 shows the monthly south vertical daylight illuminances of CIE sky type 9 within the control range of solar altitudes in March, June, September and December.
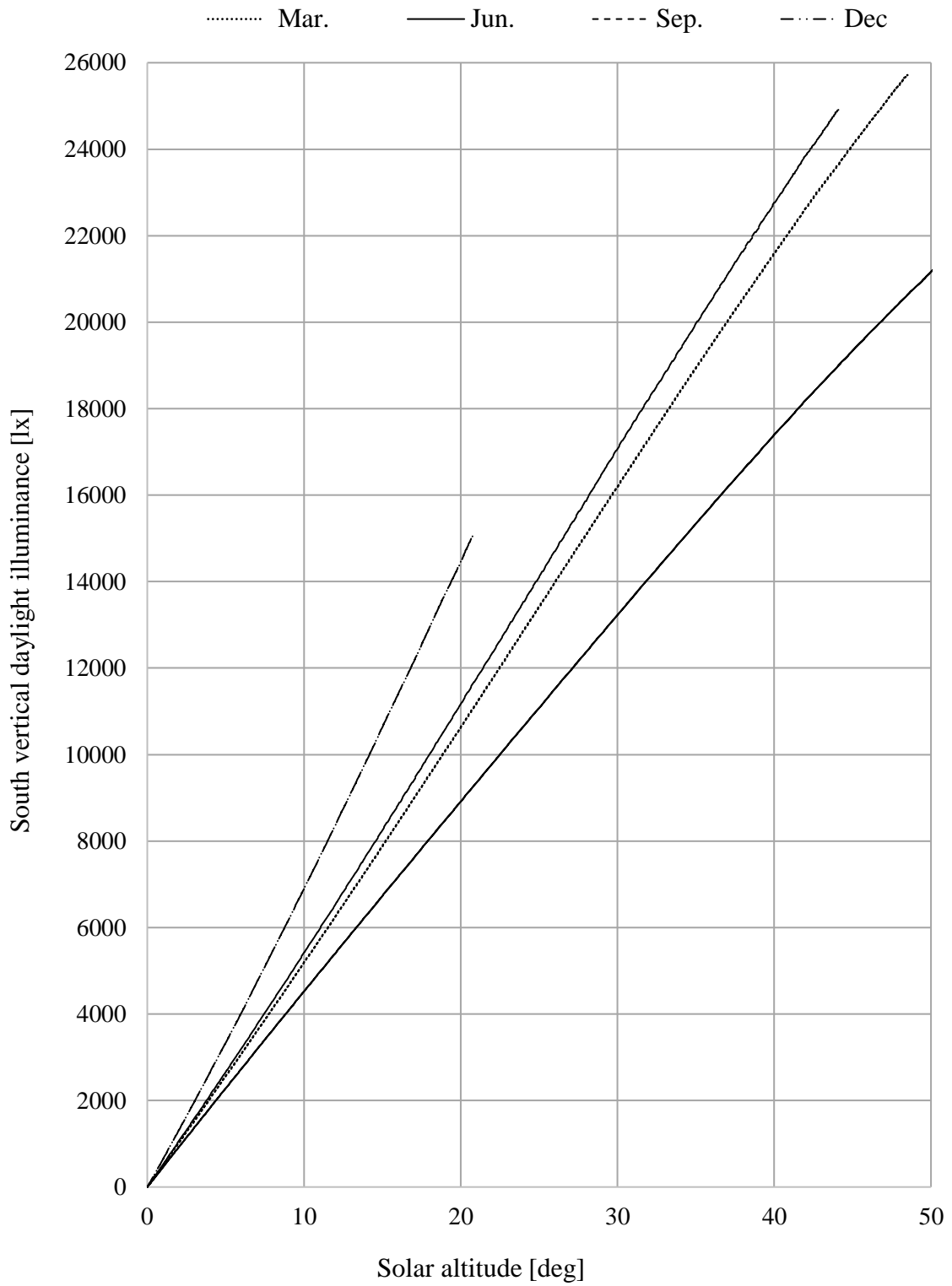
Fig. 4-6. The monthly theoretical thresholds of south vertical daylight illuminance for sunshine judgments with solar altitude (Mar., Jun., Sep. and Dec.)

As mentioned before, the window facing between the southeast and southwest, it is considered that solar altitude is appropriate as the variable for the thresholds. While for the window facing the angle between the southwest and the west (or east to southeast), the sun profile angle is more suitable than the solar altitude. By the Eq. (4-8), the west vertical daylight illuminance of sky type 9 was calculated on days of the summer solstice, the autumnal equinox and the winter solsticeand. The measured thresholds were taken to compared with the calculations and shown a good march. The Fig. 4-7 shows the monthly west vertical daylight illuminances of CIE sky type 9 within the control range of sun profile angles, in March, June, September and December.
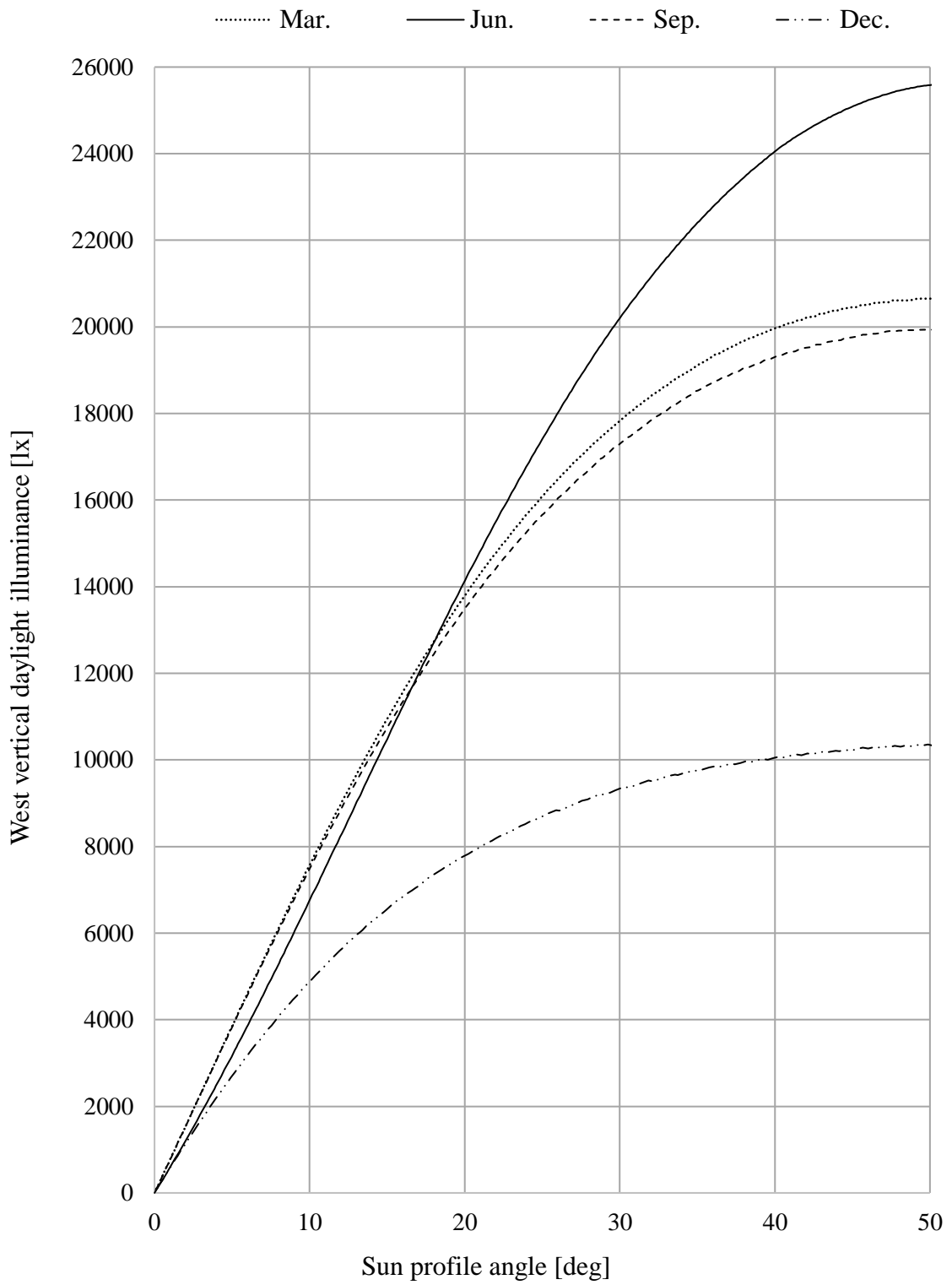
Fig. 4-7. The monthly theoretical thresholds of west vertical daylight illuminance for sunshine judgments with sun profile angle

4.3.2 Application of the thresholds to the auto-rotation PV-louver system

Because direct sunlight will cause visual disability or discomfort for indoor occupants, as well as an increase of cooling load, it is important to makes sure the safety of thresholds for sunlight judgement. Fig. 4-8 shows a sunlight judgement proceeding during a partly cloudy day on 3 March 2015 in Lyon. The great changes of the normal direct irradiance and the south vertical illuminance indicated the unstable sky conditions during the day. The orange line in upper means 120 W/m^2 normal direct irradiance, which on behalf of threshold for direct sunlight presence. The blue line in lower figure is the proposed daylight illuminance threshold for sunlight judgement. When the sensor measured the daylight illuminance greater than the thresholds, the louvers rotated to block sunshine. Otherwise, louvers were kept open to let skylight in. The proposed daylight illuminance threshold is "little lower" than the 120 W/m^2 threshold because during the process of acquiring the threshold, safety condition has taken into account.
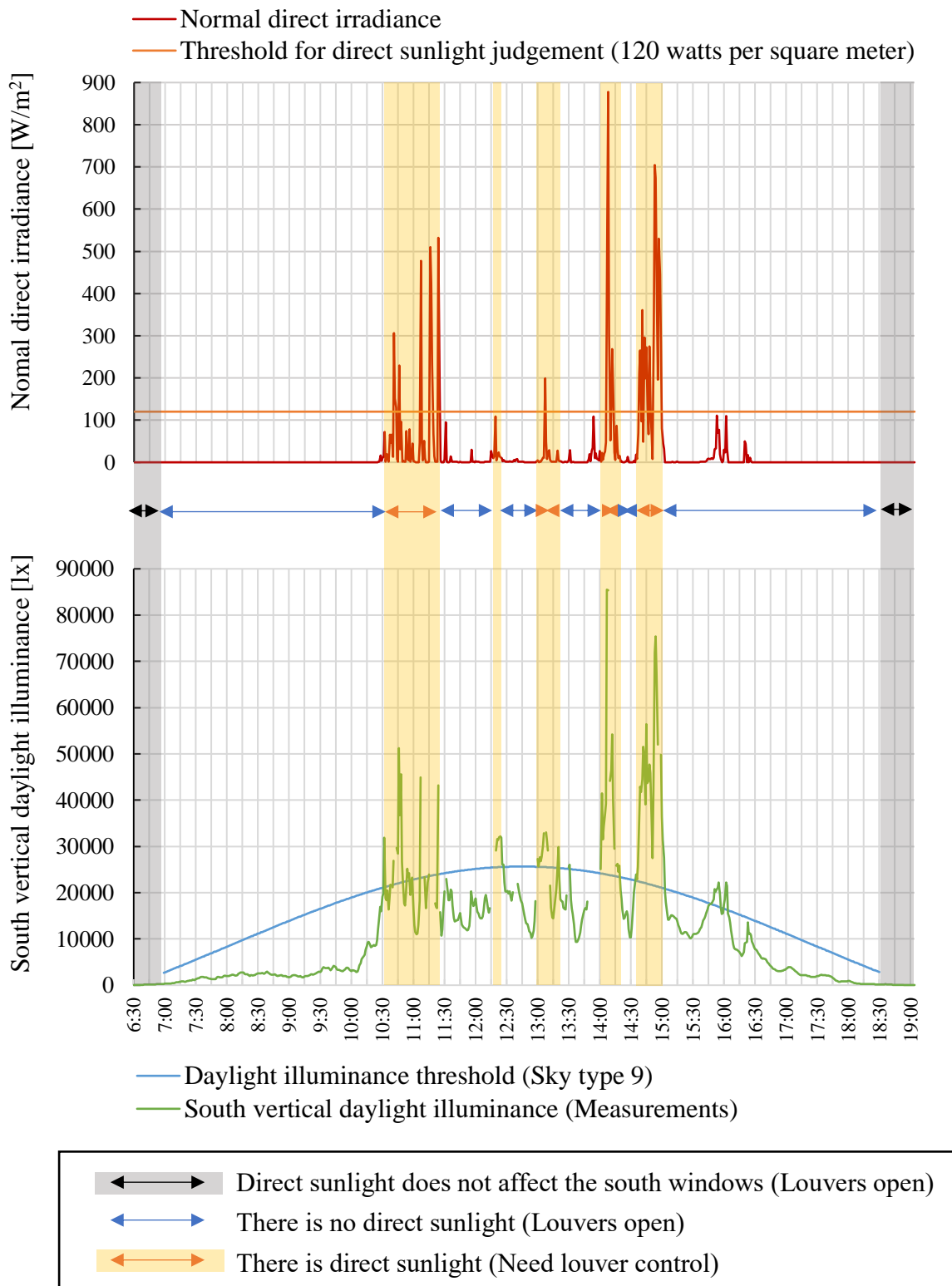
Fig. 4-8. Direct sunlight judgements using daylight illuminance threshold (3 March 2015)

In the course of actual use, when there is direct sunlight, the PV-louvers will turn following the sun. According to the law of cosines (also known as the cosine formula, cosine rule), the vertical global illuminance thresholds can be converted and applied to any surface of rotated PV-louver (except the horizontal position). When the window direction deviates from south (apply to zones in north of tropic of cancer), the PV-louver power generation may reduce but the thresholds are still available. For example, for the window directions are between east to west, the vertical global illuminance thresholds can be converted by trigonometric functions basing on the proposed south vertical illuminance thresholds.

As the angle between the window and south is $A_s{'}$ and the PV-louver tilt angle is θ, shown in Fig. 4-9, the sun-shading thresholds of global illuminance on the PV-louver can be calculated by the Eq. (4-9).
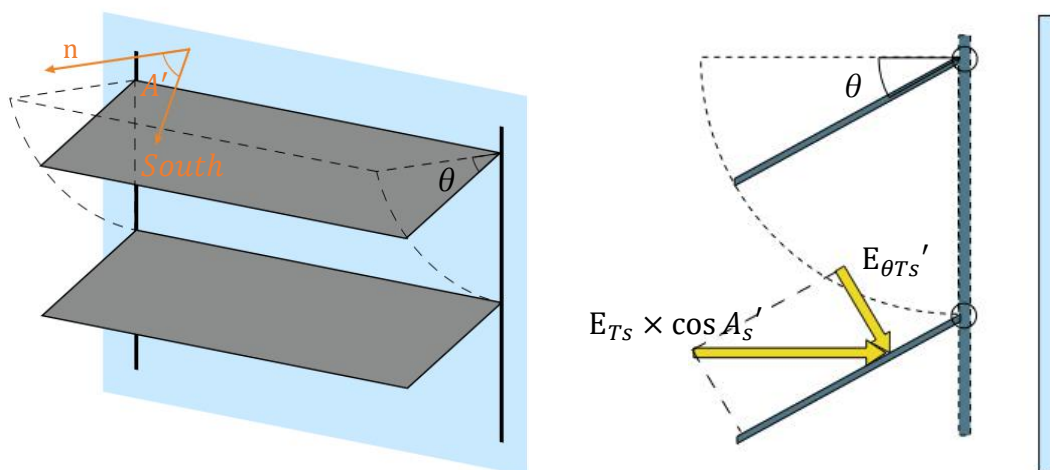

Fig. 4-9. The sun-shading thresholds of global illuminance ($E_{\theta Ts}{'}$) on PV-louver

$$E_{\theta Ts}' = E_{Ts} \times \cos A_s' \times \sin\theta \qquad\qquad \text{Eq.}\,(4-9)$$

Where $E_{\theta Ts}'$ is the sun-shading thresholds of global illuminance on PV-louver [lx]

           E_{Ts} is the sun-shading thresholds of south vertival global illuminance [lx]

           θ is the louver tilt angle [deg]

           A_s' is the angle between the window and south [deg]

4.4   Conclusion

The aim of this chapter is to propose theoretical thresholds of daylight illuminance on the PV-louvers, as functions of solar altitude or sun profile angle, to judge whether windows receive direct sunlight or not. For this purpose, this research work examines feasibility of utilizing ISO/CIE Standard General Skies to obtain theoretical thresholds. The daylight measurements at the IDMP station in Lyon are introduced to compare theoretical values and measured data. The practical use factors are taken into account into the control processes. The orientation of window is also taken into account.

It is worth noting that the measurements used to examine T_v is only from Lyon, does not represent sky conditions of other areas. However, it also showed calculated vertical diffuse illuminance of partly cloudy sky types had the same trend and the illuminance gap between sky types is very small within the control range. The adaptability of sky type 9 is expected to be further studied.

REFERENCES

[1] CIE S 011/E: 2003: Spatial Distribution of Daylight - CIE Standard General Sky.

[2] Kittler R., Perez R., Darula S., "A set of standard skies characterizing daylight conditions for computer and energy conscious design", US SK 92 052 Final Report, ICA SAS Bratislava, Polygrafia Bratislava ,1998.

[3] CIE 215:2014: Technical Report, CIE Standard General Sky Guide.

[4] Kittler R., Darula S., Kambezidis H., "Daylight climate specification based on Athens and Bratislava data", Proc. Conf. Lux Europa, Reykjavik, 442-449, 2001.

Chapter V

Impacts of the Proposed PV Facade System on Electrical Power Generation and Air-Conditioning and Lighting Energy Consumptions in a Standard Office

5.1 Simulation conditions

5.1.1 Louver control method and PV-louvers configuration

In the sections 3.2.3 and 3.2.4, a daylight-responsive control strategy and different configurations of PV-louvers were proposed to improve the energy efficiency of the PV-louver system. In order to test impacts of these solutions, this research work explored the electrical power generation, air-conditioning and lighting energy consumptions of the PV-louvers installed outside south, west and east facing windows. From the result analyses, the optimum PV-louvers configuration for different orientations was obtained.

Table 5-1 shows the analysis cases of different configurations that use cut-off angle or daylight-responsive control methods. Each case study was named using two characters. The first character stands for the three types of PV-louvers configurations; the second one stands for the two control methods. A reference case (case A0) is all louvers of Type-A closed. In this case, there is no shadow on PV-louvers. Table 5 describes basic properties of the PV-louvers

Table 5-1. Analysis cases of different configurations with cut-off angle or daylight-responsive control method

CASES	PV-louvers configuration + PV-louvers control methods
CASE A0	Type-A with PV-louvers all closed
CASE A1	Type-A with cut-off angle control method
CASE A2	Type-A with daylight-responsive control method
CASE B2	Type-B with daylight-responsive control method
CASE C2	Type-C with daylight-responsive control method

Table 5-2. Basic properties of the PV-louvers

Property	Type-A	Type-B	Type-C
PV module type	Thin-film solar cell (a-Si)		
Operating voltage	12 V		
Maximum output voltage and output current	2.5 V and 167 mA		
Power conversion efficiency	20%		
PV-louver reflectance	0.7		
Window size for PV-louvers	Length 24.6 m $\times$ Height 2.6 m		
Angle between axes of the PV-louvers and vertical plane	0°	0°	10°
PV-louver width	0.26 m	0.31 m	0.26 m
PV-louver spacing	0.26 m	0.26 m	0.26 m
Total PV area of the PV-louver system	63.96 m^2	76.75 m^2	64.95 m^2

5.1.2 A standard open office room for simulation

In this study, a Japanese standard open office (Fig. 5-1) was used to investigate impacts of the proposed PV facade system on electric power generation as well as heating, cooling and lighting energy consumptions.
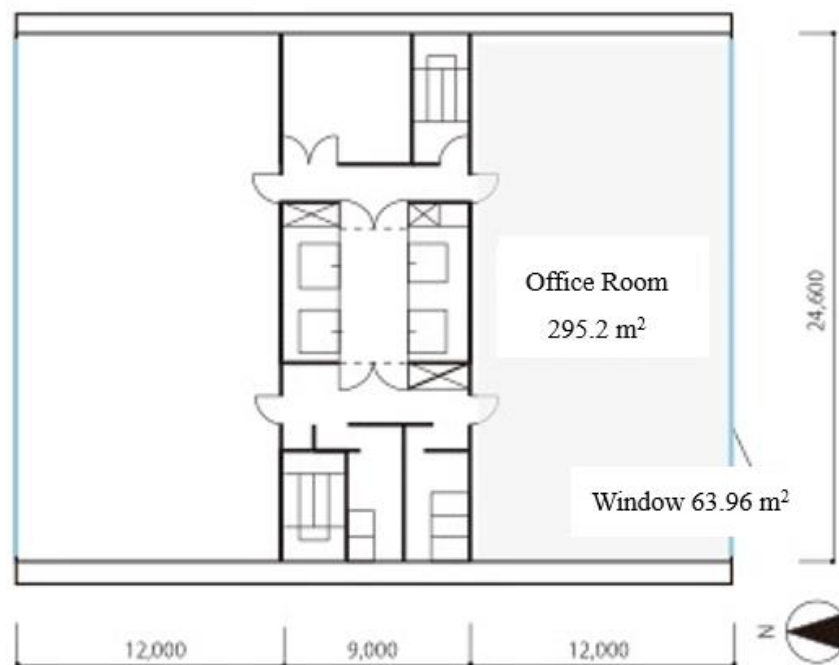

Fig. 5-1. The floor plan of the Japanese standard open office room.

The room was in a reinforced-concrete building. The room volume was 1062.72 m^3. 6-millimeter double-glazing windows were all installed with the proposed PV facade system. Forty-eight lamps of LED lighting fixtures were evenly installed on the ceiling. Table 5-3 shows the setting condition of the office room. Fig. 5-2 shows the perspective view of the office room.

Table 5-3. Setting condition of the office room

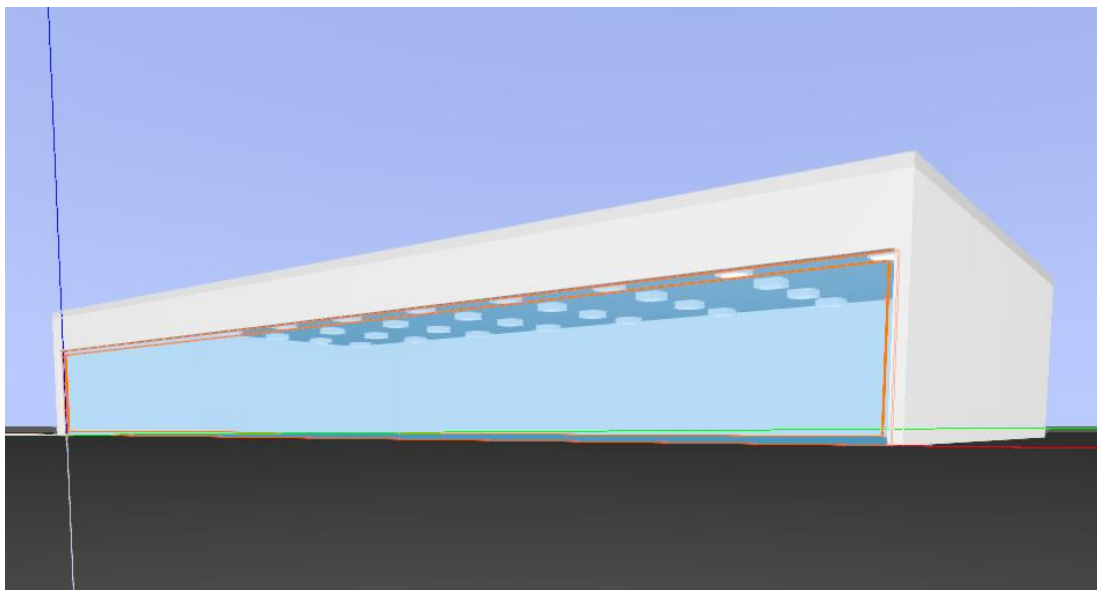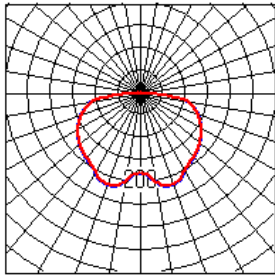| Setting position	Vaulx-en-Velin Cedex, France (4.9° E, 45.8° N)
Room size	Ceiling height 3.6 m Width 12.0 m Length 24.6 m
Reflectance of room surface	Ceiling 0.7, Wall 0.5, Floor 0.3
Window size	Height 2.6 m Length 24.6 m
Property of window	6-millimeter double-glazing Transmittance 0.66, Absorptance 0.3, Reflectance 0.1

Fig. 5-2. A perspective view of the external appearance

5.1.3 Setting conditions for the indoor luminous and thermal environments

A pair of LED embedded luminaires was installed in the room. For energy saving, the electric lights are turned off if there is enough and stable daylight. The target illuminance at work plane (0.85-meter above floor) was set at 500 lx according to the recommended illuminance levels for general office space [1]. The lighting condition was ON/OFF. Table 5-4 shows the LED luminaires specifications. Fig. 5-3 shows the layout of the LED luminaires in the proposed office room. Fig. 5-4 shows the illumination distribution when the lights are all on.

Table 5-4. LED luminaires specifications

Version: Panasonic FYY26458 LA9	
Candle power distribution	**Image**

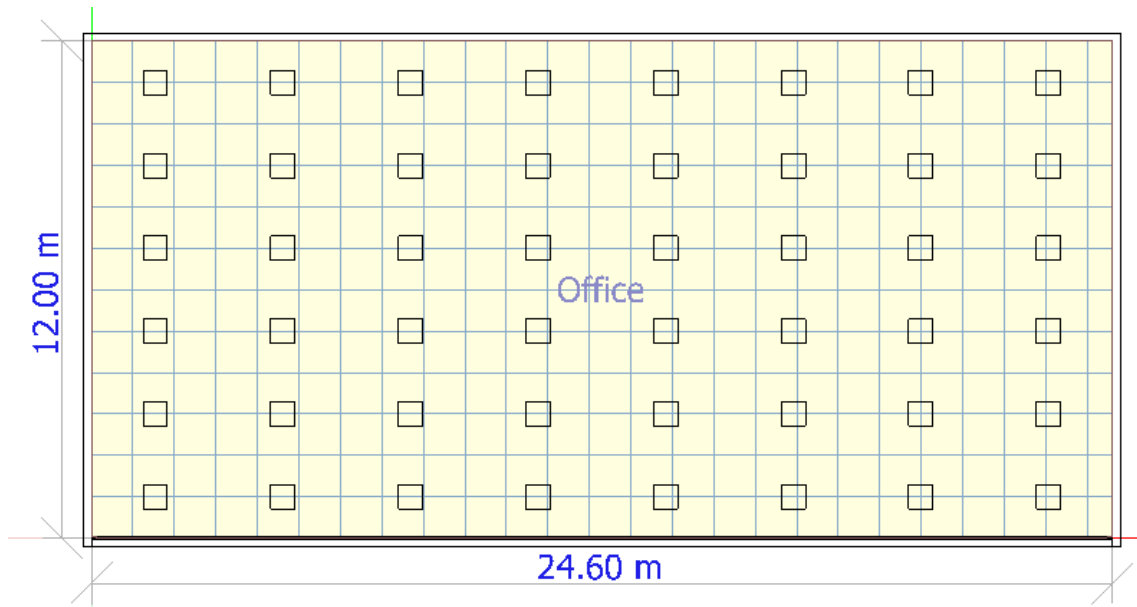|	
Size	600 mm × 600 mm × 180 mm
Consumption of electrical power	48 W
Input power source	100 – 242 V
Consumption efficiency	118.3 lm/W
Color temperature	Natural white 5000 K
Lamp luminous flux	5680 lm

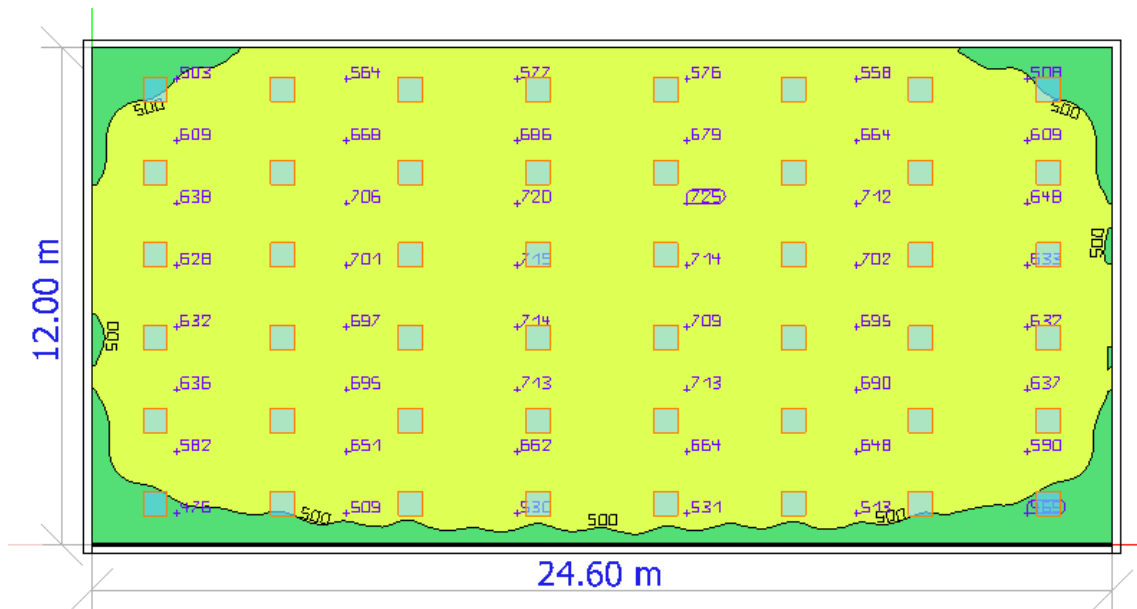Fig. 5-3. Layout of the LED luminaires in the office room (6 rows × 8 columns)

Fig. 5-4. Illumination distribution when the lights are all on (48 lamps)

The cooling and heating energy consumptions were calculated by the software *THERB for HAM* [2]. Based on detailed phenomena describing the actual building physics, the software can estimate the temperature, humidity, and heating and cooling loads of a room by segregating the room. This research used the actual data to evaluate the energy efficiency of the autonomous PV facade system. The simulation conditions for the thermal environment are shown in Table 5-5.

Table 5-5. Simulation conditions for air-conditioning consumption

Program	THERB for HAM
Subject building	An office room on the 10th floor of an eleven-story building
Meteorological data	From 1 January 2015 to 30 June 2015 and From 1 July 2016 to 31 December 2016
Persons density	0.2 person/m^2
Human body load (**Work at the room temperature of 26°**)	Sensible Heat: 55 W/person Latent Heat: 64 W/person
Cooling load for office equipment	30 W/m^2
Outside-air load	25 m^3/(hour · person)
Indoor temperature for heating	22 °C
Indoor temperature for cooling	26 °C
Cooling season	1 May ~ 30 September
Heating season	1 November ~ 31 March
Air-condoning operation period	9:00 ~ 18:00 all year round

5.2 Estimations of electrical power generation of the PV-louver system

5.2.1 Comparison of power generation of the PV-louvers with different control methods

To examine the electricity generating efficiency of different analyzed cases, the daylight measurements were used to calculate the electrical power generations of PV-louvers at one-minute intervals. In addition, the direct solar radiations measured were used to classify the sky conditions.

Firstly, the power generation per unit of area (one square meter) of a south-facing PV-louver system on a partly cloudy day were calculated. Fig. 5-5 illustrates the control method comparison between case A1 and case A2 on 4 March 2015. The red straight line presents the normal direct irradiance of 120 W/m^2. The blue zones mean that there is no direct sunlight (when the normal direct solar irradiance is below 120 W/m^2).

It shows that when there was no direct sunlight, the power generation of case A2 is greater than that of case A1. Keeping louvers open (tile angle = 0°) when there was no direct sunlight could let PV-louvers receive the maximum possible diffuse irradiance for electrical power generation.
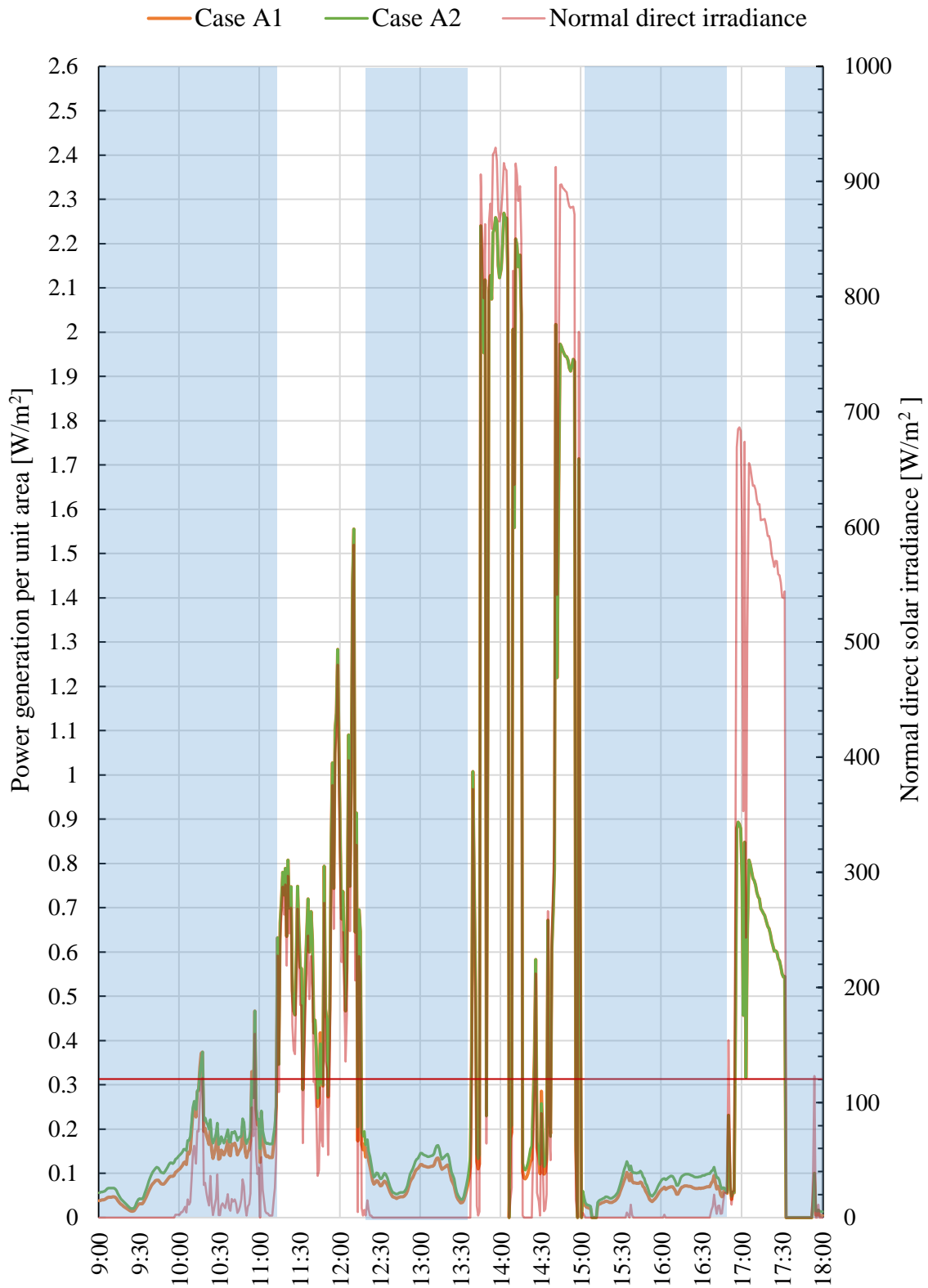
Fig. 5-5. Normal direct solar irradiance and power generations of PV-louvers in case A1 and case A2 by data on a real time basis (4 March)

5.2.2 Time series analysis of power generation of PV-louvers with different configurations

Secondly, power generations of PV-louvers with different configurations were analyzed. Fig. 5-6 illustrates the configuration comparison among case A2, case B2, case C2 and the reference case A0 on 4 March 2015. The orange line presents the sun profile angle. Same as Fig. 5-5, the blue zone means there is no direct sunlight (when the normal direct solar irradiance is below 120 W/m^2).

It shows that when there was no direct irradiance, PV-louvers in closed position had the maximum utilization rate for photovoltaic conversion and provided the maximum electrical power generation than that of PV-louvers in horizontal position. However, when there was direct irradiance and the sun profile angle was low, the PV-louvers that arranged in a slant layout (case C2) generated greater electrical power than case A0 in some periods after 14:30.
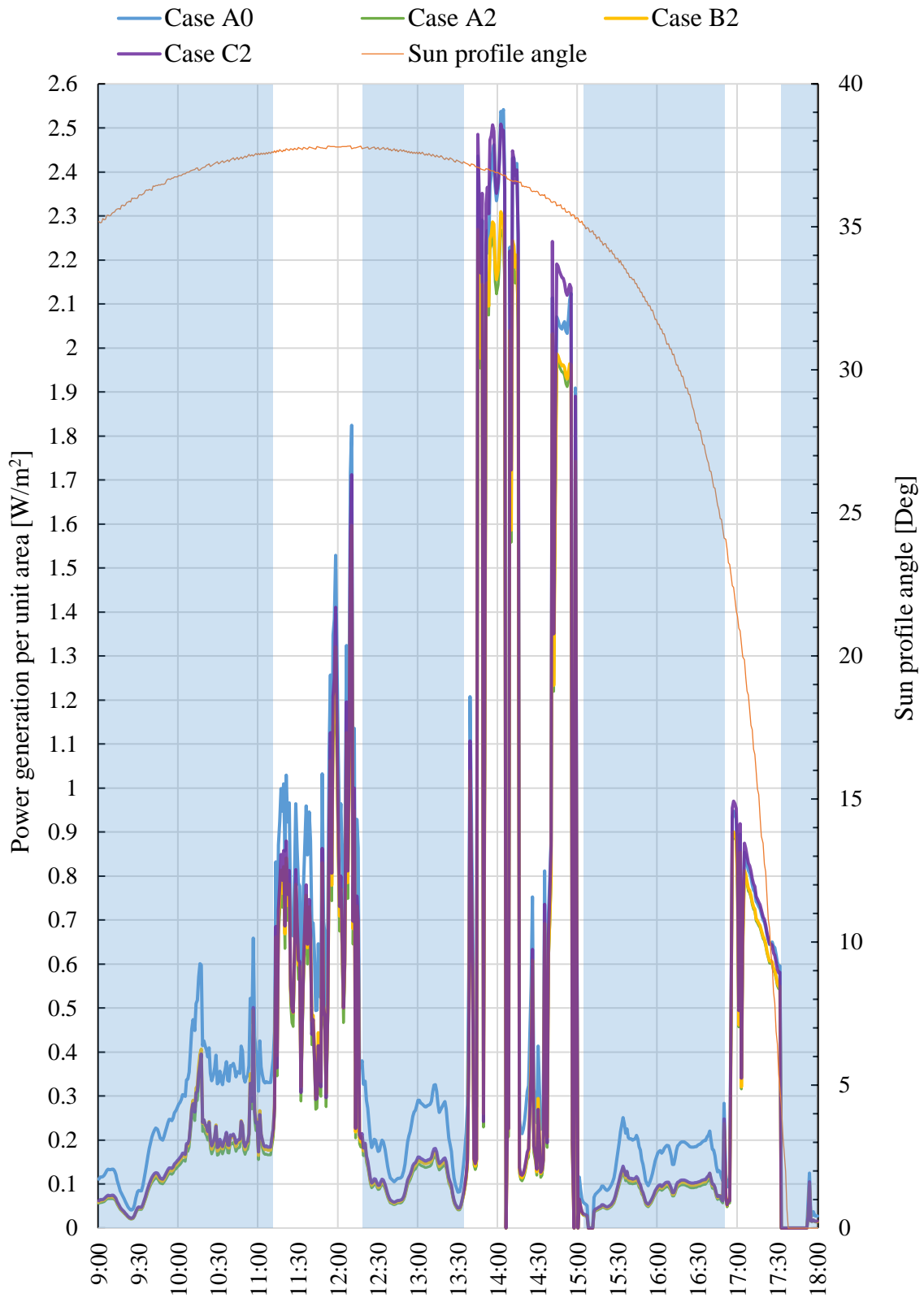
Fig. 5-6. Sun profile angle and power generations of PV-louvers in case A0, case A2, case B2 and case C2 on a real time basis (4 March)

5.2.3 Monthly and annual power generation of PV louvers for different cases

After the time series analysis in the upper section, this section continue to explore the optimized case for monthly and annual power generations of PV-louvers that were calculated with daylight measurements from 1 January 2015 to 30 June 2015 and from 1 July 2016 to 31 December 2016.

The impact of facade orientation on the electrical power generation was also examined. Table 5-6 (a)-(c) show the monthly and annual power generation per square meter of PV-louvers facing south, east and west. The results show that among south, east and west orientations, the south facing PV-louver system has the best generation capacity. Besides, with the same area of PV cells, PV-louvers arranged in a slant layout have the maximum annual power generation on either orientation, especially increased by 20% for south orientation compared to that of horizontal PV-louvers arranged vertically in line. It should be noted that in this paper, the total area of PV panels changed by the different designs of PV-louvers configuration (Table 5-2), that could affect the total electricity generation of the PV-louver system. Power generations of the PV-louver system with different configurations were examined. Fig. 5-7 (a)-(d) show the monthly and annual power generation of the PV-louver system facing south, east and west of different analyzed cases. The results show that for south orientation, case B2 generated the most energy in winter and autumn while case C2 generated the most in summer and spring (Fig. 5-7 (a)). The annual power generation of case B2 was 8856 kWh and of case C2 was 8862 kWh, both exceed the 8723 kWh of case A0. On east and west orientation, case B2 generated more energy than case C2 all year round, but less than 7033 kWh and 6743 kWh of case A0 (Fig. 5-7 (d)).

Table 5-6 (a). Power generation of south-facing PV-louvers of different cases

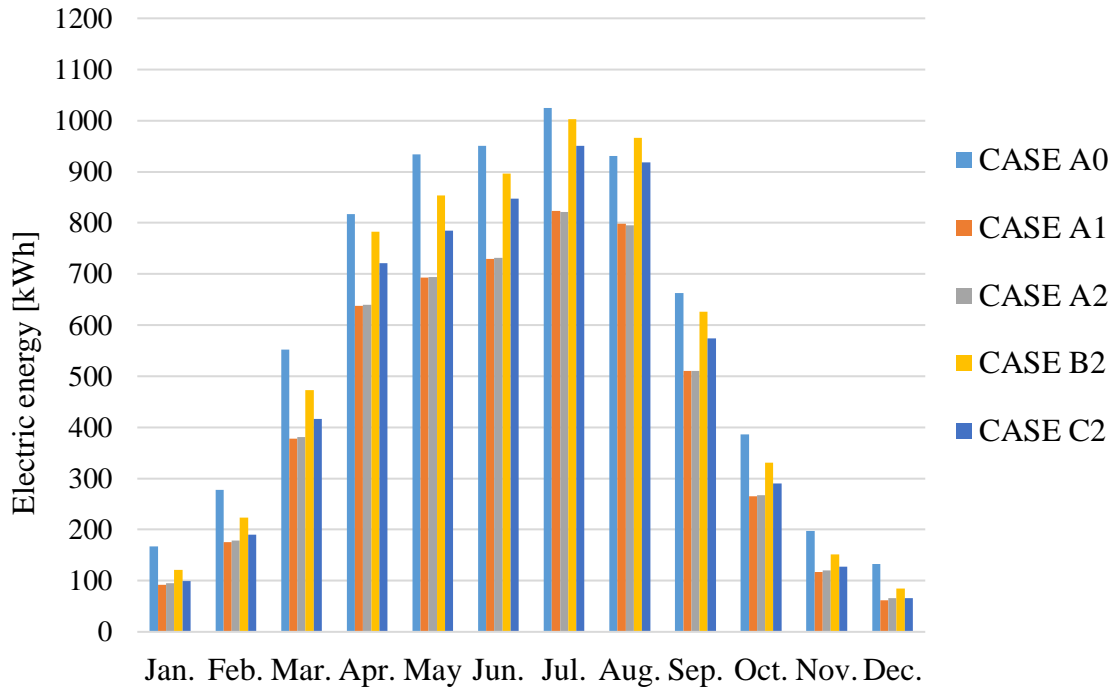| South	CASE A0	CASE A1	CASE A2	CASE B2	CASE C2
	kWh/m^2	kWh/m^2	kWh/m^2	kWh/m^2	kWh/m^2
Jan.	7.20	5.81	6.10	6.18	6.42
Feb.	8.79	7.13	7.44	7.55	8.05
Mar.	13.70	11.50	11.55	11.76	12.93
Apr.	14.68	12.51	12.51	12.64	15.36
May	11.87	8.83	8.83	9.01	11.67
Jun.	11.78	8.90	8.90	9.08	12.41
Jul.	12.62	10.00	10.01	10.17	13.80
Aug.	14.22	12.58	12.58	12.68	16.03
Sep.	15.69	13.88	13.88	14.01	16.17
Oct.	11.17	9.35	9.56	9.73	10.52
Nov.	7.92	6.47	6.73	6.82	7.14
Dec.	6.75	5.39	5.68	5.75	5.96
Annual	**136.38**	**112.34**	**113.77**	**115.39**	**136.45**
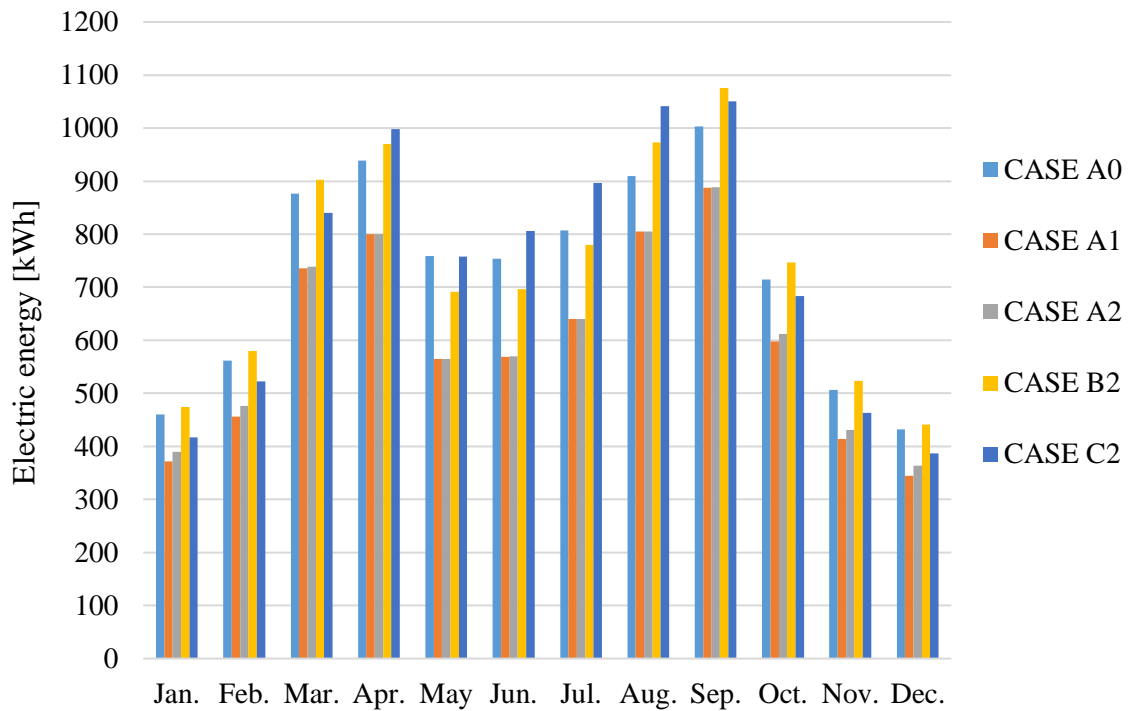
(a) South

Fig. 5-7 (a). Monthly power generation of the south-facing PV-louver system

Table 5-6 (b). Power generation of east-facing PV-louvers of different cases

| East	CASE A0	CASE A1	CASE A2	CASE B2	CASE C2
	kWh/m²	kWh/m²	kWh/m²	kWh/m²	kWh/m²
Jan.	2.62	1.43	1.49	1.58	1.54
Feb.	4.34	2.75	2.80	2.91	2.93
Mar.	8.63	5.92	5.96	6.15	6.42
Apr.	12.77	9.97	10.00	10.20	11.10
May	14.61	10.83	10.85	11.12	12.08
Jun.	14.86	11.41	11.43	11.68	13.04
Jul.	16.02	12.87	12.84	13.07	14.64
Aug.	14.56	12.47	12.44	12.59	14.14
Sep.	10.35	7.99	7.98	8.15	8.84
Oct.	6.03	4.14	4.18	4.31	4.48
Nov.	3.08	1.83	1.89	1.98	1.97
Dec.	2.08	0.97	1.03	1.11	1.02
Annual	**109.96**	**82.58**	**82.88**	**84.85**	**92.20**

(b) East

Fig. 5-7 (b). Monthly power generation of the east-facing PV-louver system

Table 5-6 (c). Power generation of west-facing PV-louvers of different cases

West	CASE A0	CASE A1	CASE A2	CASE B2	CASE C2
	kWh/m²	kWh/m²	kWh/m²	kWh/m²	kWh/m²
Jan.	3.34	2.16	2.20	2.29	2.26
Feb.	4.64	3.06	3.11	3.22	3.26
Mar.	7.88	5.17	5.23	5.42	5.62
Apr.	12.13	9.30	9.34	9.54	10.40
May	13.17	9.44	9.48	9.75	10.44
Jun.	15.03	11.60	11.62	11.87	13.19
Jul.	14.32	11.17	11.14	11.37	12.77
Aug.	10.68	8.60	8.58	8.73	9.93
Sep.	10.75	8.38	8.41	8.58	9.26
Oct.	6.21	4.32	4.38	4.51	4.67
Nov.	3.76	2.49	2.52	2.61	2.61
Dec.	3.51	2.39	2.40	2.48	2.48
Annual	**105.42**	**78.09**	**78.39**	**80.37**	**86.87**
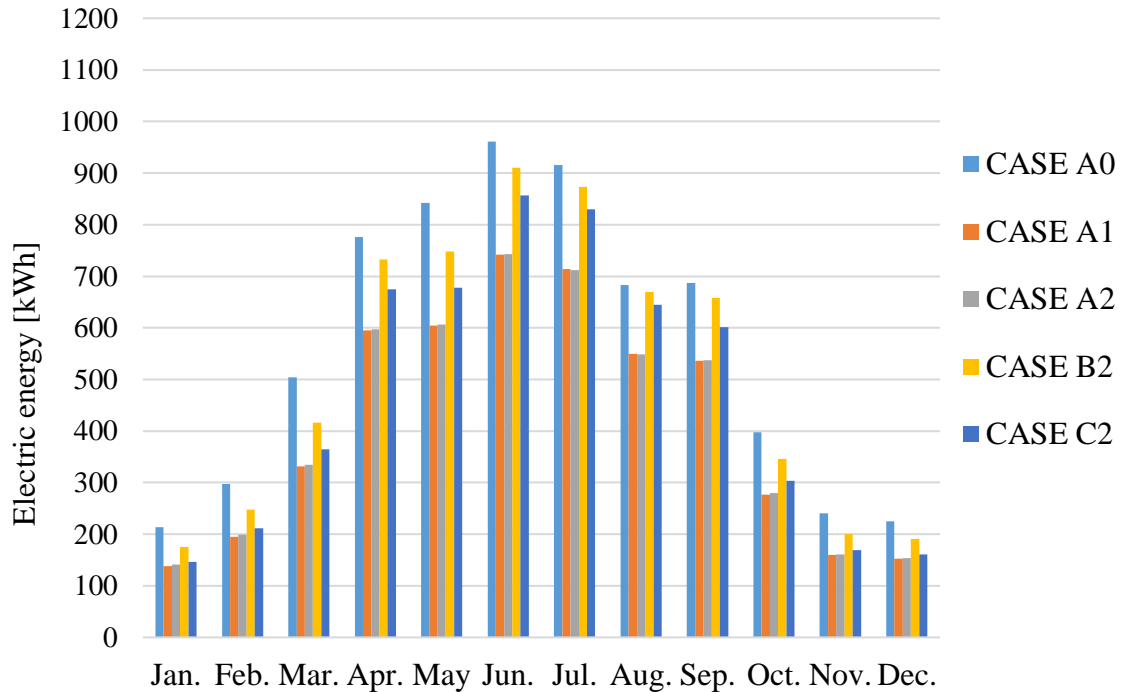
(c) West

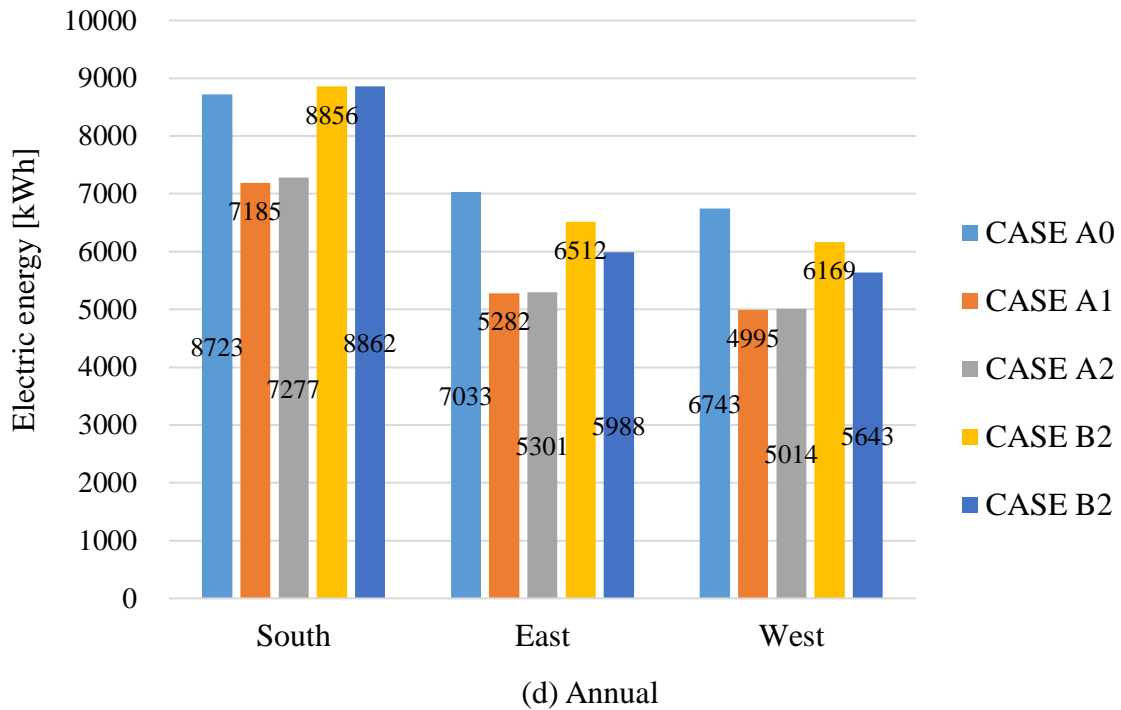Fig. 5-7 (c). Monthly power generation of the west-facing PV-louver system

Fig. 5-7 (d). Annual power generation of the PV-louver system facing south, east and west

5.3 Multi-objective optimization study for the autonomous PV facade system

5.3.1 Simulation of lighting energy consumption

To examine the impacts of different analyzed cases on lighting efficiency, the annual lighting energy consumption was calculated using daylight measurements. Firstly, daylight illuminances on work plane (0.85-meter above floor) after passing through different PV-louvers configurations were calculated at one-minute intervals. The illuminances at points of P1, P2, P3, P4 and P5 in each row were estimated. The calculating points were all on the centerline of the office room, every 2 meters away from the window wall (Fig. 5-8). If the illuminance on measure point was lower than 500 lx, the row of LED luminaires should be on. Table 5-7 shows the length of lighting hour of LED luminaires for each analysis case. For all the analyzed cases, after the fourth row,

the lights were always on (9:00~18:00 for 365 days). Therefore, the area that could be affected by PV-louver system control was within 6-meter distance from the window wall.
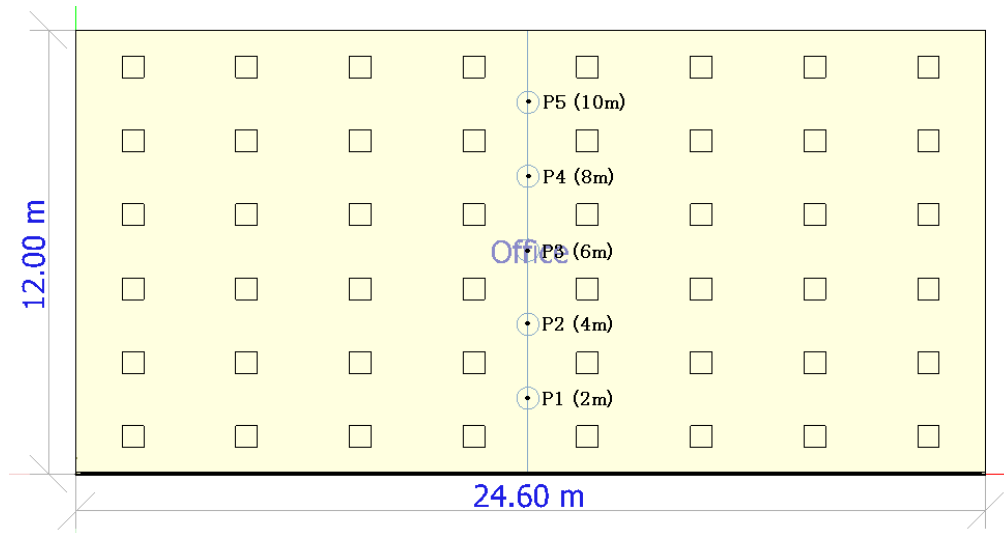

Fig. 5-8. Measure points on work plane (0.85-meter above floor)

Table 5-7. Annual lighting hours of LED luminaires for each analyzed case

ROW	CASE A0	CASE A1	CASE A2	CASE B2	CASE C2
	Hour	Hour	Hour	Hour	Hour
I	3285	2288	2114	2233	2556
II	3285	1816	1440	1529	1693
III	3285	2366	2230	2562	2416
IV	3285	3016	3005	3018	3081
V	3285	3285	3285	3285	3285
VI	3285	3285	3285	3285	3285
Total	19710	16056	15359	15912	16316

Then, after counting the required lighting hours and amount of lighting LED luminaires, the lighting energy consumption (lighting hours × LED luminaires amount × 48 W) cloud be examined. Fig. 5-9 shows the lighting energy consumption of LED luminaires by row for each analyzed case.

The simulation results showed the daylight-responsive control method could reduce lighting energy consumption by 33.11% compared to the reference case A0 and 7.36% to the cut-off angle control, which allowed more daylight quantity into the room and more possible outside viewing (Fig. 5-9).
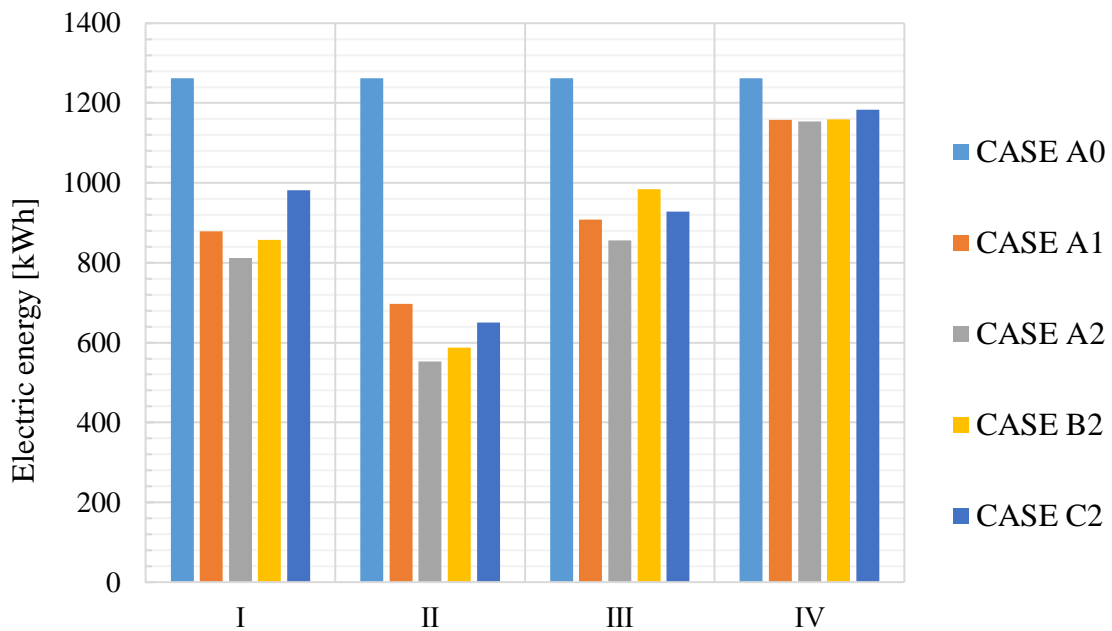

Fig. 5-9. Lighting energy consumption of LED luminaires by row for each analyzed case

5.3.2 Simulation of air-conditioning consumption

The heating and cooling energy consumption of the office room were examined. Considering the room area influenced by PV-louver controls, air-conditioning consumption was analyzed for that space for that space of 24.6 m × 6.3 m × 3.6 m (width × depth × height, 558 m3) within 6.3 m from the window wall. Table 5-8 (a)-(c) the monthly and annual air-conditioning consumption of different analyzed cases for south, east and west orientation.

Table 5-8 (a). Monthly and annual air-conditioning consumption (South)

SOUTH	CASE A0	CASE A1	CASE A2	CASE B2
	kWh	kWh	kWh	kWh
May	277	360	360	359
Jun.	681	780	780	779
Jul.	1147	1264	1264	1262
Aug.	755	880	880	878
Sep.	563	705	705	704
Cooling period	3423	3989	3989	3983
Nov.	827	777	771	760
Dec.	1578	1537	1530	1513
Jan.	1391	1350	1343	1328
Feb.	1246	1179	1174	1163
Mar.	626	505	504	498
Heating period	5669	5349	5322	5262
Annual	**9091**	**9338**	**9311**	**9245**

Table 5-8 (b). Monthly and annual air-conditioning consumption (East)

EAST	CASE A0	CASE A1	CASE A2	CASE B2
	kWh	kWh	kWh	kWh
May	271	376	378	385
Jun.	736	906	909	923
Jul.	1220	1400	1404	1422
Aug.	739	877	883	900
Sep.	455	536	540	547
Cooling period	3420	4095	4113	4178
Nov.	895	865	864	864
Dec.	1655	1631	1631	1631
Jan.	1457	1431	1430	1431
Feb.	1327	1286	1284	1283
Mar.	703	633	630	626
Heating period	6037	5846	5839	5835
Annual	**9458**	**9941**	**9952**	**10012**

Table 5-8 (c). Monthly and annual air-conditioning consumption (West)

WEST	CASE A0	CASE A1	CASE A2	CASE B2
	kWh	kWh	kWh	kWh
May	270	362	364	377
Jun.	736	887	889	912
Jul.	1211	1383	1385	1411
Aug.	707	819	821	838
Sep.	504	596	597	617
Cooling period	3429	4046	4056	4155
Nov.	871	837	834	829
Dec.	1612	1582	1579	1570
Jan.	1433	1405	1402	1396
Feb.	1300	1258	1255	1246
Mar.	681	609	604	592
Heating period	5897	5690	5674	5632
Annual	**9326**	**9737**	**9730**	**9787**

The results show that the daylight-responsive control method increased slightly the cooling consumption and faintly reduced the heating consumption due to the diffuse irradiance inflow of partly cloudy days, however for the whole year, it barely changed the annual air-conditioning consumption compared to cut-off angle control (less than 0.3%)

5.3.3 Comprehensive evaluation of energy-efficiency for the autonomous PV facade system

To obtain the optimum configuration for different orientations, comprehensive evaluation of energy efficiency for the autonomous PV facade system was reviewed. Fig. 5-10 shows the annual electrical power generation of the PV-louvers and consumptions of lighting and air-conditioning for the perimeter zone (6.3 m from the window wall) of

the office room. If the electricity produced from the PV can be used for lighting and air-conditioning of the room, using the Type-B configuration with the daylight-responsive control method required the least amount of energy for the three orientations. Specifically, narrowly improving the ratio W/S from 1 to 1.2 decreased the annual energy consumption by 26.49% for south orientation, 11.69% for east orientation and 10.94% for west orientation (Table 5-9).
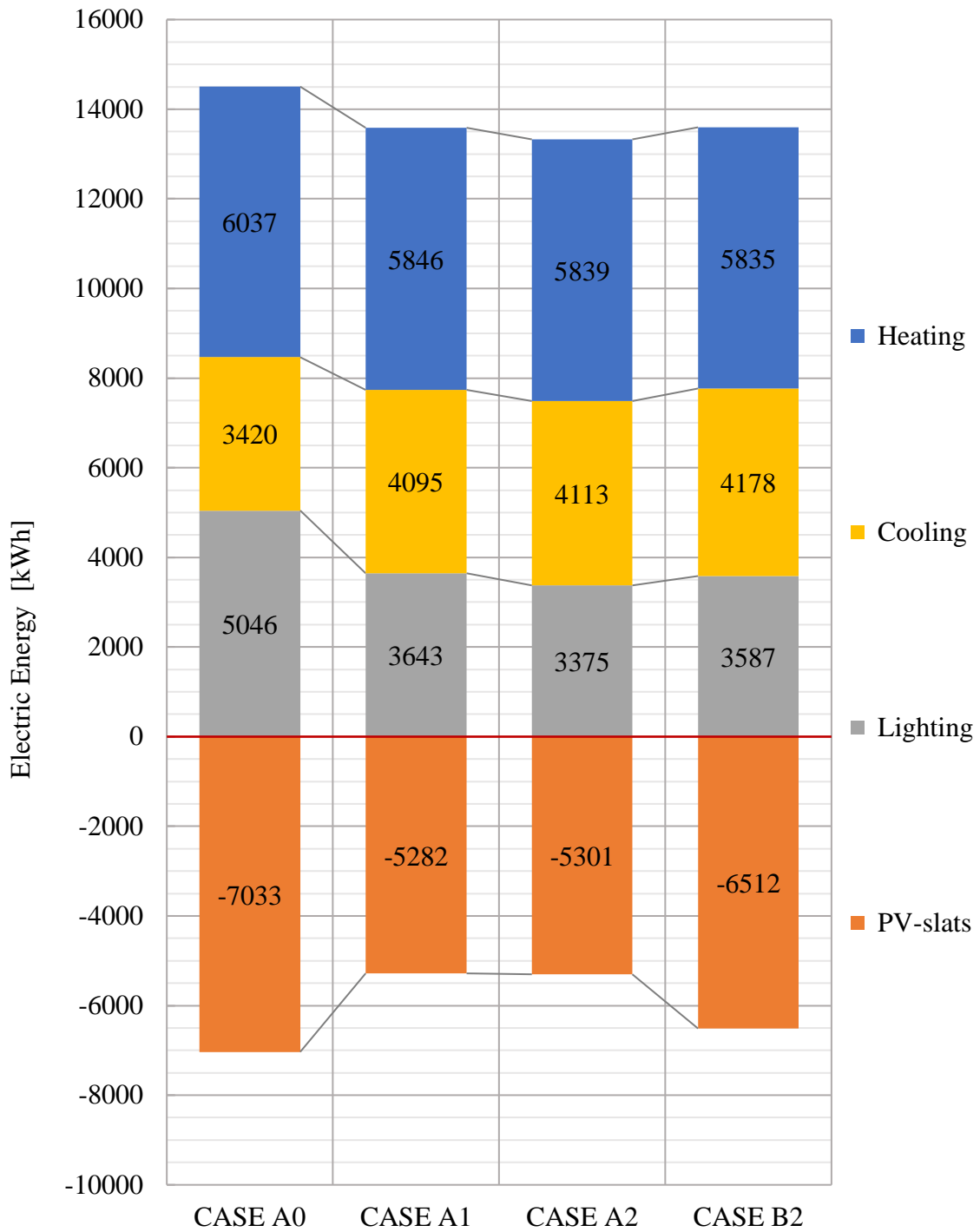
Table 5-9. Comparison of annual required energy consumption in different case

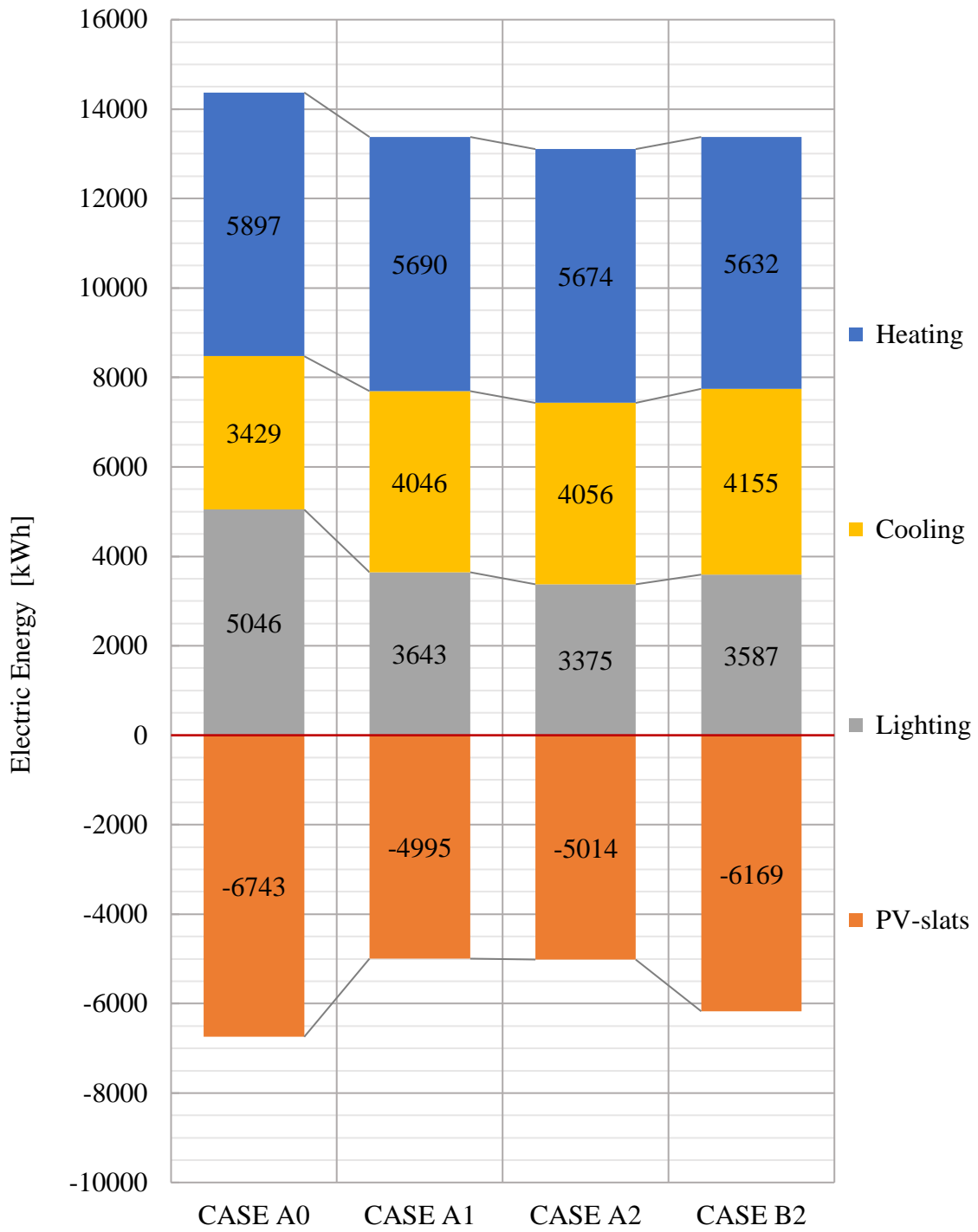| *ORIENTATION*	**CASE A0**	**CASE A1**	**CASE A2**	**CASE B2**
	[kWh]	*[kWh]*	*[kWh]*	*[kWh]*
SOUTH	5414	5796	5409	3976
EAST	7471	8302	8026	7088
WEST	7628	8385	8091	7206
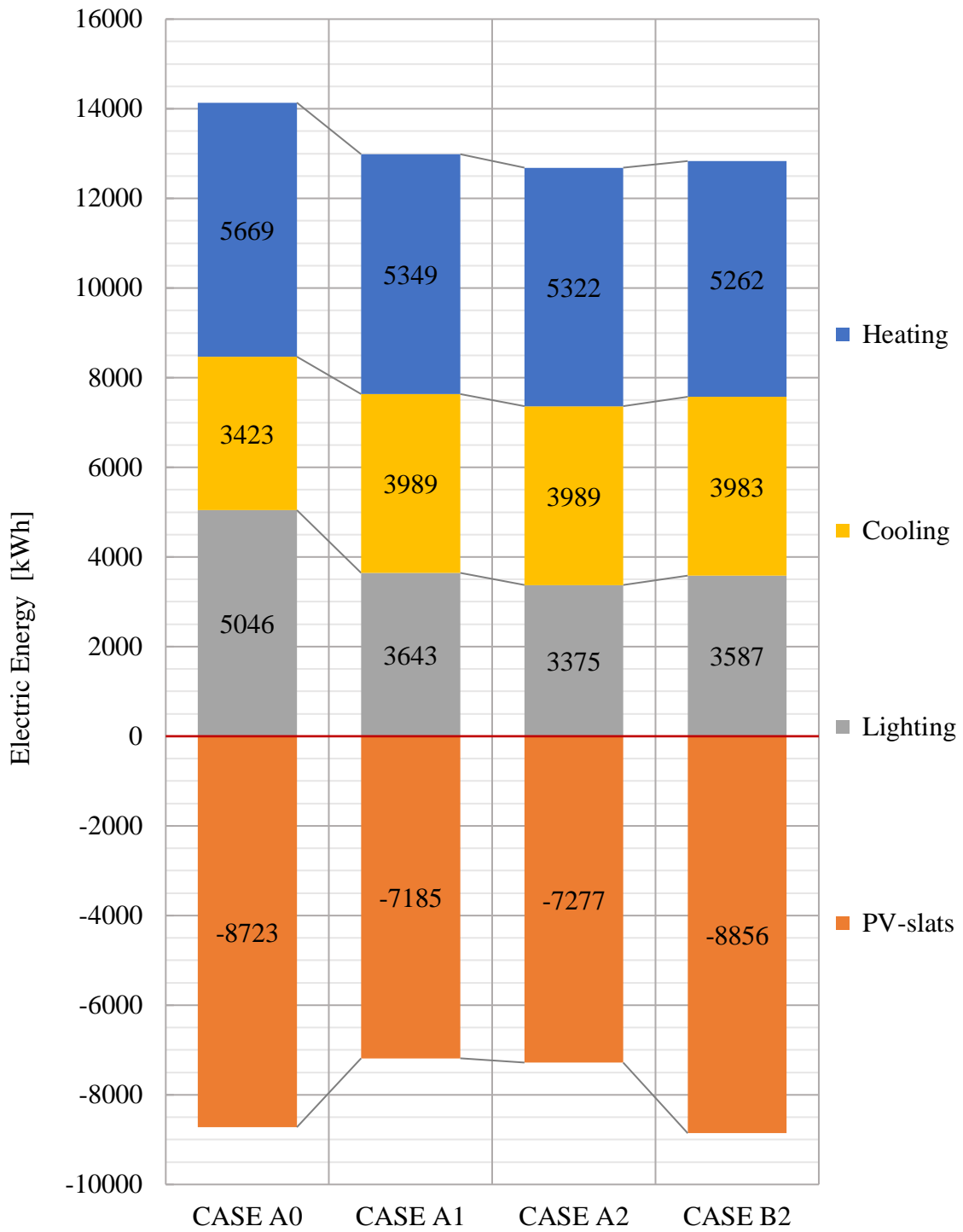
Fig. 5-10 (a). The annual electrical generation and consumptions of air-conditioning and
lighting (south orientation)

Fig. 5-10 (b). The annual electrical generation and consumptions of air-conditioning and lighting (east orientation)

Fig. 5-10 (c). The annual electrical generation and consumptions of air-conditioning and lighting (west orientation)

5.4 Conclusion

As ways to improve energy-efficiency, a daylight-responsive control strategy and two types of configuration were presented. Impacts of the facade orientation were considered. The proposed daylight-responsive strategy can benefit both its electricity generation and daylight usage without the risk of invasive direct solar radiation. This chapter conducts comprehensive analyses on electrical power generation, air conditioning and lighting energy consumptions of an open-plan office with the PV-louver system. The analysis results suggests that, for the same window area, case C2 has the highest values for maximum power generating efficiency and delivers a 20% increase in power per square meter for south orientation when compared to case A2, whose PV-louvers were vertically arranged.

The results of investigation indicate that PV-louvers arranged in a slant layout can alleviate the loss of electrical power generation caused by the partial shading effect of PV cells when the sun profile angle is high. The comprehensive evaluation of energy-efficiency including electrical power generation, air-conditioning and lighting energy consumptions indicated that the louver width should be slightly wider than the spacing in terms of the energy performance.

REFERENCES

[1] L.D. David, W.H. Kevin, G.M Richard, R.S Gary The IESNA Lighting Handbook (10th ed.), Illuminating Engineering Society of North America, New York (2011)

[2] Ozaki A., et al., : Prediction of Hygrothermal Environment of Buildings Based upon Combined Simulation of Heat and Moisture Transfer and Airflow, Journal of the International Building Performance Simulation Association, Vol.16, No.2 (2006), pp. 30-37

Chapter VI

Conclusions

6.1   Main results

This research proposed a new form of autonomous facade system with louvers integrated to photovoltaic (PV) panels that can be controlled individually. This new facade system has a new element called PV-louver, which comes with the functions of not only sun shading and power supply, commonly seen on conventional autonomous facade systems, but also integrate the additional function of daylight monitoring essential for PV-louvers control.

For the hardware side, this research conducts experiments to investigate the relationship between the daylight illuminance and the output of different type PV cell. The type of thin-film PV cells is selected for the proposed PV-louver system and an approach to utilize them for daylight sensing is obtained by experiment. Besides, improved PV-louvers configurations are proposed to solve the PV efficiency loss caused by the partial shading effects of PV cells.

For the software side, a daylight-responsive control strategy is proposed for partly cloudy and overcast sky conditions. It is based on traditional cut-off angle control method and can make better use of daylight. Besides, objective to develop a simpler and more

effective sunlight sensing approach that is viable at each window of a building, this study derived a way to use ISO/CIE Standard General Skies to obtain the theoretical daylight illuminance thresholds for sunshine judgements. The results indicate that sky type 9 can be served to get the vertical daylight illuminance thresholds, which were as functions of solar altitude or sun profile angle, to judge whether the windows receive direct sunlight or not.

As ways to improve energy-efficiency, a daylight-responsive control strategy and two types of configuration were studied through the validation of their energy performance in a predetermined open-plan office model. Impacts of the facade orientation were tested. The results suggest that, for the same window area, PV-louvers arranged in a slant layout had the highest values for maximum power generating efficiency and delivers a 20% increase in power per square meter for south orientation when compared a vertically arranged one for the same south orientation. The comprehensive evaluation of energy-efficiency including electrical power generation, air-conditioning and lighting energy consumptions showed the merit of the daylight-responsive control, and indicated that the louver width should be slightly wider than the spacing in terms of the energy performance.

6.2   Conclusion and outlook

In this research, design elements from the following aspects those were considered to increase the utility, economy and simplicity of the PV facade system: (i) Type of solar cell for the PV-louvers; (ii) PV-louver control strategy; and (iii) configuration of PV-louver system. Besides, a simpler and more effective approach that using daylight illuminances on windows (PV-louvers) for sunshine presence judgements was derived.

The measurements used to examined T_v is only from Lyon, doesn't represent sky conditions of other areas. However, the calculated vertical diffuse illuminances of the four partly cloudy sky types have the same trend and the illuminance gap between each sky type is very small within the control range. The adaptability of CIE sky types is expected to be further studied.

The calculations were based on theories, they meant the maximal possible power generation of each cases. Because of the partial shading effect of PV cells, a tiny shading of the PV-louver may reduce the PV power generation and total energy performance of the system. By designing an arrangement of PV modules on louvers with the precondition of avoiding the areas where shadows would be casted upon them on a regular basis may be one way to solve this problem. This aspect will be the next step to optimize the PV facade system.